Characterizing the mechanisms of resistance to the novel antimicrobial 4-hydroxy-2-nonenal by the model pathogen *Listeria monocytogenes*

Hannah Tabakh

A dissertation
submitted in partial fulfillment of the
requirements for the degree of

Doctor of Philosophy

University of Washington
2020

Reading Committee:
Joshua Woodward, Chair
Joseph Mougous
Ram Savan

Program Authorized to Offer Degree:
Microbiology

University of Washington

Abstract

Characterizing the mechanisms of resistance to the novel antimicrobial 4-hydroxy-2-nonenal by the model pathogen *Listeria monocytogenes*

Hannah Tabakh

Chair of the Supervisory Committee:
Associate Professor, Joshua J. Woodward
Department of Microbiology

Pathogens encounter numerous antimicrobial responses, including the reactive oxygen species (ROS) burst. ROS-mediated oxidation of host membrane poly-unsaturated fatty acids (PUFAs) generates the toxic αβ-carbonyl 4-hydroxy-2-nonenal (4-HNE). Though studied extensively in the context of sterile inflammation, 4-HNE's role during infection remains limited. Here we found that 4-HNE is generated during bacterial infection and that the intracellular pathogen *Listeria monocytogenes* induces a specific set of genes in response to 4-HNE exposure. A component of the *L. monocytogenes* 4-HNE response is the expression of the genes *rha1* and *rha2* which code for two NADPH-dependent oxidoreductases that collectively counter 4-HNE toxicity by converting 4-HNE to the less toxic product 4-hydroxynonanal (4-HNA). Heterologous expression of *rha1/2* in *Bacillus subtilis* significantly increased bacterial resistance to 4-HNE both *in vitro* and following phagocytosis by murine macrophages. Our work demonstrates that 4-HNE is a previously unappreciated component of ROS-mediated toxicity and that *L. monocytogenes* has evolved specific countermeasures to survive within its presence. In

addition to the above-mentioned work, we also developed a saturated transposon library in *L. monocytogenes* that we then used to determine the essential genes of *L. monocytogenes* using a transposon sequencing (Tn-seq) approach. This methodology could be used in the future to further probe the genetic determinants of *L. monocytogenes* resistance to 4-HNE.

Table of Contents

Acknowledgements……..……4
List of figures……..……6
List of tables……...……7

Chapter 1: Introduction and background……..……8
1.1 Innate immune sensing and response: a brief introduction……8
1.2 Reactive oxygen species: an overview……..……8
1.3 Innate immunity and antimicrobial ROS……9
1.4 Arachidonic acid, lipid peroxidation and innate immunity……..…11
1.5 4-HNE: a toxic product of lipid peroxidation……...…12
1.6 4-HNE eukaryotic detoxification schemes……..…14
1.7 4-HNE and bacteria -- state of the field……...……16
1.8 Introduction to *Listeria monocytogenes* as a model pathogen……17

Chapter 2: 4-hydroxy-2-nonenal antimicrobial toxicity is neutralized by the intracellular pathogen *Listeria monocytogenes*……19
2.1 Introduction……...……19
2.2 Results……....20
2.2.1 4-HNE accumulates during L. monocytogenes infection……..…20
2.2.2 4-HNE causes damage through the targeting of nucleophilic protein moieties and L. monocytogenes is uniquely resistant to 4-HNE-mediated death.……23
2.2.3 L. monocytogenes expresses 4-HNE detoxification enzymes that contribute to its survival in the presence of 4-HNE……25
2.2.4 Recombinant Rha1 and Rha2 metabolize 4-HNE to 4-HNA……..……..…31
2.2.5 Ectopic expression of rha1 and rha2 confers 4-HNE resistance to the sensitive bacteria B. subtilis……..……33
2.3 Discussion……...……36
2.4: Postscript -- candidate genes with no obvious roles in 4-HNE resistance……39

Chapter 3: TnSeq development in *Listeria monocytogenes* and potential applications for the study of 4-HNE resistance……41
3.1 Introduction……..……...41

3.1.1 The potential utility of Tn-seq for understanding L. monocytogenes physiology……..41
3.1.2 Introduction to TnSeq……..41
3.2 Results……..42
3.2.1 The L. monocytogenes genome is 7% essential genes……42
3.2.2 Overview of the L. monocytogenes essential genes……44
3.2.3 A closer look at L. monocytogenes essential genes with unknown functions……..45
3.3 Conclusions and future directions……47
3.3.1 Tn-seq as a potentially powerful tool for assessing L. monocytogenes physiology……47
3.3.2 Tn-seq for understanding L. monocytogenes 4-HNE resistance……48

Chapter 4: Perspectives and future directions……50
4.1 Introduction……50
4.2 Why two enzymes that do the same thing?……50
4.3 Why 4-hydroxynonanal?……51
4.4 Other resistance schemas -- *rha1* and *rha2* are not everything……51
4.5 *L. monocytogenes* potentially subverts immunomodulatory function of 4-HNE……52
4.6 Conclusion……52

Chapter 5: Materials and Methods……54
5.1 Strains and routine growth conditions……54
5.2 Bacterial infection and exogenous 4-HNE TIB73 dot blot……54
5.3 Mouse infections……55
5.4 4-HNE histology……55
5.5 *L. monocytogenes* 4-HNE PBS dot blots cytosolic 4-HNE assessment……56
5.6 RNA extraction from broth cultures of *L. monocytogenes*……57
5.7 RNA-sequencing……57
5.8 qRT-PCR……58
5.9 Intracellular RNA extraction……58
5.10 Survival assays bacterial panel……59
5.11 *L. monocytogenes* competition experiments……59
5.12 *L. monocytogenes* protein aggregation assay……60
5.13 Purified protein expression and enzyme kinetics……61
5.14 Chemical reduction of 4-HNE……61

5.15 Thin layer chromatography (TLC)……..…61
5.16 *B. subtilis* growth curves……..……62
5.17 *B. subtilis* and *L. monocytogenes* rich media dot blots……..…62
5.18 *L. monocytogenes* macrophage infection……..63
5.19 *B. subtilis* macrophage survival assay……64
5.20 Tn-seq library preparation and sequencing ……..…64

References……65

Acknowledgements

I'd like to thank my advisor, Joshua Woodward, for his mentorship and guidance through the completion of this thesis work. Thanks for being patient of my fear of chemistry-related lab injuries, however far-fetched. This work would not have been completed without all your support.

Huge thanks to all the Woodward lab members, past and present, with a special shout-out to fellow grad students Alex Pollock and Shivam Zaver for helpful scientific discussions as well as extremely non-scientific (and often emotionally life-saving) after-work and lunch hangs. I'd also like to thank senior graduate student (as you were senior to me when I joined) Adelle McFarland, both for your initial groundwork for this project as well as your patience in teaching me immunology. Also, a big thanks to Aruna Menon, who helped with so much of the labor of this project and with whom I could always get a cup of tea.

Enormous thanks to my classmates, Ariana Samadpour, Erin Garcia de Jesus and Hannah Ledvina. You guys were the best cohort, and I miss you all. A special thanks to Hannah L for being my name-twin, as well as an amazing scientist and friend.

I'd like to say thanks to all the other awesome members of the UW Microbiology Graduate Program, especially Rochelle Glover, Dan Holmes, Monica Cesinger, and Kaitlyn LaCourse. Our department has the best grad students, for sure.

I'd also like to thank my friends outside the Department, for reminding me that there is life outside the lab – Kanichi Garcia Nakata, Zach Gottesman, Nick Englund, Polina Berenstein, Juliet Evans Jacobson, Liz Baroi, Rachel Banning-Lover, Anna Shelpakova, Ella Shkiperova, Jono Go, Morgan Crawford, Steven Cohen, Erik Krasner-Karpen, Boris Krichevsky … and everyone else who came to visit Seattle while I have been in grad school or hosted me when I ventured outside the PNW for a change of scenery. I hope to be able to see you all on the other side of 2020 sooner rather than later.

Also huge, huge thanks to the DTE lab gang – Anum Azam Glasgow, Jeff Glasgow, Sergey Boyarskiy and Steph Davis Lopez. You made grad school look so fun, I couldn't help but join up too! Of course, goes almost without saying, big thank you to DTE herself – Danielle Tullman-Ercek, who took a chance and hired me as an 18-year-old baby and helped me grow into a real adult scientist.

A big thank you to my parents: Roman and Katya Tabakh, who supported my scientific proclivities throughout my life and are always there to remind me that although it is important to work hard… it is also important to not forget to do the things that bring you joy and keep you sane.

And, last but not least, a giant thanks to my husband, Kris Tonthat, who has put up with me for almost a decade and has always been there for me, even if it had to be over Skype from halfway around the world. I couldn't have done it without you.

List of figures

Figure1. ROS generation in a eukaryotic cell during phagocytosis……...10
Figure2. Hock rearrangement to form 4-HNE……...12
Figure3. 4-HNE molecular structure……..……...13
Figure4. 4-HNE reactivity with biological macromolecules….....13
Figure5. 4-HNE detoxification schemes in eukaryotic cells….....15
Figure6. 4-HNE adduct accumulation during *L. monocytogenes* infection….....21
Figure7. There is no significant 4-HNE adduct accumulation in the murine liver….....22
Figure8. 4-HNE accumulates in the spleen during murine *L. monocytogenes* infection….....23
Figure9. 4-HNE impacts bacterial viability, replication and damage to intracellular proteins…….....24
Figure10. 4-HNE exposure induces a large transcriptional change in *L. monocytogenes*….....26
Figure11. 4-HNE specifically induces *rha1* and *rha2* expression…….....27
Figure12. *rha1* and *rha2* expression is induced during intracellular infection…….....28
Figure13. Competitions of WT versus mutant *L. monocytogenes* in 4-HNE….....28
Figure14. 4-HNE protein adduct accumulation is increased in ∆*rha1*∆*rha2 L. monocytogenes*….....29
Figure15. 4-HNE does not lead to significant protein aggregation in *L. monocytogenes*.....30
Figure16. ∆*rha1*∆*rha2 L. monocytogenes* lacks a robust infection phenotype….....31
Figure17. Homology predictions of active sites of Rha1 and Rha2…….....32
Figure18. *In vitro* characterization of Rha1 and Rha2 functionality…….....33
Figure19. Expressing both of the functional *rha1* and *rha2* forms in *B. subtilis* enhances growth in 4-HNE….....34
Figure20. Expressing *rha1/2* WT in B*. subtilis* aids in the bacterium's survival in 4-HNE….....35
Figure21. Ectopic expression of *rha1/2 in B. subtilis* confers a PHOX-dependent survival advantage in primary bone marrow macrophages…….....36
Figure22. Model or *rha1*/*2* mediated resistance in *L. monocytogenes*….....37
Figure23. Gene expression of *lmo2829* and positive control *rha2* during treatment with various aldehydes….....40
Figure24. Tn-seq workflow schematic….....42
Figure25. Essential genes that overlap between *B. subtilis* and *L. monocytogenes*.....44
Figure26. *dnaK*, *dnaJ* and *grpE* are all essential in *L. monocytogenes*….....45
Figure27. *lmo2487* is a novel *L. monocytogenes* essential gene.....47
Figure28. *L. monocytogenes* death upon 4-HNE exposure in PBS….....48

List of tables

Table 1. RNA-seq dataset of L. monocytogenes treated with 4-HNE versus mock….....73
Table 2. Tn-seq dataset of essential *L. monocytogenes* genes matched with essential *B. subtilis* genes.....93

Chapter 1: Introduction and background

1.1: Innate immune sensing and response: a brief introduction

The initial defenses against invading pathogens in a body are physical barriers and clearing mechanisms such as mucus[1], cilia[2] and skin[3]. However, these barriers are sometimes breached by pathogenic bacteria. Once this occurs, the innate immune system is the next point of defense. The innate immune system comprises a host of cells expressing germline-encoded recognition receptors, called pattern recognition receptors (PRRs) for specific pathogen-associated molecular patterns (PAMPs)[4]. PAMPs are defined as components of pathogens that are invariable, essential for the survival of the pathogen, and absent in the host, allowing for "self-nonself" differentiation[5]. A well-studied and important group of PRRs are the Toll-like receptors, or TLRs. TLRs are surface and endosomal membrane-embedded proteins that sense a wide range of PAMPs, including bacterial membrane lipopolysaccharides, or LPS (TLR4)[6], peptidoglycan (TLR2)[7] , flagellin (TLR5)[8] , unmethylated pathogen-associated CpG DNA (TLR9)[9] and viral single-stranded RNA (TLR7)[10].

Once a TLR engages with the appropriate PAMP, it triggers a conformational change in the Toll/interleukin-1 receptor domain (TIR) of the TLR, which leads to the recruitment of adaptor proteins, including Myeloid differentiation factor 88 (MyD88) and TIR-domain containing adaptor molecule (TRIF)[11] . These adaptor protein-TLR interactions lead to proinflammatory signaling cascades and the release of a multitude of immunomodulatory and antimicrobial and antiviral factors, such as the inflammatory cytokines tumor necrosis factor (TNF) and interleukin 6 (IL-6), as well as type I interferons, among many others[12]. In addition to cytokine release, TLR activation leads to the production and release of reactive oxygen species[13], which I will discuss in greater detail in the following section.

1.2: Reactive oxygen species: an overview

Reactive oxygen species (ROS) is an umbrella term referring to radical and non-radical molecules formed through the partial reduction of oxygen[14]. These include superoxide anion (O_2^-), hydrogen peroxide (H_2O_2), hydroxyl radical ($OH^\bullet$), ozone (O_3), hypochlorous acid (HOCl), organic peroxides (ROOR') and peroxyl radicals ($ROO^\bullet$). These molecules are difficult to distinguish from one another within cells and challenging to measure, meaning that although the term "ROS" is extremely broad and encompasses a variety of chemically distinct molecules, many of the nuances of their distinctions are unknown or poorly studied[15,16]. However, in recent years there has been a renewed effort to understand how exactly this family of molecules functions within the eukaryotic cell, and therefore a more detailed picture of the many facets of ROS biology has been brought to light.

Although often thought of as exclusively damaging agents whose accumulation within the cytosol should be avoided, low levels of ROS actually serve homeostatic functions within eukaryotic cells. ROS have been found to be an important component of regulating various cellular functions and signaling cascades[15,17], including NF-kB activation[18], glycolysis[19], ion channel conductance [17,20], and replication fork formation in DNA [21], among others. In this chapter, however, we will focus on the role of ROS not as regulators of homeostasis, but rather as direct antimicrobials in the context of innate immunity.

1.3: Innate immunity and antimicrobial ROS

ROS have been studied for over sixty years in the context of infectious disease. In 1961, polymorphonuclear leukocytes were found to produce ROS in the form of hydrogen peroxide [22,23], and in 1977 it was discovered that ROS contributed to increased antimicrobial activity of macrophages [22,23], from which point the significant role of ROS in innate immune antimicrobial defense has been observed in hundreds of studies[24].

ROS is produced in neutrophils and to a lesser extent in macrophages[25]. Once the phagocytes sense invading bacteria via their PRRs, it leads to bacterial engulfment into a

phagosome compartment and the assembly of the NADPH oxidase (NOX) complex at the phagosome membrane[26]. There is also growing evidence that mitochondria are an important source of intracellular ROS, called mitochondrial ROS (mROS), during infection[27–29]. NOX generates superoxide anions (O_2^-) through an NADPH-dependent reaction, which is the initial source of all the downstream ROS generated within the phagocyte. Superoxide is cytotoxic to bacteria directly, but it is also converted to a variety of oxygen species through multiple enzymatic and spontaneous reactions. Superoxide is converted to hydrogen peroxide by superoxide dismutase, which can be further transformed to highly toxic hypochlorous acid by the enzyme myeloperoxidase [30]. In addition to enzymatically derived ROS, hydroxyl radicals ($OH^{\bullet}$) are formed within the phagosome through iron-mediated Fenton chemistry[31] as is the highly reactive peroxynitrite[32], which is formed through the spontaneous reaction of superoxide anion with nitric oxide. Nitric oxide is another antimicrobial small molecule which is generated by the inducible nitric oxide synthase enzyme (iNOS) upon immune activation[33] (Figure 1).

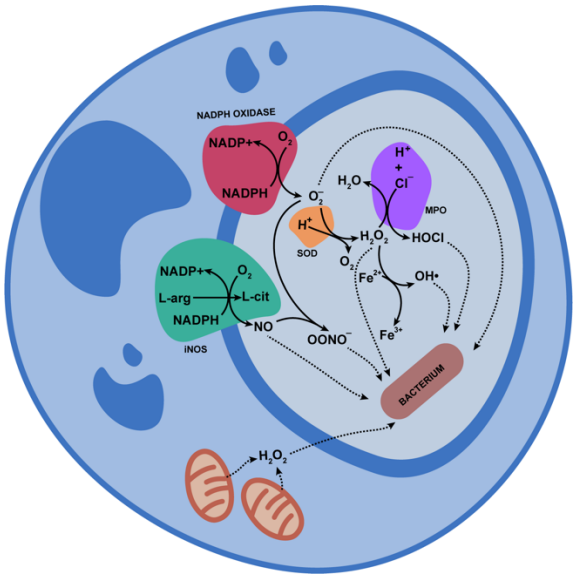

Figure 1. **ROS generation in a eukaryotic cell during phagocytosis.** A pictorial representation of various sources of ROS that a bacterium encounters during phagocytosis by a eukaryotic cell.

Once ROS is generated during infection, it is able to directly damage the invading pathogen. ROS molecules lead to double strand breaks in DNA through guanine base oxidation[34],

iron-sulfur containing proteins sustain damage through oxidation of their Fe-S clusters[35], the cells sustain direct protein damage through oxidation of amino acids[36] and there is evidence of lipid peroxidation of bacterial membranes[36,37].

These antimicrobial ROS effects are very important for the successful clearance of invading pathogens. Humans with chronic granulomatous disease, a disorder caused by a congenital defect in their NOX, are acutely susceptible to life-threatening bacterial infections[38], while mutations leading to reduced functionality of the macrophage NADPH oxidase have been associated with increased susceptibility to *Mycobacterial* infections[39], and defective NOX activation in patients with alcoholic hepatitis increased their vulnerability to *E. coli* infection[40]. In sum, ROS are a class of potent antimicrobial molecules which play an important role in innate immunity.

1.4: Arachidonic acid, lipid peroxidation and innate immunity

ROS generation is not the only effect of PRR-mediated bacterial sensing by the eukaryotic host. Another important component of the innate immune response to a sensed pathogen is the release of the n-6 polyunsaturated fatty acid arachidonic acid from the eukaryotic cell membrane and the formation of the suite of arachidonic acid-derived immunostimulatory molecules, referred to as the eicosanoids [40,41]. The eicosanoid synthesis is initiated by the phospholipase A_2 enzyme-mediated release of arachidonic acid from the host membranes. The free arachidonic acid is then enzymatically converted to prostaglandins by the cyclooxygenase enzymes and to leukotrienes by the lipooxygenase enzymes[42]. Eicosanoids are crucial to modulating the duration and scale of the inflammatory immune response and play both anti- and pro-inflammatory roles[43].

In addition to its enzymatic conversion to the eicosanoids, arachidonic acid also undergoes non-enzymatic peroxidation to a variety of toxic products including malondialdehyde, acrolein, crotonaldehyde, 4-oxo-2-nonenal (4-ONE) and 4-hydroxy-2-nonenal (4-HNE)[44,45]. The following section will take a deeper look at the chemistry, biological roles and detoxification

schemes of the arachidonic oxidation product 4-HNE.

1.5: 4-HNE -- a toxic product of lipid peroxidation

4-HNE is a major product of the peroxidation of n-6 fatty acids, primarily arachidonic acid. It is formed once arachidonic acid is liberated from the membrane by phospholipase A_2 and reacts with a hydroxyl radical, oxidized iron ($Fe^{2+/3+}$) or an iron-containing heme group, leading to the formation of a lipid radical, which then undergoes peroxidation [46]. This peroxidized lipid undergoes carbon-carbon bond Hock cleavage, forming an aldehyde, which is followed by further peroxidation, the binding of oxygen to form the hydroxyl group and a final reduction reaction leading to the generation of the $\alpha\beta$-aldehyde 4-HNE [47,48] (Figure 2).

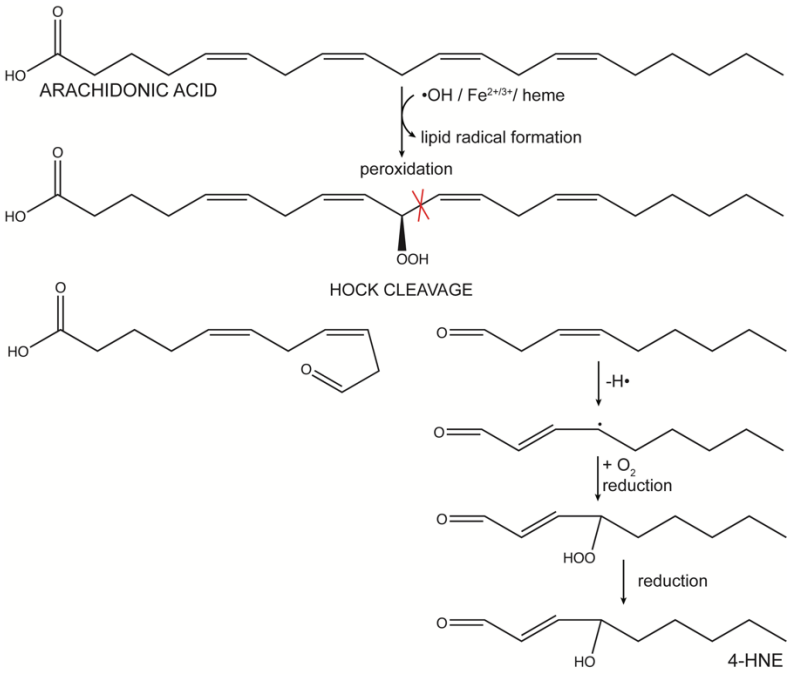

Figure 2. **Hock rearrangement to form 4-HNE.** HNE formation occurs through a multistep process of lipid radical formation, peroxidation, Hock cleavage and reduction.

The molecular structure of 4-HNE leads to biologically relevant chemical properties. 4-HNE has a hydrophobic and hydrophilic end, which leads to 4-HNE being preferentially partitioned into cell membranes while easily traversing the membrane into the aqueous cytosol. 4-HNE is highly reactive due to the presence of multiple reactive groups. The conjugated double bonds as well as the hydroxyl group withdraw electrons from the C3 position, increasing its electropositivity

and making it susceptible to attack from nucleophilic amino acids, while the carbonyl group can react with amino groups on proteins [46] (Figure 3).

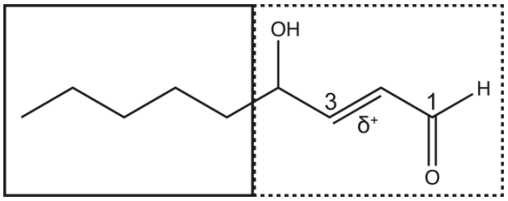

Figure 3. 4-HNE molecular structure. Due to the presence of two highly electron-withdrawing groups adjacent to the C3 position 4-HNE's carbon-carbon double bond is particularly susceptible to attack from nucleophiles. Hydrophobic portion of the molecule indicated by solid line box. Hydrophilic portion indicated by dashed line box.

4-HNE readily forms conjugates with multiple macromolecules within the cell, which leads to often irreversible damage. 4-HNE damages DNA through the formation of 6-(1-hydroxy-hexanyl)-8-hydroxy-1,N2-propano-2′-deoxyguanosine (4-HNE-dG), a bulky exocyclic adduct on guanosine (Figure 4A). This leads to mutagenesis through the increase in G to T transversions[49].

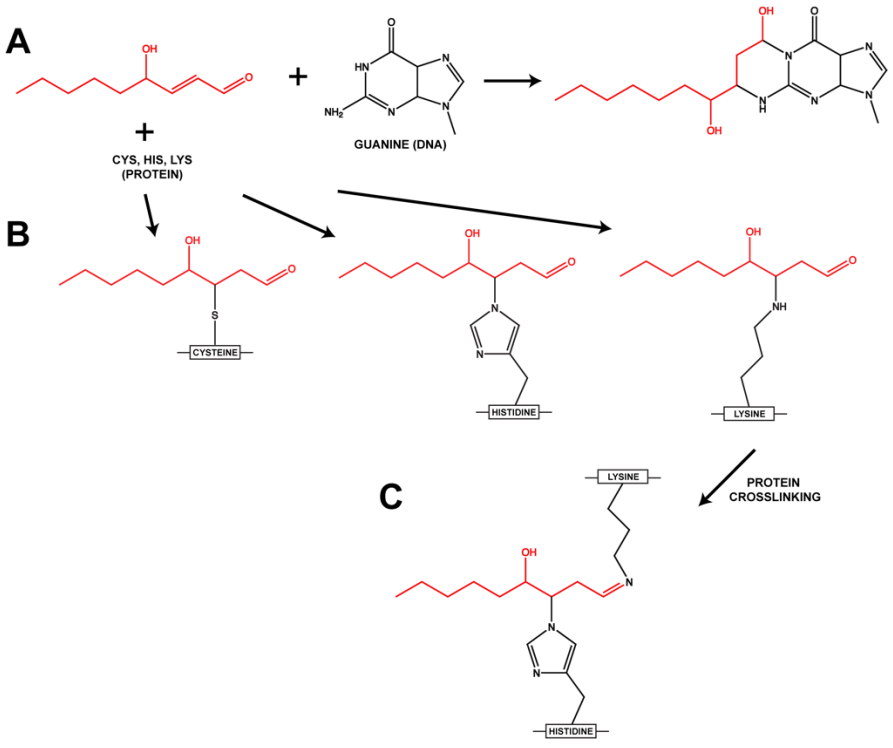

Figure 4. **4-HNE reactivity with biological macromolecules**. 4-HNE is indicated in red. **(A)** 4-HNE reacts with DNA and forms 4-HNE-dG, a bulky exocyclic product. **(B)** 4-HNE readily conjugates with nucleophilic amino acids and can lead to **(C)** protein crosslinking through Schiff base formation with lysine.

4-HNE also has significant reactivity towards nucleophilic amino acids, with the strongest

preference towards cysteine, followed by histidine and lysine[50]. The reaction between 4-HNE and nucleophilic protein moieties is thought to proceed quickly, on the order of seconds to minutes[51] (Figure 4B). In addition to 4-HNE protein conjugation via Michael addition across the double bond, 4-HNE can lead to protein crosslinking through Schiff base formation between the amine group of lysine and the carbonyl group of 4-HNE[52] (Figure 4C).

4-HNE's reactivity towards nucleophilic amino acids means that 4-HNE-protein adduction leads to significant perturbation in protein function. These alterations in activity vary widely, and 4-HNE has been shown to impact cell signaling[53,54]; enzyme activity, mainly through inactivation[55,56,57]; membrane transport[58,59]; and regulation of apoptosis[60,61]. Due to 4-HNE's capability to impact so many intracellular functions and its ready generation upon the initiation of inflammatory processes, it has been implicated in many human diseases[62]. 4-HNE has been shown to contribute to the pathologies of atherosclerosis[63], Alzheimer's [64,65], Parkinson's[66], multiple sclerosis[67], diabetes and insulin resistance[68], cancer[69,70], atherosclerosis[63], inflammatory bowel disease[71] and cataracts[71,72], among others. All these deleterious effects mean that 4-HNE levels must be tightly controlled, and eukaryotic cells have multiple mechanisms of 4-HNE detoxification to prevent 4-HNE mediated cell damage accumulation.

1.6: 4-HNE eukaryotic detoxification schemes

Eukaryotic organisms have multiple detoxification schemes for 4-HNE (Figure 5). 4-HNE's toxicity is driven by its high reactivity due the presence of two resonant double bonds as well as the general reactivity of an aldehyde group. Therefore, detoxification is driven through the elimination of resonance and/or the aldehyde moiety. Eukaryotic organisms have evolved multiple enzymes capable of performing such reactions, which broadly fall into three groups: reduction, oxidation or glutathione transfer. Reduction can proceed at either the double carbon-carbon bond or at the carboxyl group. Double carbon-carbon bond reduction is performed by alkenal/one oxidoreductases and forms the product 4-hydroxynonanal (4-HNA)[71–74]. The reduction of the

carbonyl group is performed by both the aldo-keto reductase and alcohol dehydrogenase enzyme families, forming the alcohol 1,4-dihydroxynonene (1,4-DHN)[75]. Oxidation of the carbonyl bond to the corresponding carboxylic acid and the formation of 4-hydroxynonenoic acid (4-HNEA) is performed by aldehyde dehydrogenases and P450 enzymes[76,77]. Finally, glutathionylation across the carbon-carbon double bond is a reaction that occurs spontaneously but is catalyzed by the glutathione-s-transferases, forming glutathionyl-4-hydroxynonenal (GS-HNE), which is then reduced to glutathionyl-1,4-dihydroxynonene (GS-DHN) by aldose reductases[78]. These glutathionylated products are then excreted out of the cell by the RLIP76 exporter [78,79]. In addition to enzymatic detoxification, 4-HNE toxicity can also be ameliorated non-enzymatically through buffering agents, including the quenching reactions with the endogenous peptides carnosine and GHK (Gly-His-Lys) as well as the small molecule hydrogen sulfide (H_2S)[80].

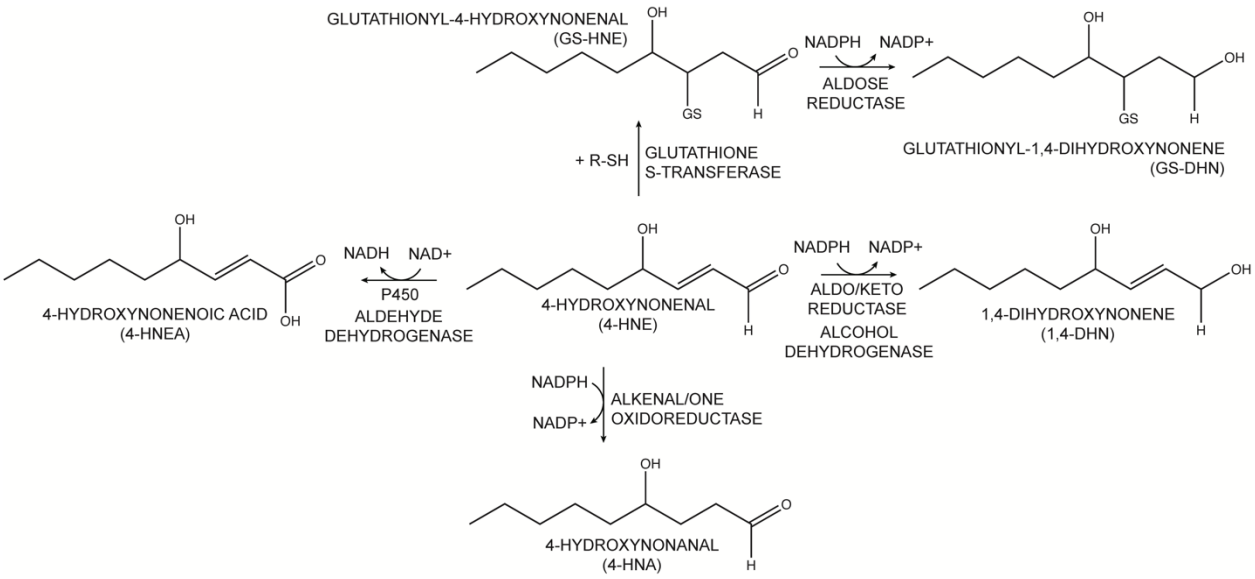

Figure 5. 4-HNE detoxification schemes in eukaryotic cells. To detoxify 4-HNE the cells must eliminate the molecule's resonant double bonds. This can occur through oxidation, reduction or conjugation reactions and eukaryotic cells encode enzymes capable of performing all three processes.

In addition to directly dealing with 4-HNE toxicity, eukaryotic cells also have multiple pathways of responding to, and clearing of, 4-HNE damaged macromolecules. As mentioned above, 4-HNE reacts with proteins, DNA, and lipids, and these damaged cell components must be dealt with to allow the cell to survive. One major pathway of 4-HNE-damaged protein clearance

is via the proteasome, particularly the 20S proteasome[81,82], a well-characterized component of the eukaryotic proteasomal response[83]. A caveat in this clearance scheme is that 4-HNE has been found to inhibit the proteasome, both through direct reactions with proteasomal nucleophilic moieties[84] and by making 4-HNE-ylated proteins resistant to proteolysis[85]. This fact suggests that proteasomal degradation cannot be the only process by which 4-HNE-damaged proteins are recycled in the cell. Another known 4-HNE-protein adduct clearance mechanism is autophagy. Autophagy is the process by which major eukaryotic cytoplasmic components and organelles get degraded within a specialized vacuole called the autophagosome[86]. 4-HNE is known to trigger autophagy[87] and 4-HNE-adducted proteins can be cleared from the cell in this manner[88], though the literature evidence for this pathway is less robust than for proteolysis. Interestingly, although 4-HNE-protein adduct clearance is a major problem for 4-HNE exposed cells, there are no known enzymes capable of removing 4-HNE that is covalently bound to a protein[89].

Proteins are not the only macromolecules damaged by 4-HNE that the cell must deal with. 4-HNE-mediated DNA damage appears to be cleared primarily by the nucleotide-excision repair (NER) pathway[90] , which is effective, but can lead to mutagenesis. This makes 4-HNE a mutagenic, and therefore carcinogenic, molecule[91,92]. Overall, eukaryotic cells have multiple overlapping and redundant mechanisms for protecting themselves against 4-HNE toxicity.

1.7 4-HNE and bacteria -- state of the field

Although 4-HNE has been studied for decades in the context of sterile inflammation, as noted above, and is a known downstream product of PRR activation, particularly TLR stimulation[93], its role during bacterial infection has been significantly understudied. Release of polyunsaturated aldehydes during diatom blooms in the ocean is known to cause bacterial die-offs[94], confirming that a wide variety of bacteria are potentially susceptible to the toxicity of 4-HNE and related molecules. Studies of 4-HNE during bacterial infection and commensalism have primarily investigated how 4-HNE enhances damage to the eukaryotic host or modulates

response to bacterial presence. Examples include 4-HNE exacerbation of inflammation during inflammatory bowel disease (IBD), a disorder partially driven by gut bacterial penetration into systemic circulation[71,94]; the human gut commensal *Enterococcus faecalis* driving macrophage polarization and 4-HNE generation which leads to DNA damage and eventual oncogenic transformation[95]; the inhibition by 4-HNE of the *Chlamydia pneumoniae*-dependent activation of the NF-kB transcription factor[96]; and the induction of 4-HNE accumulation by *Porphyromonas gingivalis*, potentially promoting atherosclerosis development[97]. Overall, there has been very limited research into how 4-HNE impacts bacteria during infection. However, it is likely that 4-HNE, a known component of the inflammatory response, is toxic to invading bacteria. This also opens up the possibility that bacteria can defend themselves against this toxicity. In this work, I will lay out a novel mechanism by which *Listeria monocytogenes* is capable of detoxifying 4-HNE and surviving in its presence.

1.8: Introduction to *Listeria monocytogenes* as a model pathogen

Listeria monocytogenes is a Gram-positive, non-spore-forming, rod-shaped bacterium whose lifestyle includes both a saprophytic component as well as the potential to become a deadly intracellular pathogen upon entry into a eukaryotic organism[98]. This entry typically occurs when *L. monocytogenes* is ingested on food contaminated with the bacteria[99]. Once *L. monocytogenes* is within the host organism, it is capable of nimbly shifting from its environmental niche lifestyle to one of pathogenesis[100], where it utilizes a suite of virulence factors to escape the phagocytic vacuole, multiply within the safe environment of the eukaryotic cytosol and then utilize actin-based motility to propel itself into neighboring cells, propagating the infectious cycle[101,102].

L. monocytogenes has served as a model intracellular pathogen in laboratories worldwide for decades. It is amenable to genetic manipulation, easy to grow in rich and defined broth and on plates, is capable of surviving both in anaerobic and aerobic environments, can be used for both cell culture and murine infection studies and is a relatively low handling risk BSL-2 pathogen

compared to other intracellular pathogens such as *Mycobacterium tuberculosis, Coxiella burnetii* and *Francisella tularensis*[103,104]. Multiple discoveries in pathogenesis research have been made using *L. monocytogenes* that had broader implications outside of the Listerial field. This includes the discovery that the bacterial second messenger cyclic-di-AMP is a potent activator of the type I interferon response[105,106], that multiple intracellular bacterial species use actin-mediated motility to traverse between cells during infection[102,107], and the significant role of host-derived lipoic acid in bacterial pathogenesis[108,109]. All these factors mean that *L. monocytogenes* is an excellent model for studying the interplay between host and pathogen. In this thesis, I present work detailing how *L. monocytogenes* detoxifies the novel antimicrobial molecule 4-HNE and the broader implications of this work for other host-associated bacteria.

Chapter 2: 4-hydroxy-2-nonenal antimicrobial toxicity is neutralized by the intracellular pathogen *L. monocytogenes*

2.1: Introduction

Innate immune detection of bacterial infection initiates a complex inflammatory response characterized by production of cytokines and small molecule mediators involved in driving antimicrobial immunity. A key aspect of intrinsic cellular immunity is the production of highly reactive molecules, including reactive oxygen (ROS) and nitrogen (RNS) species [110]. Unlike the highly specific targeting of infectious agents by adaptive immune responses, ROS and RNS exhibit indiscriminate toxicity toward biological systems through their capacity to react with lipid, amino acid, and nucleic acid moieties that are conserved among both eukaryotic host and invading microbe [111,112]. While such indiscriminate noxious metabolite production provides protection against infection, many bacterial pathogens have evolved a diverse array of mechanisms to directly detoxify or repair damaged cellular components following ROS and RNS encounters [24,113].

ROS and RNS encompass a broad group of distinct molecules. While nitric oxide, hydrogen peroxide, hypochlorite, and superoxide are well characterized molecular components of the innate immune response, these molecules give rise to numerous secondary metabolites that may also contribute to host defense against infection. An initial characteristic of the inflammatory response is the mobilization of arachidonic acid from cellular membranes. While typically involved in generation of eicosanoids, arachidonic acid exposure to oxygen radicals derived from the ROS burst leads to peroxide-mediated structural rearrangement and the generation of breakdown products, the best studied of which is 4-hydroxy-2-nonenal (4-HNE), a highly reactive membrane-permeable molecule[42]. Over the last 40 years, the production of 4-HNE has been well documented at sites of sterile inflammation and has been associated with many disease pathologies, including atherosclerosis [114], Alzheimers' [115], diabetes [68], obstructive

pulmonary disease [116] and chronic liver disease[117]. Although arachidonic acid mobilization and reactive oxygen species generation are well-known and well-studied components of innate immune responses, there are a dearth of studies characterizing the role of 4-HNE during infectious disease.

In this study, we demonstrate that 4-HNE is generated during bacterial infection both in cell culture and *in vivo*, is able to penetrate the bacterial cell envelope and access the cytoplasm, and that 4-HNE generation leads to bacterial growth delay or death. We observed that the intracellular bacterial pathogen *L. monocytogenes* is highly resistant to the bactericidal effects of 4-HNE and that several specific transcriptional responses are induced in response to toxic 4-HNE exposure, including two enzymes, *rha1* and *rha2*, whose loss sensitizes *L. monocytogenes* to 4-HNE toxicity. Through *in vitro* analysis of recombinant Rha1 and Rha2, we found that they both reduce 4-HNE in an NADPH-dependent-manner to the less toxic saturated aldehyde 4-hydroxynonanal (4-HNA). And finally, when *rha1/2* are expressed in the 4-HNE sensitive and avirulent organism *B. subtilis*, they significantly increase bacterial survival in the presence of 4-HNE both *in vitro* and following phagocytosis by murine macrophages. Our findings are consistent with the premise that 4-HNE is a heretofore unrecognized component of ROS-mediated antimicrobial defense and that pathogens have specific and multifaceted detoxification systems used to evade 4-HNE-mediated cytotoxicity in order to promote infection.

2.2: Results

2.2.1: 4-HNE accumulates during *L. monocytogenes* infection.

4-HNE is a highly reactive electrophilic αβ-unsaturated aldehyde that undergoes Michael addition with nucleophilic amino acids, resulting in stable conjugates that correlate with cellular levels of free 4-HNE. Monoclonal antibodies to these adducts are routinely used to monitor 4-HNE levels in cells [48]. To investigate 4-HNE production during bacterial infection, we infected murine hepatocytes with *L. monocytogenes* for 6 hours and quantified 4-HNE conjugates using

dot blots of whole cell lysates at various times post-infection which we then compared to adducts accumulated after incubating the cells with 10μM purified 4-HNE. We found that at 6 hours post infection 4-HNE adducts accumulate to a similar level as with the addition of 10μM purified 4-HNE relative to β-actin control (Figure 6).

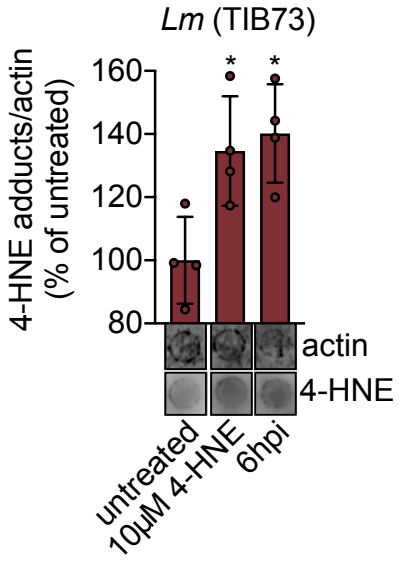

Figure 6. 4-HNE adduct accumulation during *L. monocytogenes* infection. TIB73 cells were either untreated and uninfected, treated for 10 minutes with 10μM 4-HNE in PBS, or infected for 6 hours with *L. monocytogenes*. The cells were then lysed and blotted for actin and 4-HNE-adducts. Data is technical quadruplicates and representative of two independent experiments. Statistics is an ordinary one-way ANOVA comparing untreated to treated and to infected. Error bars are +/- SD. *, $p < 0.05$.

To interrogate the impact of bacterial infection on host production of 4-HNE *in vivo*, mice were infected intravenously with *L. monocytogenes* constitutively expressing GFP. At 48 hours post infection, tissues were harvested, fixed, and analyzed by immunohistochemistry. Clear foci of infection were visible in the liver with no change in the abundance of 4-HNE protein conjugates (Figure 7). In the spleen, however, the bacteria were diffusely distributed throughout the organ and the entire spleen of the infected mouse exhibited increased staining for 4-HNE protein conjugates (Figure 8A-D).

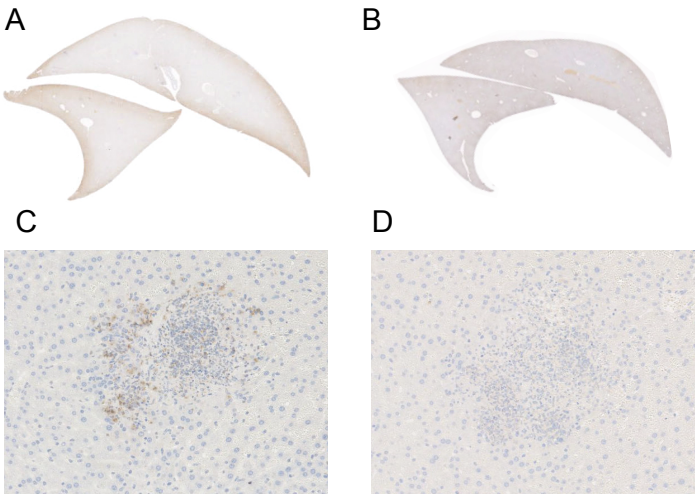

Figure 7. There is no significant 4-HNE adduct accumulation in the murine liver. At 48 hours post infection with GFP+ *L. monocytogenes* the murine liver immunohistochemistry analysis shows no accumulation of anti-4-HNE signal in either **(A)** infected or **(B)** uninfected livers. At 10x magnification there are **(C)** clear foci of GFP reactivity in the infected liver, indicating *L. monocytogenes* presence, but still **(D)** no visible anti-4-HNE signal**.**

The grossly different observations between the liver and spleen were somewhat surprising given our previous observation that infection of murine hepatocytes with *L. monocytogenes in vitro* induced accumulation of 4-HNE conjugates. These observations are likely a consequence of several factors. The liver is a major site of small molecule detoxification and hepatocytes are known to produce high levels of many of the 4-HNE metabolizing proteins, including aldo-keto reductases, alcohol dehydrogenase, and the 4-HNE glutathione transferase, GSTA4[118]. Additionally, the immune driven mobilization of arachidonic acid and ROS precursors that lead to 4-HNE generation may result in elevated accumulation of this host aldehyde in the spleen.

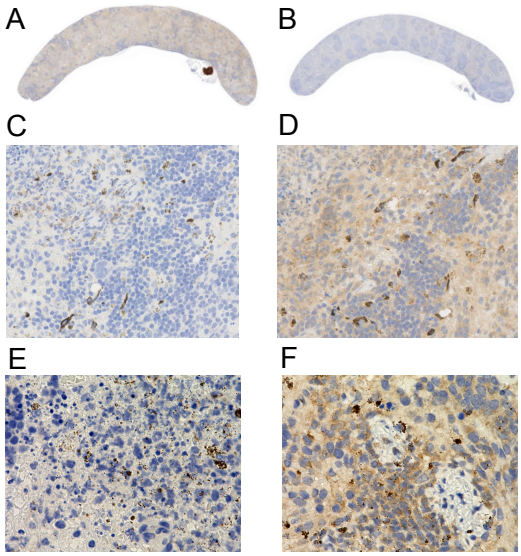

Figure 8. 4-HNE accumulates in the spleen during murine *L. monocytogenes* infection. At 48 hours post infection with GFP+ *L. monocytogenes* anti-4-HNE signal is readily apparent. **(A)** infected spleen anti-4-HNE **(B)** spleen uninfected anti-4-HNE **(C)** infected spleen anti-GFP 25x magnification **(D)** infected spleen anti-4-HNE 25x magnification **(E)** infected spleen anti-GFP 100x magnification **(F)** infected spleen anti-4-HNE 100x magnification.

At higher levels of magnification, we observed that 4-HNE conjugates were not evenly distributed among all cells. The majority of cells exhibited diffuse and constant staining and a subset showed very dark and robust staining for 4-HNE conjugates. At 100x magnification, the most pronounced signal for 4-HNE conjugates had punctate staining resembling the staining of the bacteria with anti-GFP antibody (Figure 8E-F), consistent with 4-HNE conjugate formation on the bacteria. While these observations do not provide quantitative measures of 4-HNE levels, they establish that 4-HNE was indeed elevated following bacterial infection and suggest that bacteria encounter and may be directly chemically modified by this metabolite during infection.

2.2.2: 4-HNE causes damage through the targeting of nucleophilic protein moieties and *L. monocytogenes* is uniquely resistant to 4-HNE-mediated death.

Electrophilic stress due to 4-HNE conjugation to proteins causes eukaryotic cells to undergo apoptosis following intermediate 4-HNE exposure (5-40μM) and necrosis at higher concentrations (40-100μM)[119]. However, due to 4-HNE's lipophilicity it is believed to accumulate

to significantly higher levels (0.3-5mM) near and within membranes than what is typically considered cytotoxic[120–122].

To characterize bacterial sensitivity to 4-HNE toxicity, we exposed a range of both Gram-positive and Gram-negative bacteria to a wide range of 4-HNE concentrations and assessed viability. We observed variability in survival, ranging from a 4-log reduction in CFU for *B. subtilis* and *Francisella novicida,* a 2-log reduction for *Staphylococcus aureus*, a log reduction for *E. coli,* a half-log reduction for *Enterococcus faecalis* to less than a 40% reduction for *L. monocytogenes* (Figure 9A) The variability in survival didn't appear to track with bacterial phylum or their pathogenicity styles, as *L. monocytogenes* and *F. novicida*, both intracellular pathogens, had markedly different survival capabilities in 4-HNE. The decimation of *F. novicida* by 4-HNE may be due to the fact that *F. novicida* is known to block the generation of ROS by NADPH oxidase[123,124], therefore preventing the generation of 4-HNE and eliminating the need to develop defense mechanisms against its toxicity.

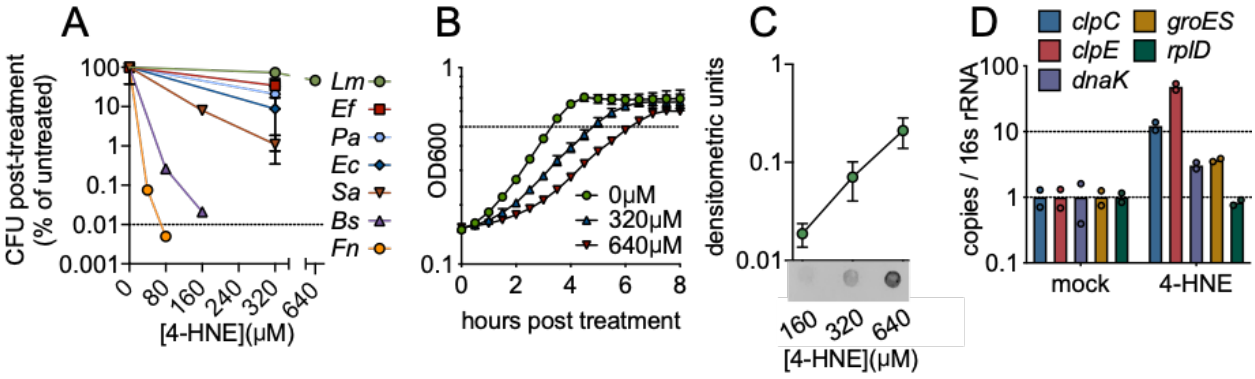

Figure 9. 4-HNE impacts bacterial viability, replication and damage to intracellular proteins. (A) survival of mid-log (0.4-0.8 OD600) *Listeria monocytogenes (Lm), Enterococcus faecalis (Ef), Pseudomonas aeruginosa (Pa), Escherichia coli (Ec), Staphylococcus aureus (Sa), Bacillus subtilis (Bs) and Francisella novicida (Fn)* exposed to 4-HNE in PBS for 1 hour at 37C. **(B)** growth of *L. monocytogenes* in TSB with various concentrations of 4-HNE added at time zero. **(C)** anti-4-HNE dot blot of soluble bacterial lysates from mid-log *L. monocytogenes* suspended in PBS and treated with increasing concentrations of 4-HNE. **(D)** qRT-PCR measurement of expression of indicated genes in mid-log *L. monocytogenes* in TSB treated with 640μM 4-HNE for 20 minutes. Expression normalized to 16S levels. Data in (A) and (B) are biological triplicate, (C) and (D) in biological duplicate. All are representative of at least two independent experiments.

We observed a dose dependent decrease in growth of *L. monocytogenes* with increased exposure to 4-HNE (Figure 9B). The significant resistance of *L. monocytogenes* to 4-HNE

exposure was unexpected. Due to the conserved nature of 4-HNE targets, we hypothesized that 4-HNE would exert similar damaging effects on bacteria as on eukaryotic cells. Thus, we first interrogated the ability of 4-HNE to generate protein adducts in *L. monocytogenes*. Dot blots of *L. monocytogenes* bacterial cell lysates indicated an increase in 4-HNE-protein adducts that correlated with increased 4-HNE exposure (Figure 9C), establishing that this aldehyde penetrates the bacterial cell envelope and impacts cytosolic proteins.

4-HNE adduct accumulation can result in protein misfolding and crosslink-induced aggregation. Eukaryotic cells clear 4-HNE damaged proteins through proteasome and autophagy-mediated pathways[125]. Bacteria target damaged proteins for degradation through the proteases that comprise the heat shock response[126]. This pathway is primarily transcriptionally regulated [127], so RT-qPCR was performed on a subset of heat shock genes representing two major groups of heat shock genes *in L. monocytogenes*: HrcA-regulated chaperones and CtsR-regulated proteases[128]. When *L. monocytogenes* was exposed to 640μM 4-HNE for 20 minutes, the four genes tested (*clpC, clpE, dnaK, groES*) were significantly induced compared to vehicle controls, while the control gene *rplD*, was unaffected (Figure 9D).

These data, combined with the dot blot results, support the hypothesis that 4-HNE causes protein damage to which *L. monocytogenes* mounts a heat shock response. The elevated induction of cellular proteases relative to chaperones may indicate that *L. monocytogenes* primarily combats electrophilic 4-HNE stress through turnover of damaged proteins rather than chaperone-mediated stabilization. Collectively, these observations suggest that despite formation of protein adducts and delayed growth following exposure, *L. monocytogenes* has a uniquely robust capacity to survive 4-HNE toxicity even among closely related organisms.

2.2.3: *L. monocytogenes* expresses 4-HNE detoxification enzymes that contribute to its survival in the presence of 4-HNE.

Our data suggest that *L. monocytogenes* is exposed to 4-HNE during infection and that only high concentrations of this aldehyde impact its growth. We hypothesized that *L. monocytogenes* may express genes involved in countering the cytotoxic effects of 4-HNE. To probe further, we performed global transcriptome analysis during 4-HNE exposure using RNA sequencing. Over one hundred genes were induced greater than 10-fold in response to 4-HNE exposure, including several of the heat shock genes previously identified by qRT-PCR analysis (Figure 10, Table 1).

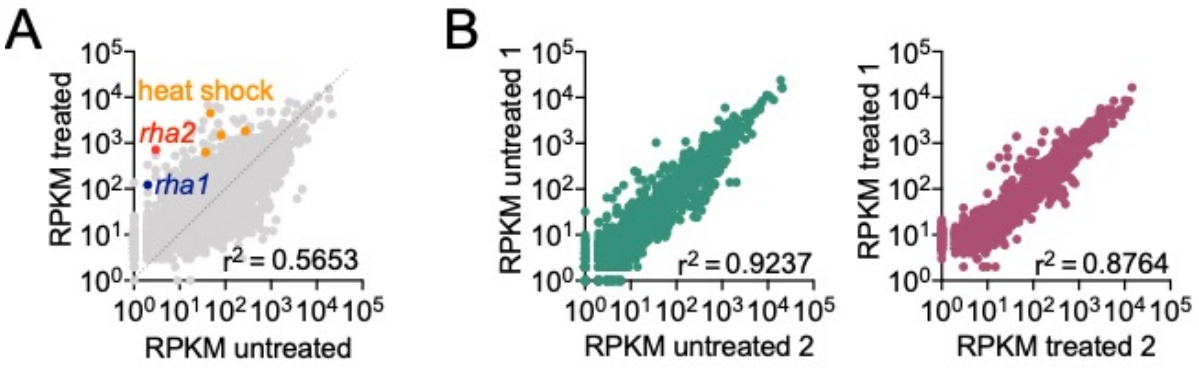

Figure 10. 4-HNE exposure induces a large transcriptional change in *L. monocytogenes.* (A) global gene expression of mid-log *L. monocytogenes* in TSB treated with 640μM 4-HNE or ethanol control for 20 minutes. Genes of interest *rha1*, *rha2* and heat shock are indicated in blue, red and orange, respectively. **(B)** comparison of the two biological replicates of untreated and treated samples between themselves as a control for data reproducibility. RPKM: reads per kilobase million

Eukaryotic cells utilize several reductases to detoxify 4-HNE[80]. Two reductases were highly induced in our global transcriptome, *lmo0103* and *lmo0613*, which we refer to as *rha1* and *rha2* (**r**eductase of **h**ost **a**lkenals 1 and 2), respectively. Phyre2 analysis of Rha1 predicted high structural homology to CLA-ER, a flavin-dependent enone reductase from *Lactococcus plantarum* (PDB: 4QLY)[129]. A Phyre2 analysis of Rha2 revealed structural similarity to a few crotonyl-CoA carboxylase/reductases (PDBs: 3KRT, 4Y0K, and 5A3J) and a plant chloroplast oxoene reductase (PDB: 5A3V), two enzymes with the capacity to reduce enone-containing lipophilic substrates. Given the predicted reductase activity of Rha1 and Rha2 and their structural similarity to proteins that metabolize enone-containing compounds, we further investigated their role in 4-HNE resistance.

Induction of *rha1* and *rha2* in response to 4-HNE exposure was found to be 34 and 90-fold, respectively, by RT-qPCR. To assess the specificity of their induction, we exposed *L. monocytogenes* to a sublethal concentration of a panel of aldehydes including 4-HNE; 4-HHE (4-hydroxy-2-hexenal), a similar but shorter chain αβ-unsaturated aldehyde produced from the oxidation of ω-3 fatty acids [130]; methylglyoxal, a reactive byproduct of glycolysis; propionaldehyde, an alpha hydrogen aldehyde; and malondialdehyde, another product of lipid peroxidation[121] (Figure 11A-B). Both *rha1* and *rha2* were most strongly induced by 4-HNE exposure, with much less induction by 4-HHE and negligible induction with the other tested compounds (Figure 11C).

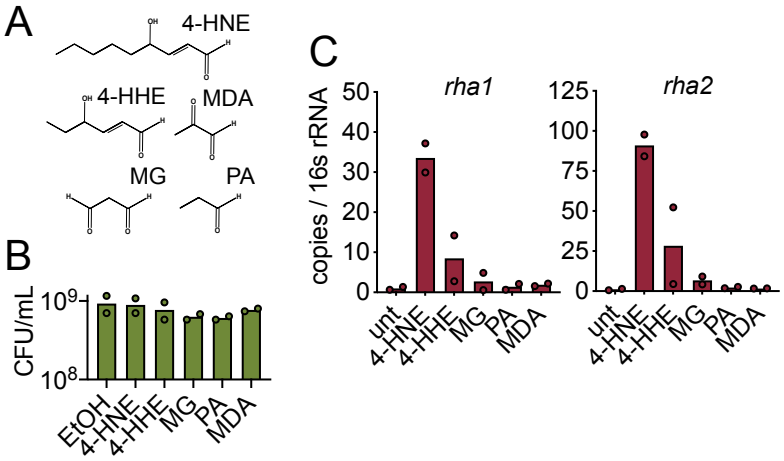

Figure 11. 4-HNE specifically induces *rha1* and *rha2* expression. (A) panel of aldehydes used for expression assessment: 4-HNE (4-hydroxynonenal), 4-HHE (4-hydroxyhexanal), MDA (malonaldehyde), MG (methylglyoxal) and PA (propionaldehyde). **(B)** CFU post treatment in TSB media for 20 minutes with 500μM of the indicated aldehydes or mock (ethanol). There was no survival differences between mock and treatment. **(C)** qRT-PCR analysis of expression of *rha1* and *rha2* after treatment with 500μM of the indicated aldehyde for 20 minutes. Experiments in biological duplicate and representative of at least two independent experiments.

We next assessed if these genes are induced by *L. monocytogenes* during intracellular infection. At 6 hours post-infection of macrophages, we found that there was significant induction of both genes compared to growth in BHI broth (Figure 12). Together these transcriptional studies suggested that the *rha1/2* genes are not components of a general aldehyde response but rather specific responses to 4-HNE encountered during infection.

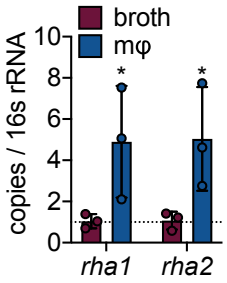

Figure 12. *rha1* and *rha2* expression is induced during intracellular infection. At 6 hours post infection in J774 macrophages (mϕ) there is significant induction of both *rha1* and *rha2* in intracellular *L. monocytogenes* compared to control broth-grown bacteria. Statistics are an unpaired t-test between ΔΔCt values of broth samples versus intracellular samples. Error bars are +/- SD. *, $p < 0.05$.

These intriguing transcriptional results suggested that *rha1* and *rha2* may function in 4-HNE resistance. Individual and double mutants of these genes were generated and assessed by competition experiments for survival relative to WT *L. monocytogenes* following 4-HNE exposure. Control mixtures left untreated in PBS exhibited no significant difference between mutant and control strains (Figure 13A).

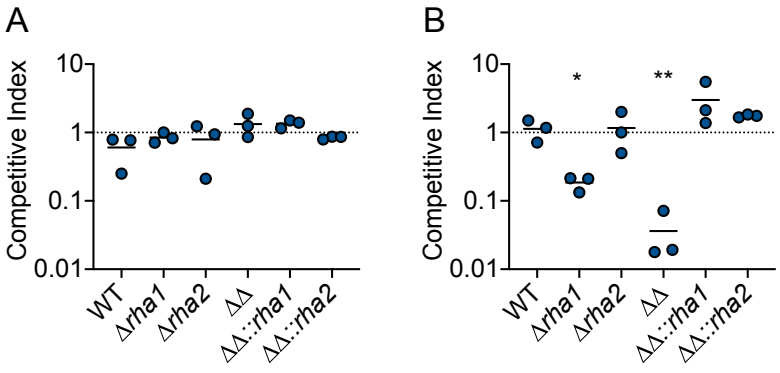

Figure 13. Competitions of WT versus mutant *L. monocytogenes* in 4-HNE. A 1:1 ratio of WT and the mutant strain resuspended in PBS and **(A)** left untreated an **(B)** treated with 640μM 4-HNE for an hour at 37C. Statistics are unpaired t-tests between WT and mutant *L. monocytogenes* competition pairs. Error bars are +/- SD. *, $p < 0.05$; **, $p < 0.01$.

Among mixtures exposed to 640 μM 4-HNE, unmarked WT and marked WT showed no significant difference in 4-HNE survival. Loss of *rha2* had no effect on 4-HNE survival while Δ*rha1* had a modest 5-fold reduction relative to WT. However, the *Δrha1Δrha2* mutant exhibited a 50-fold competitive defect compared to WT *L. monocytogenes* that was rescued by either *rha1* or

rha2 expression in *trans*, demonstrating that both genes must be absent for the toxic effect to manifest (Figure 13B).

The WT, *Δrha1Δrha2, Δrha1Δrha2::rha1* and *Δrha1Δrha2::rha2* strains were also assessed for relative 4-HNE adduct accumulation by dot blot. We found that at 3 hours post exposure in TSB media there was a significant 2-fold increase in 4-HNE adduct accumulation in the *Δrha1Δrha2 L. monocytogenes* compared to WT (Figure 14).

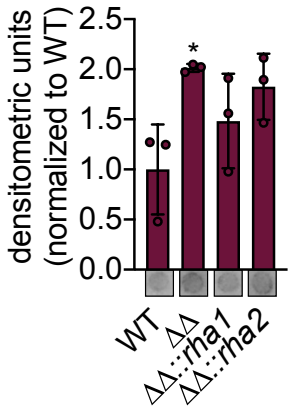

Figure 14. 4-HNE protein adduct accumulation is increased in *Δrha1Δrha2 L. monocytogenes.*
Bacteria were normalized in TSB by OD and treated with 640μM 4-HNE for 3 hours at 37C, then blotted for anti-4-HNE protein adducts. Statistics are an ordinary one-way ANOVA of WT versus the mutants. Error bars are +/- SD. *, $p < 0.05$.

Interestingly, although there was a modest reduction in adduct levels in both complement strains, neither fully restored WT levels of adduct formation, even though either *rha1* or *rha2* complementation fully restored survival in our competition experiment. This may suggest that perhaps there is a very narrow range “tipping point” concentration of 4-HNE that leads to death that isn’t necessarily reflected in crude adduct accumulation measurements. We also assessed total aggregation levels of WT L. monocytogenes and *Δrha1Δrha2* when exposed to 4-HNE. We found that in WT *L. monocytogenes* 4-HNE does not lead to significant protein aggregation compared to untreated control, especially compared to the positive control of a 10-minute 56C

heat shock (Figure 15). In addition, the *Δrha1Δrha2* mutant does appear to have only a modest (10-15%) and not statistically significant increase in protein aggregation accumulation with 4-HNE treatment compared to WT. This suggests that the difference in WT versus *Δrha1Δrha2* survival in 4-HNE is probably not primarily driven by protein aggregation but rather more likely by the extensive carbonylation in the double mutant compared to WT *L. monocytogenes*, in addition to other potential unexplored 4-HNE-mediated damage.

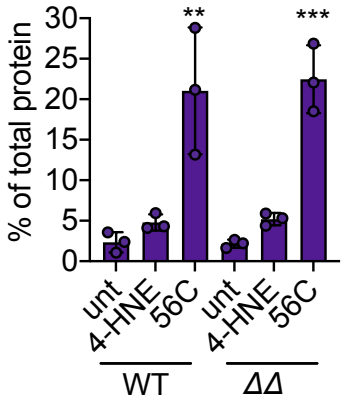

Figure 15. **4-HNE does not lead to significant protein aggregation in *L. monocytogenes.*** WT and Δ*rha1*Δ*rha2 L. monocytogenes* were untreated, treated with 4-HNE for 1 hour at 37C, or heat-shocked at 56C for 10 minutes. Statistics are an ordinary one-way ANOVA of untreated versus the treated samples. Error bars are +/- SD. **, $p < 0.01$; ***, $p < 0.001$.

We then transitioned to *in vivo* and tissue culture analyses of the *Δrha1Δrha2* strain. *Δrha1Δrha2 L. monocytogenes* was used to infect macrophages and mice. During cellular infection, we observed a ~50% reduction in CFU at 2 hours post-infection (Figure 16A), which rebounded to WT levels at later time points. In mice infected via intravenous injection no significant phenotype was observed at 48 hours post infection in either the spleen or the liver (Figure 16B).

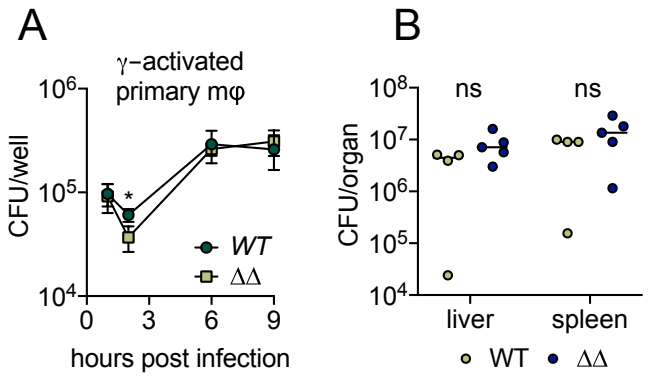

Figure 16. Δ*rha1*Δ*rha2 L. monocytogenes* lacks a robust infection phenotype. (**A)** primary γ-activated primary mϕ infected with WT and Δ*rha1*Δ*rha2 L. monocytogenes*. There is a modest CFU reduction at 2 hours post infection of the Δ*rha1*Δ*rha2* mutant compared to WT *L. monocytogenes*. **(B)** 48-hour intravenous murine infection with WT and Δ*rha1*Δ*rha2 L. monocytogenes*. There is no significant difference between the WT and mutant. Statistics are unpaired t-tests comparing WT and Δ*rha1*Δ*rha2*. Error bars are +/- SD. *, $p < 0.05$.

Overall, the findings presented here provide evidence that Rha1 and Rha2 are specific and important for 4-HNE resistance, though other factors likely contribute to *L. monocytogenes* capacity to counteract this metabolite *in vivo*.

2.2.4: Recombinant Rha1 and Rha2 metabolize 4-HNE to 4-HNA

In order to determine if these putative enone reductases can directly utilize 4-HNE as a substrate, we generated recombinant Rha1 and Rha2 proteins. As controls for these studies, we generated catalytically dead variants of the two proteins by mutating amino acids predicted to be involved in flavin binding by Rha1 (asparagine-47) and NADPH coordination by Rha2 (tyrosine-195) to alanine (Figure 17).

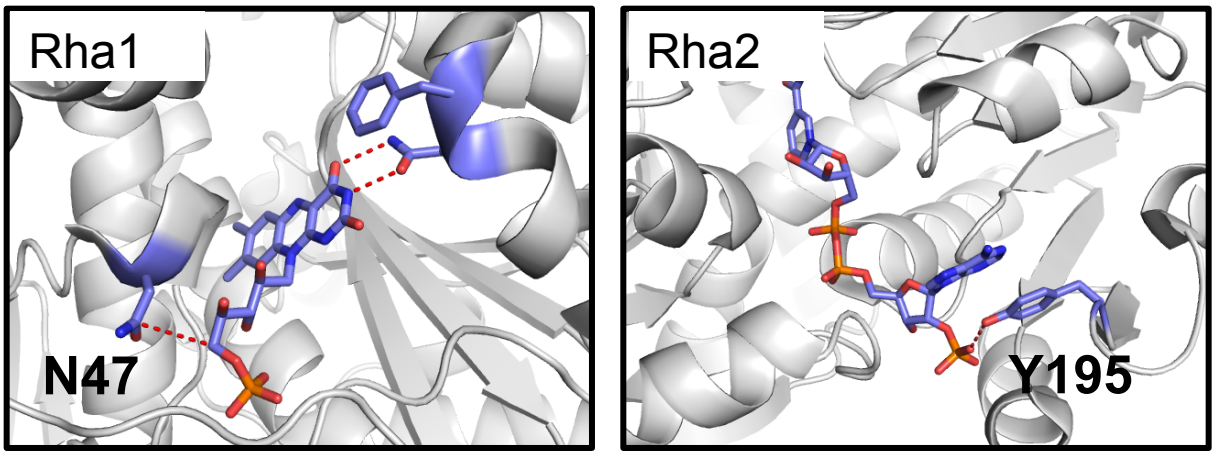

Figure 17. Homology predictions of active sites of Rha1 and Rha2. Phyre2 structural homology predicted structures that model that **(A)** the asparagine-47 coordinates the FMN in Rha1 and **(B)** tyrosine-195 coordinates NADPH in Rha2. Mutating both residues to alanine should effectively abrogate activity of both enzymes.

All proteins were expressed and characterized for NADPH oxidation in the presence and absence of 4-HNE. Only the WT variants of Rha1 and Rha2 exhibited NADPH oxidation upon addition of 4-HNE (Figure 18A), consistent with their capacity to mediate NADPH dependent reduction. We then measured NADPH oxidation of Rha1 and Rha2 using the aldehyde panel we previously used for our expression specificity analysis (Figure 11A). We found that both Rha1 and Rha2 showed the most robust NADPH oxidation in the presence of 4-HNE, although Rha2 in particular showed modest but non-negligible NADPH oxidation with 4-HHE, perhaps suggesting a wider substrate range for Rha2 than Rha1 (Figure 18B).

Finally, we wanted to determine what product or products Rha1 and Rha2 reduce 4-HNE into. Generally, NADPH-dependent 4-HNE reduction can occur at either the carbon-carbon double bond, generating the saturated aldehyde 4-hydroxynonanal (4-HNA), or on the carboxyl aldehyde moiety, generating the alcohol 1,4-dihydroxynonene (1,4-DHN)[131]. To elucidate which of these two products Rha1 and Rha2 may be generating, we performed thin-layer chromatography (TLC) on their enzymatic products. We concurrently ran a set of positive controls for either 1,4-DHN or 4-HNA generation, using the human enzyme AKR1C1 as the positive control for 1,4-DHN production[132] and the *Arabidopsis thaliana* enzyme P1-ZCr as the positive control for

4-HNA[74]. We also chemically generated 1,4-DHN as an additional control. We found that after one-hour incubation at room temperature, both Rha1 and Rha2 converted a fraction of 4-HNE to 4-HNA in a NADPH-dependent manner (Figure 18C-D), conclusively proving that both enzymes have the capability to directly detoxify free 4-HNE to 4-HNA (Figure 18E).

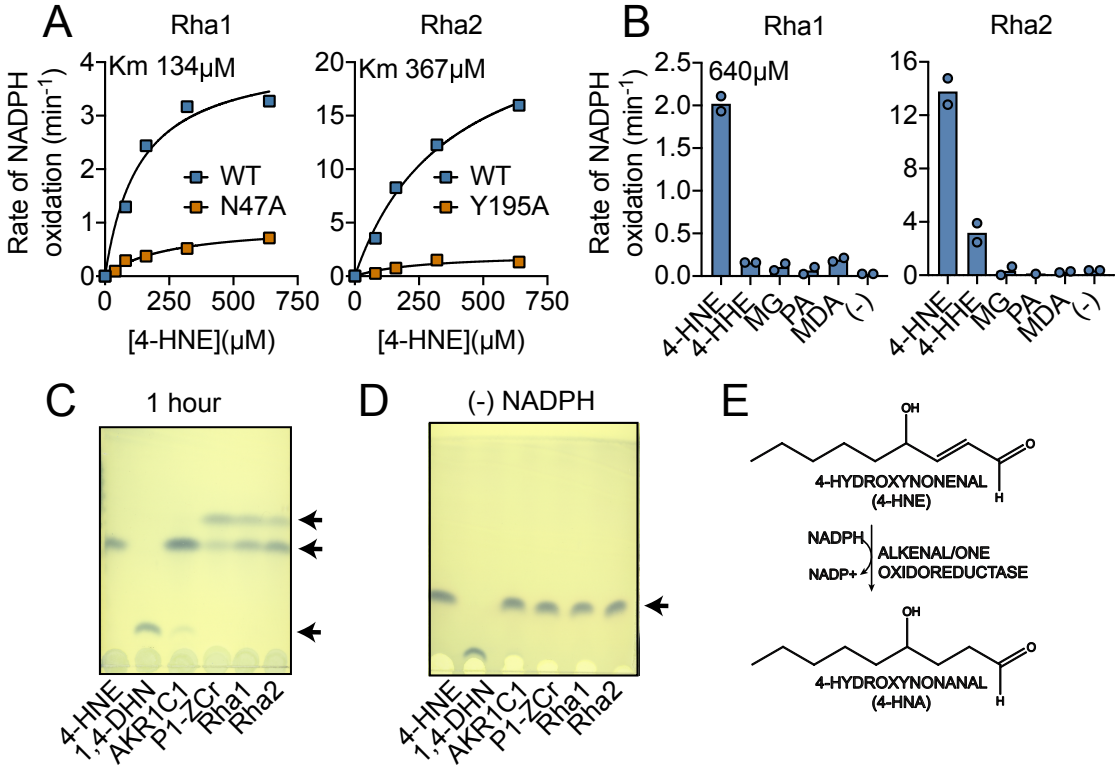

Figure 18. *In vitro* characterization of Rha1 and Rha2 functionality. (A) Rates of NADPH oxidation (200μM) by WT (blue) and mutant (orange) variants of Rha1 and Rha2 in the presence of 4-HNE **(B)** NADPH oxidation rate by Rha1 and Rha2 in the presence of various aldehydes **(C)** TLC plate showing the generation of a product above 4-HNE in the Rha1, Rha2 and P1-ZCr lanes after 1 hour of reaction at room temperature, which is predicted to be 4-HNA. There is also the chemically generated 1,4-DHN control as well as AKR1C1 **(D)** TLC plate showing no product generation by any of the enzyme panel in the absence of NADPH, confirming that the products shown in panel C are enzymatically derived **(E)** schematic of the reduction reaction of 4-HNE to 4-HNA.

2.2.5: Ectopic expression of *rha1* and *rha2* confers 4-HNE resistance to the sensitive bacteria *B. subtilis*.

Based on our recombinant protein data, we hypothesized that Rha1 and Rha2 could confer 4-HNE resistance to a sensitive organism. To this end, each gene and corresponding catalytically dead variant were expressed individually and in combination in *B. subtilis*, which

exhibited 300-fold more sensitivity than *L. monocytogenes* upon 4-HNE exposure (Figure 9A). Consistent with our observations of the *L. monocytogenes rha* deletion mutants, expression of *rha2* in *B. subtilis* had no effect on growth in the presence of 4-HNE, *rha1* gave modest protection against 640μM 4-HNE, and expression of both *rha1* and *rha2* had the largest growth rescue, reducing lag time by up to 3 hours (Figure 19).

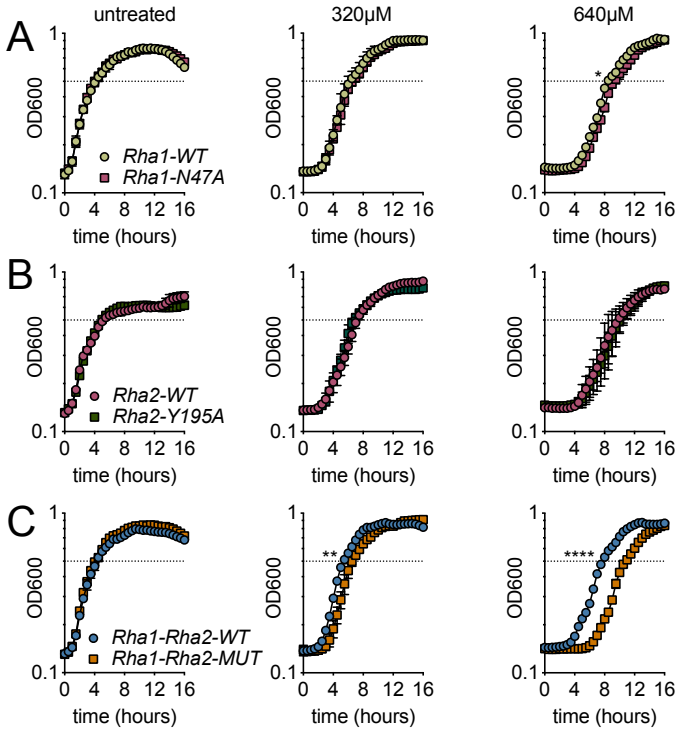

Figure 19. Expressing both of the functional *rha1* and *rha2* forms in *B. subtilis* enhances growth in 4-HNE. *B. subtilis* expressing either the functional or catalytically dead versions of *rha1* and *rha2* grown in the presence of 0, 320 and 640μM 4-HNE**. (A)** *B. subtilis* expressing rha1 WT and N47A (catalytically dead) **(B)** *B. subtilis* expressing rha2 WT and Y195A (catalytically dead) **(C)** *B. subtilis* expressing both rha1 and rha2 WT and rha1 and rha2 MUT (catalytically dead). Statistics are unpaired t-tests comparing WT and dead enzyme time-to-OD 0.5. Error bars are +/- SD. *, $p < 0.05$; **, $p < 0.01$; ****, $p < 0.0001$.

We then focused on *B. subtilis* expressing both *rha1* and *rha2* genes, as this strain had the most robust phenotype. When assessed for bacterial survival following 4-HNE treatment, *B. subtilis* expressing the functional enzymes exhibited nearly a 2-log survival advantage relative to the control strain expressing enzymatically dead *rha1/2* (Figure 20A). Additionally, soluble cellular fractions from *B. subtilis* exposed to 4-HNE and probed for 4-HNE protein adducts by dot blot

revealed a ~70% reduction in 4-HNE conjugates in the *B. subtilis* strain expressing both of the active *rha1* and *rha2* genes versus their catalytically dead counterparts (Figure 20B).

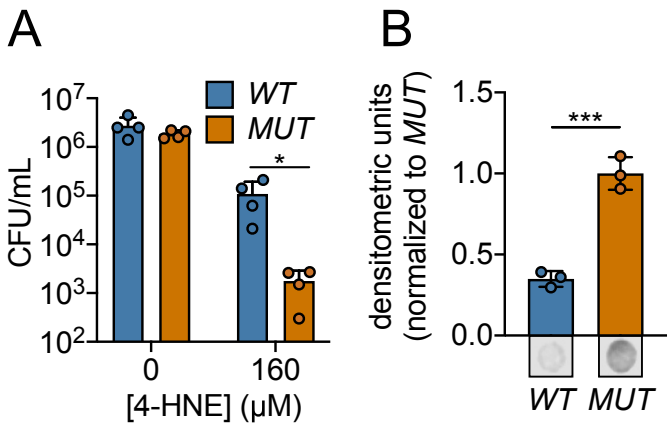

Figure 20. Expressing *rha1/2* WT in *B. subtilis* aids in the bacterium's survival in 4-HNE. (A) B. subtilis expressing rha1/2 WT and MUT treated for 1 hour with 160μM 4-HNE and plated for CFU (B) B. subtilis expressing rha1/2WT and MUT treated with 640μM 4-HNE in TSB for 3 hours and then assessed for 4-HNE adduct formation.

To determine if 4-HNE resistance conferred by *rha1/2* could contribute to bacterial survival within mammalian cells, *B. subtilis rha1/2* strains were assessed for viability following phagocytosis by primary bone marrow-derived macrophages. We found that *B. subtilis* expressing the active forms of Rha1 and Rha2 maintained a significantly higher CFU over the course of eight hours than the *B. subtilis* expressing the catalytically dead form (Figure 21A). To determine whether this survival advantage was due to 4-HNE resistance, we measured *B. subtilis* survival within bone marrow-derived macrophages from *gp91$^{phox-/-}$* mice deficient in oxidase cytochrome b-245, which are unable to produce the reactive oxygen burst and therefore 4-HNE[121]. Consistent with the role of *rha1* and *rha2* in resistance to a ROS-derived factor, the protective effect of WT *rha1/2* expression was eliminated in the absence of *gp91^{phox}* (Figure 21B). Together, these observations revealed that expression of *rha1* and *rha2* in *B. subtilis* imparts resistance to 4-HNE toxicity and impacts bacterial survival in the host cell's ROS burst.

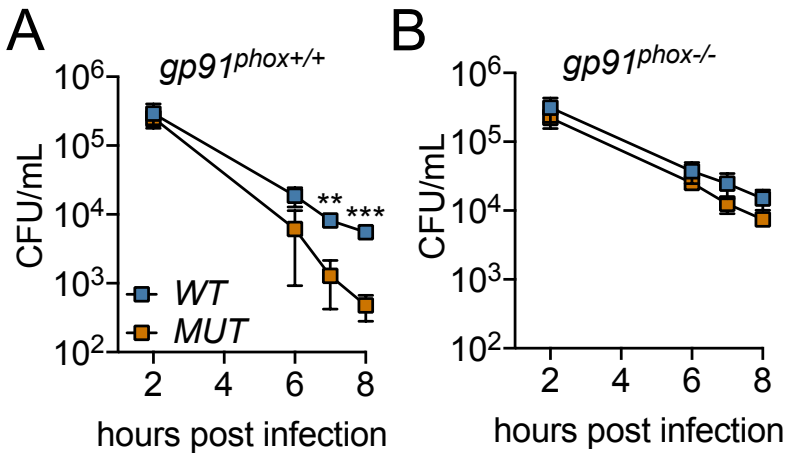

Figure 21. Ectopic expression of *rha1/2* in *B. subtilis* confers a PHOX-dependent survival advantage in primary bone marrow macrophages. (A) *B. subtilis* expressing either WT *rha1/2* or MUT *rha1/2* were added to gamma activated WT primary murine bone marrow macrophages. CFU was assessed at 2, 6, 7 and 8 hours post infection. **(B)** *B. subtilis* expressing WT and MUT *rha1/2* added to gamma activated *gp91*$^{phox-/-}$ murine macrophages.

2.3: Discussion

In this study, we provide evidence that ROS-derived metabolite 4-HNE accumulates during *L. monocytogenes* infection both in tissue culture and in mice. We also show that 4-HNE exhibits antimicrobial effects on several bacterial species and that in the highly resistant intracellular pathogen *L. monocytogenes*, exposure to this aldehyde induces a specific and robust transcriptional profile. Among the highest induced genes are components of the heat shock response, consistent with aldehyde induced protein damage, a known effect of 4-HNE exposure. In addition, two genes, *rha1* and *rha2* are highly and specifically induced by 4-HNE exposure, and these two enzymes reduce 4-HNE to 4-HNA in an NADPH-dependent manner *in vitro*. Disruption of *rha1* and *rha2* in *L. monocytogenes* results in a decrease in viability in the presence of 4-HNE, and heterologous expression of *rha1* and *rha2* in *B. subtilis* conferred increased tolerance to 4-HNE toxicity in this non-pathogenic and 4-HNE-sensitive organism. Rha1 and Rha2 expression in *B. subtilis* also allowed for greater survival following phagocytosis by bone marrow derived macrophages in a manner entirely dependent upon phagocyte ROS generation. Together this work supports the conclusion that 4-HNE represents one of the individual molecular components

of ROS-mediated host defense through its direct antimicrobial effects on bacteria and that pathogens have likely evolved complex mechanisms of surviving its encounter within eukaryotic hosts (Figure 22).

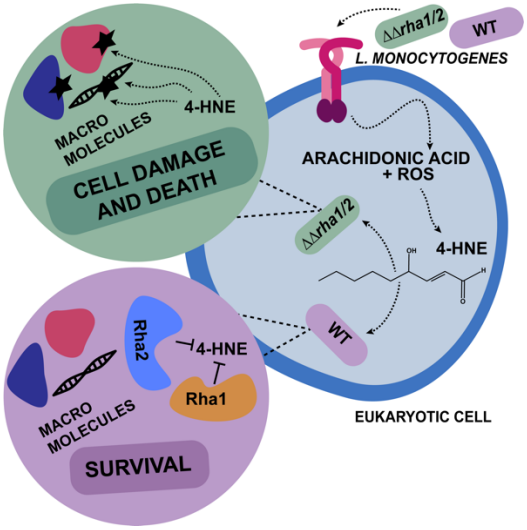

Figure 22. Model or *rha1/2* mediated resistance in *L. monocytogenes*.

There are many parallels between the chemical and biological functions of 4-HNE and other toxic metabolites that function in antimicrobial defense. The freely diffusible and highly reactive diatomic gas nitric oxide (NO) is produced during infection[133,134] and has a direct role in preventing bacterial growth[135]. However, due to the conservation of its reactive targets, elevated levels of NO also exert pathological effects during both sterile inflammation and acute infections[136,137]. 4-HNE is membrane diffusible, highly reactive, and contributes to disease pathology due to its cytotoxic activity toward eukaryotic cells. These parallels, together with our findings that bacterial infection induces 4-HNE production are consistent with the premise that 4-HNE represents a component of ROS-mediated host defense, among such other toxic metabolites as superoxide, hydrogen peroxide, and hypochlorite.

While a role for 4-HNE in host antimicrobial defense has yet to be appreciated in mammals, plants utilize a variety of lipophilic molecules generated by the oxidation of polyunsaturated fatty acids (PUFAs), collectively referred to as oxylipins. While generally

considered to be involved in signal transduction, many oxylipins can directly inhibit bacterial growth[138] and 4-HNE itself is a component of the oxylipin burst in soybean where it serves an anti-fungal function[139]. Because 4-HNE is one of several distinct metabolites produced following oxidation of PUFAs in mammals, it is conceivable that other reactive byproducts of this process also contribute to microbial defense in a similar manner.

To survive within the sterile tissues of eukaryotic hosts, bacterial pathogens often counteract the toxic effects of the immune response. Our discovery of two genes that confer synergistic resistance to 4-HNE in *L. monocytogenes* begin to provide insight into the mechanisms by which 4-HNE toxicity might be overcome. Our in vitro protein studies demonstrated that Rha1 and Rha2 both metabolize 4-HNE to 4-HNA, meaning that enzymatically, they have redundant function. Redundancy in bacterial resistance to ROS is a relatively common phenomenon, including the need to eliminate five individual enzymes in *Salmonella enterica* Serovar Typhimurium to exhibit a phenotype in the presence of hydrogen peroxide[140] and simultaneous disruption of four enzymes in *Bacillus anthracis* to observe a phenotype in the presence of superoxide[141]. Such redundancy in bacterial detoxification programs likely decreases the chances that genetic drift or other genomic damage would render an organism defenseless against oxidative stress. It is also possible that there are subcellular localization differences between Rha1 and Rha2, leading to the requirement of both proteins for robust 4-HNE detoxification.

While Rha1 and Rha2 both contribute to 4-HNE resistance, the *Δrha1Δrha2 L. monocytogenes* strain still exhibits several logs of survival benefit relative to the related organism *B. subtilis*, suggesting that other mechanisms of 4-HNE resistance remain to be identified. Among the many uncharacterized genes induced during 4-HNE exposure, *lmo0796* shows homology to *bcnA*, a secreted lipocalin in *Burkholderia cenocepacia* which sequesters long-chain lipophilic antibiotics[142]. 4-HNE, with its long hydrophobic tail, could conceivably be neutralized in an

analogous manner. It is possible many intrinsic resistance properties of *L. monocytogenes* are not reflected through transcriptional responses. For instance, addition of amine containing constituents on the cell's surface through lysinylation of teichoic acids and/or lipids, as well as deacetylation of peptidoglycan, may provide a nucleophile reactivity barrier that prevents 4-HNE entry into the bacterial cell. Additionally, αβ-unsaturated aldehydes have preferential reactivity toward sulfhydryl groups, including cysteine and glutathione, and it is expected that thiolate depletion would be the major mechanism of 4-HNE toxicity[143]. Indeed, the thiol responsive transcription factor spxA1 was induced >2-fold in response to 4-HNE and the magnitude of heat shock gene induction mirrored results reported for *B. subtilis* following diamide treatment, a potent inducer of disulfide stress[144]. While our findings provide initial molecular insight into one pathogen's resistance to 4-HNE, it is clear that many details are yet to be revealed.

Taken together, our findings extend the range of antimicrobial molecules generated through the reactive oxygen burst to include the byproducts of lipid peroxidation. Additionally, bacteria whose infection cycles involve intimate exposure to these molecules, such as *L. monocytogenes*, have specific and finely regulated detoxification and protection programs against this toxicity. Future investigation of the impacts of 4-HNE on a diverse array of organisms with varied infection models will highlight the importance of this metabolite on host defense and the varied mechanisms by which pathogens counteract its toxicity to promote infection.

2.4: Postscript -- candidate genes with no obvious roles in 4-HNE resistance

Although we were able to conclusively demonstrate that two of our 4-HNE treatment global transcriptional analysis top hits, *rha1* and *rha2*, play a direct role in 4-HNE resistance and detoxification, many of the other genes we had selected for follow-up did not appear to have any role in 4-HNE resistance.

The first such gene was *lmo2829*, annotated as a putative nitroreductase, or an enzyme capable of reducing double bonds. It was specifically and robustly induced by 4-HNE treatment

(Figure 23). However, purified enzyme showed no discernable activity against 4-HNE and the genetic disruption of *lmo2829* showed no phenotype.

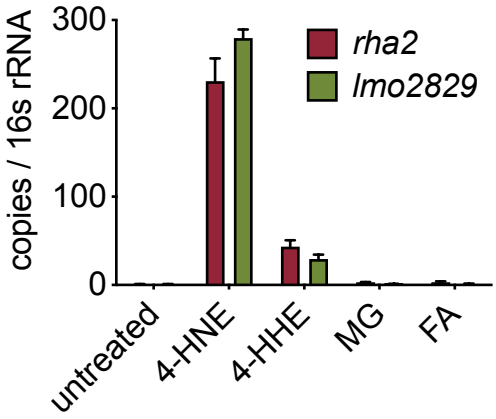

Figure 23. Gene expression of *lmo2829* and positive control *rha2* during treatment with various aldehydes. L. monocytogenes treated for 20 minutes in TSB with 500μM of 4-HNE, 4-HHE, methylglyoxal (MG) or formaldehyde (FA) and assessed for gene expression by qRT-PCR.

Two other promising genes were *lmo0880* and *lmo0646*. These genes encode, respectively, for a putative sortase-anchored LPXTG motif protein and a putative glyoxalase, and were robustly induced by 4-HNE treatment (*lmo0880*: 137-fold; *lmo0646*: 61.5-fold by RNA-seq). We hypothesized that Lmo0880 could interact with 4-HNE outside the cell, while Lmo0646 might be performing direct 4-HNE detoxification through a glyoxalase-like pathway[145]. However, neither disruption had any effect on *L. monocytogenes* survival in 4-HNE, nullifying both hypotheses.

Overall, although we were able to untangle a very small part of the *L. monocytogenes* 4-HNE resistance with our discovery and characterization of *rha1* and *rha2*, there were multiple false starts and fruitless pursuits, underscoring both the immense strength and inherent weaknesses of large non-biased datasets such as RNA-seq.

Chapter 3: Tn-seq development in *L. monocytogenes* and potential applications for the study of 4-HNE resistance.

3.1: Introduction

3.1.1: The potential utility of Tn-seq for understanding *L. monocytogenes* physiology

As discussed in Chapter 1, *L. monocytogenes* is an important model organism for the study of virulence, and many discoveries in pathogenesis have been made using *L. monocytogenes*. Therefore, it is crucial to study the basic physiology of *L. monocytogenes*, as it would enhance our understanding of any downstream discoveries of its virulence and pathogenesis mechanisms. To this end, one of the basic things that is important to know about *L. monocytogenes* is its suite of essential genes. The fastest, most high-throughput and least biased way to accomplish this is through the generation of a saturated library of transposons in wild-type *L. monocytogenes* and performing transposon sequencing (Tn-seq) to determine which genes are indispensable for bacterial survival. In the next section we will cover the development of bacterial Tn-seq, what Tn-seq methodology entails and what kind of information can be gleaned from the generated data.

3.1.2: Introduction to TnSeq

Tn-seq was invented in 2009 and initially used to determine the essential genes in the bacterium *Streptococcus pneumoniae*[146]. The principle behind the methodology is to determine which genes in a bacterium are essential for survival in a given condition by comparing the genetic fitness of a pool of different mutants. Each mutant has a single unique transposon insertion, making it possible to sequence out from within the transposon to determine the genomic locus of the insertion. When this sequencing is performed using massively parallel methods on highly saturated mutant pools (meaning each gene has multiples of unique insertions, helping to prevent

false signals in the data), it generates a detailed map of transposon locations within the genome. Finally, these data can be analyzed to determine what genes are selected for or against in any given treatment condition (Figure 24).

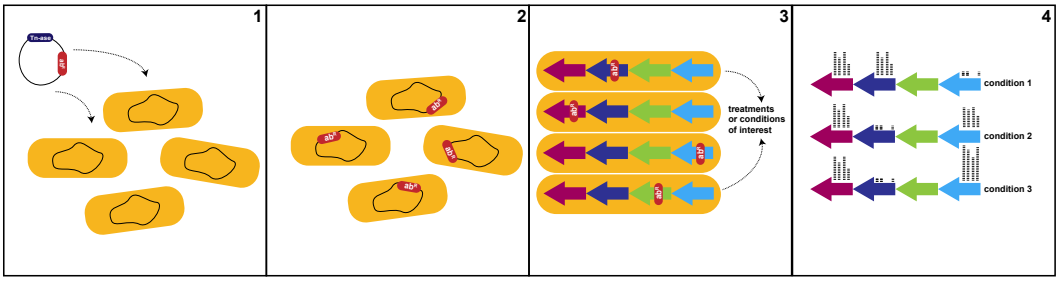

Figure 24. Tn-seq workflow schematic. 1 – plasmid carrying a transposase and antibiotic selection-containing transposon is transformed into bacteria. 2 – the transposon is randomly inserted throughout the bacterial genome by the transposase. 3 – the pool of transposon mutants is exposed to a treatment and/or growth condition of interest. 4 – the pool is sequenced and the location of all the transposons is mapped. These data *are* then used to determine what genes are deleterious, beneficial or neutral in any given treatment or condition.

Since its invention over a decade ago, Tn-seq has been used with great success to understand the genetic landscape of many different bacteria in a variety of conditions, including determining the essential genes in *Mycobacterium tuberculosis*[147], understanding the mechanism of host glutathione utilization in *Francisella tularensis*[148] and dissecting the contribution of carbohydrate utilization to murine infection of *Borrelia burgdorferi*[149], among many others.

Overall, Tn-seq is a powerful technique that allows researchers to get a broad systemic view of the genomic landscape of any given bacteria amenable to transposon mutagenesis. In the following section, I present the results of my Tn-seq experiment to better understand the landscape of essential genes in *L. monocytogenes*.

3.2: Results

3.2.1: The *L. monocytogenes* genome is 7% essential genes

To determine which genes in *L. monocytogenes* are essential for the bacteria's survival

we generated a saturated (150,000 individual insertions) transposon library in the WT 10403s *L. monocytogenes* background. Once generated, we sequenced our library using an Illumina HiSeq and analyzed the data for essentiality using TnSeq Explorer[150]. We found that using our stringent cutoff for essentiality (Essentiality Index average between two biological replicates equal to or less than 1) that 214 genes in the *L. monocytogenes* genome were deemed essential for survival (Table 2). As *L. monocytogenes* 10403s has 2,979 genes total, this makes roughly 7% of the genome essential[151]. This is in line with other bacterial essentiality analyses, with the *Bacillus subtilis* 168 genome encoding roughly 7% essential or indispensable genes[152], the *E. coli* K-12 genome encoding about 8% essential genes[153], and *Pseudomonas aeruginosa* genome being about 6.6% essential genes[154].

Most of the genes we found to be essential in *L. monocytogenes* were unsurprising, including proteins encoding tRNA synthetases, proteins involved in DNA replication and chromosome condensation, ribosomal proteins, translation and transcription factors, protein quality control proteins, cell wall synthesis proteins, cell division machinery, nucleotide biosynthesis enzymes, cofactor synthesis enzymes, metal ion transport channels and iron-sulfur cluster biosynthesis proteins.

To get a better idea of any uniquely Listerial essential genes, we cross referenced the *B. subtilis* essential genome with our *L. monocytogenes* essential genes, as *B. subtilis* is a close relative of *L. monocytogenes* but its genome and essential genes are significantly better studied. We found, unsurprisingly, that the majority of genes overlapped -- 156 genes in total were essential in both bacteria, roughly two-thirds of all essential genes in both organisms (Figure 25). These overlapping genes mostly coded for the widely known essential factors listed above. However, 58 genes were essential in *L. monocytogenes* but not in *B. subtilis* and 97 were essential in *B. subtilis* but not *L. monocytogenes*. We decided to focus on the 58 *L. monocytogenes*-specific essential genes and explore a few further, to perhaps aid in deepening our understanding of *L. monocytogenes* physiology and metabolism.

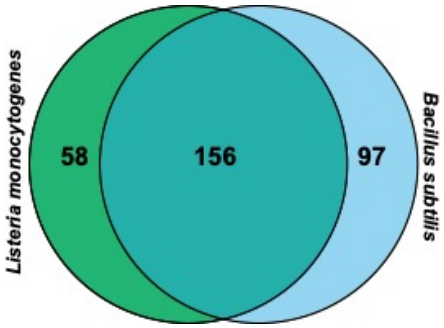

Figure 25. Essential genes that overlap between *B. subtilis* and *L. monocytogenes*.

3.2.2: Overview of the *L. monocytogenes* essential genes

When we looked more closely at essential genes in *L. monocytogenes* that did not overlap with *B. subtilis* essential genes, we found some expected genes, such as the *dacA* (*lmo2120*) cyclic di-AMP synthase, which is essential in *L. monocytogenes* because it is the only enzyme for synthesizing this essential second messenger present in the *L. monocytogenes* genome, while *B. subtilis* encodes three cyclic di-AMP synthesizing enzymes, preventing their detection in an essential gene panel[155]. Another easily explained difference between *L. monocytogenes* and *B. subtilis* was the essentiality of components of the mevalonate pathway (*lmo0010-lmo0012, lmo1414-lmo1415, lmo0825*) in *L. monocytogenes*, as this branch of terpenoid biosynthesis is missing in *B. subtilis,* which utilizes the methylerythritol phosphate pathway instead[156].

Some differences between *B. subtilis* and *L. monocytogenes* essential genes are a little more difficult to explain. For example, in our *L. monocytogenes* dataset, three heat shock response genes, *dnaK, dnaJ* and *grpE,* were all found to be essential (Figure 26).

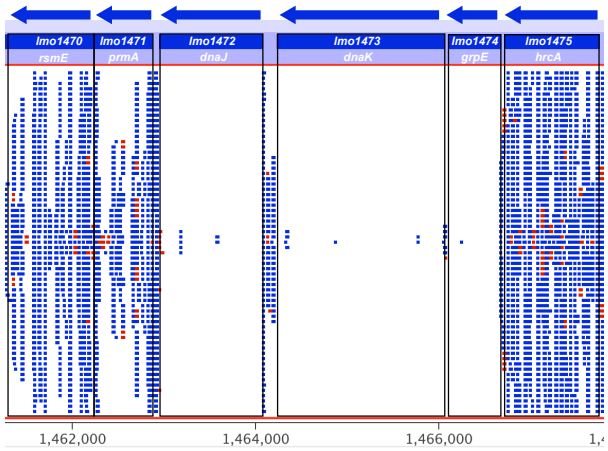

Figure 26. dnaK, dnaJ and grpE are all essential in *L. monocytogenes*. The genetic context of *dnaJ*, *dnaK* and *grpE* is shown here. Each blue or red box is a unique transposon read. Blue reads are sense reads, red anti-sense. It is clearly visible here that *dnaJ*, *dnaK* and *grpE* all accumulated almost no transposon hits, indicating essentiality. Data alignment shown here was generated using SeqMonk software.

This was surprising to us, as heat shock genes are not essential in many bacteria they have been studied in, including *E. coli* and *B. subtilis* [152,157]. However, *dnaK* is essential in *Mycobacterium smegmatis* and *Mycobacterium tuberculosis,* where DnaK is required for the solubilization of newly synthesized peptides[158,159]. It was also found that upon disruption of both of the *dnaJ* genes in *M. tuberculosis*, the function of *dnaJ*, a cofactor involved in DnaK activation, becomes essential[158]. *DnaK* is also essential in *Caulobacter crescentus*, where it serves as a gene regulator by inhibiting the activity of the heat shock sigma factor sigma-32[160]. Although we are not certain if the essentiality of *dnaK, dnaJ* and *grpE* in *L. monocytogenes* is due to their roles in protein folding or through a *C. crescentus*-like secondary yet unstudied role, their apparent indispensability to *L. monocytogenes* survival is an important and previously unknown factor for further *L. monocytogenes* physiology research.

3.2.3: A closer look at *L. monocytogenes* essential genes with unknown functions

In addition to finding that well-characterized genes are essential in *L. monocytogenes*, there were a handful of genes with no known function that also came out in our essentiality analysis. This is a particularly intriguing group of genes, since generally, factors essential for

survival are involved in evolutionarily ancient and well-conserved cellular functions and therefore have been studied and characterized in many different organisms. Therefore, factors of unknown function that are essential in *L. monocytogenes* could point to something that could be important for furthering our understanding of the specifics of its biology.

A few essential genes from the *L. monocytogenes* dataset which have no obvious function were *lmo1028, lmo2487*, and *lmo2562*. Although *lmo1028* is a putative unknown protein, analysis of its genomic context suggests it plays a role in RNA degradation, as it's in an operon with the essential gene *lmo1027*, the Listerial *rnjA* zinc-dependent RNA hydrolase homolog[161]. *Lmo2562* was also of lesser interest as it is in an operon with the essential arginyl-tRNA synthetase, suggesting a role in protein synthesis. Therefore, we focused our attention on elucidating the possible function of *lmo2487*, a protein containing a domain of unknown function (DUF). *lmo2487* is putatively predicted to be the first gene in a 4-gene operon, within which none of the genes have been studied. From simple bioinformatics the homologies of the other genes in the operon, we found that *lmo2484* codes for a putative membrane protein and *lmo2485* codes for a protein containing a truncated PspC (phage shock protein C) domain. This was unexpected, as PspC proteins are generally cytoplasmic membrane integrated Gram-negative proteins involved in stress response[162]. Finally, *lmo2486* also codes for a protein with a domain of unknown function and no putative functionality prediction. In addition, the other three genes in the operon are not essential, sustaining many transpositions (Figure 27A). We ran a Phyre2 structural homology analysis[163] to try to begin to understand the potential function of the *lmo2487* protein product. Our homology analysis produced an unexpected result, wherein the closest structural homologs to the *lmo2487* peptide product were bacterial adhesin proteins. When superimposed using Chimera[164] to the closest predicted structural homolog, a *Bacteroides fragilis* adhesin (PDB: 3PET) it is readily apparent how well the structures align, with clear tertiary structure similarity (Figure 27B).

.

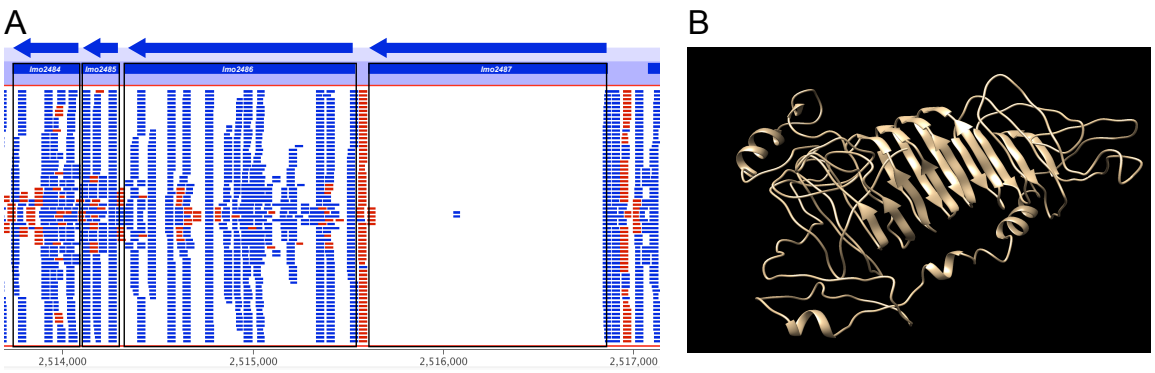

Figure 27. *lmo2487* is a novel *L. monocytogenes* essential gene. (A) a lack of transpositions in the *lmo2487* ORF indicates essentiality **(B)** structural model of Lmo2487 by Phyre2 prediction software.

PSORTb localization prediction software[165] assessed the *lmo2487* protein product as localized to the cytoplasm, further deepening the mystery, as adhesins are typically surface associated[166].

Our next approach to elucidate Lmo2487's function was to do a literature search. We found that *lmo2487* gene expression is regulated by the LisRK signal transduction system, which is an important part of *L. monocytogenes* response to nisin and cephalosporin antimicrobials[167,168]. This, combined with the fact that at least one other component of the *lmo2487* operon appears to be involved in membrane-associated stress response, made us hypothesize that *lmo2487* plays a role in cell wall and/or membrane integrity of *L. monocytogenes*.

Although we were unable to experimentally determine what role *lmo2487*, or the other few putatively unknown essential genes, are playing, we believe that the presence of these unstudied genes in our *L. monocytogenes* essential dataset effectively demonstrates the utility of the Tn-seq approach to studying *L. monocytogenes* physiology and generally of the importance of understanding the basic underpinnings of *L. monocytogenes* biology.

3.3: Conclusions and future directions

3.3.1: Tn-seq as a potentially powerful tool for assessing *L. monocytogenes* physiology

Overall, we believe that the data we present above demonstrates the utility of a Tn-seq

based approach for the study of *L. monocytogenes* physiology. Possible future uses for Tn-seq in *L. monocytogenes* would be to expand the treatments of the wild type library, such as passaging the library through macrophages or mice, or treatments with toxic molecules, such as nitric oxide or 4-HNE. It is also possible to generate transposon libraries in various *L. monocytogenes* mutant backgrounds and analyze differences in transposon densities. Similar work has been done in a plethora of other bacteria and there is a wide range of experimental opportunities that is now available in the Listerial field, including the potential for a deeper understanding of *L. monocytogenes* 4-HNE resistance.

3.3.2: Tn-seq for understanding *L. monocytogenes* 4-HNE resistance

There are a few possible approaches for using Tn-seq to assess *L. monocytogenes* 4-HNE resistance. The first is to grow the WT library in the presence of 4-HNE or mock vehicle treatment and compare the two treatments. However, there is a potential issue with this approach, as *L. monocytogenes* does not appear to die at significant levels when exposed to 4-HNE in rich media (Figure 11B). A possibly more effective way to utilize Tn-seq for 4-HNE survival assessment is to treat *L. monocytogenes* suspended in PBS, a condition in which *L. monocytogenes* does eventually succumb to about a half-log of 4-HNE induced death (Figure 28).

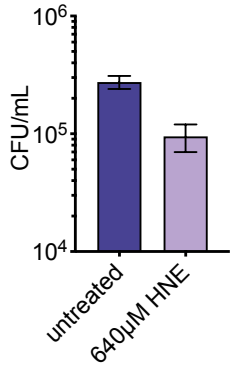

Figure 28. *L. monocytogenes* death upon 4-HNE exposure in PBS. *L. monocytogenes* was exposed to 640μM 4-HNE in PBS at 37C for 1 hour and CFU were enumerated on an LB plate.

Another approach to take is to generate transposon libraries in the *ΔΔrha1/2* background

to determine what other factors contribute to *L. monocytogenes* survival in 4-HNE. All of these are interesting directions to take the study of 4-HNE effects on bacterial physiology in general and *L. monocytogenes* in particular.

Chapter 4: Perspectives and future directions

4.1: Introduction

In this thesis, I show that 4-hydroxy-2-nonenal, or 4-HNE, is a previously unappreciated component of the reactive oxygen species burst during bacterial infection and that the intracellular pathogen *Listeria monocytogenes* is highly resistant to its toxicity. This resistance is partially due to *L. monocytogenes* expression of two novel NADPH-dependent 4-HNE reductases, *rha1* and *rha2*. Rha1/2 exert their activity on 4-HNE by reducing the carbon-carbon double bond and reducing 4-HNE to 4-HNA, 4-hydroxynonanal, a less toxic saturated aldehyde product. This enzymatic capability allows heterologous *rha1/2* expression to partially rescue the survival of a sensitive bacterium, *Bacillus subtilis,* in purified 4-HNE and during intracellular macrophage phagocytosis. This is the first time it has been demonstrated that 1) 4-HNE accumulates during bacterial infection, 2) *L. monocytogenes* is highly resistant to its toxicity and 3) *L. monocytogenes* encodes specific detoxification enzymes against 4-HNE.

In the second part of this thesis, I discussed the adaptation of the Tn-seq essentiality assessment protocol for *L. monocytogenes*, its successful application to determine the *L. monocytogenes* essential genome and how Tn-seq could be a powerful tool to continue to probe *L. monocytogenes* anti-4-HNE defenses. Both parts of this study open up many potential new directions of research.

4.2: Why two enzymes that do the same thing?

The first very evident question one might ask about this work is how come there are two enzymes that perform the same enzymatic reaction in tandem? It's possible that the difference between *rha1* and *rha2* functionality could be intracellular localization, especially since *rha1* is structurally homologous to quinone reductases involved in the electron transport chain, suggesting potential membrane-association. Overall, there is a lot left to explore to better

understand the reasons for the concurrent necessity of both *rha1* and *rha2* in anti-4-HNE defense.

4.3: Why 4-hydroxynonanal?

Another immediately obvious step for follow-up is -- why this resistance mechanism? In eukaryotic biology, the NADP-dependent double-bond hydrogenation of 4-HNE to 4-HNA is exceedingly rare, or at least poorly studied, with only a few papers in the last twenty years demonstrating such an enzymatic mechanism of defense [73,74]. This enzymatic mechanism is somewhat puzzling as 4-HNA still contains an aldehyde moiety and is therefore reactive with nucleophilic proteins, presumably exerting toxicity within the cell. However, although 4-HNA's aldehyde moiety makes it a theoretically less-ideal detoxification product, many bacterial genomes encode for many aldehyde detoxification schemes, some of which have been well-studied, such as the aldehyde dehydrogenase AdhA of *B. subtilis* [169] and AldH from *E. coli* [170]. Perhaps *rha1/2* are simply the first in a complicated cascade of this pathway of 4-HNE detoxification and other enzymes -- maybe homologs of familiar genes, such as the above mentioned aldehyde dehydrogenases, or maybe something novel and heretofore unstudied -- are capable of further reducing the aldehyde double bond and fully saturating 4-HNA.

4.4: Other resistance schemas -- *rha1 and rha2* are not everything

Although in this work we conclusively demonstrate that *rha1/2* are important components of the anti-4-HNE *L. monocytogenes* response, the differential in survival between WT and *ΔΔrha1/2 L. monocytogenes* is a modest 1.5-log defect for the mutant strain (Figure 13B), suggesting that there are other components to *L. monocytogenes* multi-log survival advantage over the closely related but 4-HNE sensitive bacterium *B. subtilis* (Figure 9A). There are many possibilities as to why simply disrupting two enzymes didn't completely eliminate *L. monocytogenes* 4-HNE resistance. It is likely there are many other components of the 4-HNE

transcriptional response that could contribute to *L. monocytogenes* survival. We had found that over 350 genes were significantly induced over 2-fold upon 4-HNE treatment (Table 1), leaving us with hundreds of genes we have not explored in this study for their potential contributions to 4-HNE resistance.

It is also possible that genes that are not induced by brief 4-HNE exposure play significant roles in survival. These genes would not be detected through transcriptional analysis and would only be detected through transposon mutagenesis and Tn-seq. Finally, it might be that components of the *L. monocytogenes* essential genome could contribute to its enhanced 4-HNE survival, making them undetectable through most conventional assessments.

4.5: *L. monocytogenes* potentially subverts immunomodulatory function of 4-HNE

In addition to 4-HNE's direct antimicrobial properties I present in this thesis, it has a well-known role as an immune modulator. It is possible that not only do the 4-HNE detoxification genes encoded by *L. monocytogenes* allow the bacterium to escape the aldehyde's direct toxicity, but that this 4-HNE-to-4-HNA conversion diminishes the proinflammatory pathways activated by 4-HNE. 4-HNE is known to activate the NF-κB inflammatory pathway through its reaction with the Src protein [171], and through the promotion of extracellular export of HSP70 [172]. 4-HNE may also increase inflammation through its positive regulation of TNF-α expression [173,174]. This robust evidence of 4-HNE as a pro-inflammatory molecule could mean that reducing total 4-HNE within the eukaryotic cell via direct detoxification could benefit *L. monocytogenes* not just through the elimination of bacterial-targeted toxicity, but also through tamping down the inflammatory pathways regulated by 4-HNE.

4.6: Conclusion

This thesis lays the groundwork for multiple different and interesting potential research directions. The field is wide-open and full of potential novel discoveries about ROS, 4-HNE, and

the intricacies of the 4-HNE resistance mechanisms of *L. monocytogenes*.

Chapter 5: Materials and Methods

5.1: Strains and routine growth conditions

Unless otherwise specified, *L. monocytogenes* was grown at 37°C degrees in tryptic soy broth (TSB) media and *E. coli* at 37°C degrees in Luria-Bertani (LB) media with appropriate antibiotic selection. Unless otherwise noted, *B. subtilis* was struck on LB plates with appropriate antibiotics and induction agent overnight at 30°C, after which the biomass was scraped off the plates, resuspended in LB media, passed 6 to 10 times through a 27-gauge needle to break up clumps and chains, then normalized to an OD_{600} of 1. When required for selection, antibiotic concentrations used in this study were as follows – *L. monocytogenes* selections: streptomycin 200µg/mL, chloramphenicol 5µg/mL; *E. coli* selections: ampicillin 50µg/mL; *B. subtilis* selections: chloramphenicol 10µg/mL; tissue culture: gentamicin 50µg/mL.

5.2: Bacterial infection and exogenous 4-HNE TIB73 dot blot

TIB73 cells were infected with *L. monocytogenes* following a previously developed protocol [175]. Exogenous 4-HNE (Cayman Chemical, #32100) was added to uninfected TIB73 cells by first washing the cells with sterile PBS and then adding 2mL sterile PBS containing a final concentration of 10µM 4-HNE for 10 minutes. TIB73 cells were lysed in whole cell lysis buffer (50 mM Tris pH 7.5, 150 mM NaCl, 1% Triton X-100) with EDTA (1 µM) and Halt Protease Inhibitor Cocktail (Thermo Fisher Scientific, #78442). Protein concentration was determined using the Pierce BCA protein assay kit (Fisher Scientific, #PI23227). Lysates were resuspended in 1X PBS to achieve 2µg of protein per 3µl, which was the volume spotted out onto nitrocellulose membrane (Bio-Rad, #1620115). The nitrocellulose was then dried, blocked for 45 minutes in 5% dry milk, washed 3 times with TBS-T (Tris-buffered saline with 0.1% Triton X-100) and primary 4-HNE antibody was added at 1:200 dilution (Abcam, #ab46545). The antibody was left on overnight at 4°C rocking. Primary actin antibody (Abcam, #ab8226) was added at 1:1000 for 3 hours at room

temperature. The primary antibodies were then washed off with TBS-T 3 times and secondary antibodies (Licor, #926-32211, #926-68072) were added at 1:8000 for 45 minutes at RT. The secondary antibodies were then washed with TBS-T twice, then TBS once and the blot was imaged on a Licor Odyssey Fc. Relative densitometric analysis was performed using Licor Image Studio software.

5.3: Mouse infections

L. monocytogenes was grown overnight statically at 30°C degrees in Brain Heart Infusion (BHI) broth, then backdiluted using 1.2 mL of overnight culture to 4.8 mL of fresh BHI and grown for 1 hour at 37°C degrees shaking. OD_{600} of these cultures were taken and, using the conversion of 1 OD = $1.7x10^9$ CFU, diluted to $5x10^5$ CFU/mL with PBS. 200µl were then injected into female mice between 6-8 weeks of age retro-orbitally ($1x10^5$ CFU/mouse) and livers and spleens were harvested at 48 hours post infection. Livers were homogenized in 10mL of cold 0.1% IGEPAL and spleens were homogenized in 5mL using a Tissue Tearor Model 985370 (Biospec Products) at 10,000 RPM for 5 seconds/organ. Homogenates were diluted in PBS and plated on LB plates to enumerate CFU. All protocols were reviewed and approved by the Institutional Animal Care and Use Committee at the University of Washington.

5.4: 4-HNE histology

Two female mice were infected as outlined above, in addition to one uninfected control mouse. The livers and spleens were harvested at 48 hours post infection and placed in 10% neutral buffered formalin for 24 hours, after which the organs were removed from formalin and placed in PBS for 24 hours. Paraffin embedded tissues were sliced and prepared as slides. Slides were then deparaffinized for 30 minutes at 60°C. All subsequent manipulations were performed on a Leica Bond Automated Immunostainer. Antigen retrieval for GFP was performed by HIER 2 (EDTA) treatment for 20 minutes at 100°C. Antigen retrieval for 4-HNE was performed by citrate

treatment for 20 minutes at 100°C. Then a Leica Bond peroxide block was performed for 5 minutes at room temperature, and normal goat serum (10% in TBS) was added for 20 minutes at room temperature. Primary antibody was added (GFP 1:500), (Rab IgG 1:1000), (4-HNE 1:200) in Leica Primary antibody diluent, for 30 minutes at room temperature. Leica Bond Polymer was added for 8 min at room temperature, after which the samples were washed with Leica Bond Mixed Refine (DAB) detection solution twice for 10 minutes at room temperature. Hematoxylin Counterstain was added for 4 minutes and the samples were cleared to xylene. Finally, samples were mounted with synthetic resin mounting medium on a 1.5cm coverslip and imaged with a Hamamatsu Nanozoomer Whole Slide Scanner and a Keyence BZ-X710 Microscope.

5.5: *L. monocytogenes* 4-HNE PBS dot blots cytosolic 4-HNE assessment

L. monocytogenes were sub-cultured from overnight stationary cultures 1:100 into fresh media and grown to mid-log (0.4-0.8 OD_{600}). The bacteria were normalized to OD 1, washed twice with sterile PBS and resuspended in sterile PBS. A range of 4-HNE concentrations were added to the bacteria and the samples were placed at 37°C for 30 minutes. Upon completion, the bacteria were washed twice with PBS and spun at 10,000g for 5 minutes, then resuspended in fresh PBS. The bacteria were then sonicated using a narrow tip sonicator at 20% power, 1 second on 1 second off for 10 seconds and placed on ice. The bacteria were then spun at 4C at 10,000g for 30 minutes. The subsequent lysate was transferred to fresh Eppendorf tubes containing Halt Proteinase and Phosphatase Inhibitor (Thermo Fisher Scientific, #78442) and stored at -80°C until use. For the dot blots, the protein concentration was normalized using BCA (Fisher Scientific, #PI23227) and 3µg in 3µL was spotted onto nitrocellulose membrane (Bio-Rad, #1620115). The nitrocellulose was then dried, blocked for 45 minutes in 5% dry milk, washed 3 times with TBS-T and primary 4-HNE antibody was added at 1:200 dilution (Abcam, #ab46545). The antibody was left on overnight at 4°C rocking. The primary antibody was then washed off with TBS-T 3 times and secondary antibody (Licor, #926-32211) was added at 1:8000 for 45 minutes at RT. The

secondary antibody was then washed off with TBS-T twice, TBS once and the blot was imaged on a Licor Odyssey Fc. Relative densitometric analysis was performed using Licor Image Studio software.

5.6: RNA extraction from broth cultures of *L. monocytogenes*

L. monocytogenes stationary phase overnights were subcultured 1:100 into fresh TSB media and grown shaking at 37°C to mid-log (0.4-0.8 OD_{600}). Then a final concentration of 640μM 4-HNE (Cayman #32100) or vehicle (100% ethanol) was added to the bacteria, which continued to grow at 37°C shaking for 20 minutes. After 20 minutes, ice cold 100% methanol was added in equal volume to the culture flask and placed at -20C overnight. The next day the bacteria were spun down and resuspended in 400μL AE buffer (50mM NaOAc pH 5.2, 10mM EDTA in molecular grade water). The resuspended bacteria were then mixed with 400μL acidified 1:1 phenol:chloroform pH 5.2 (Fisher Scientific, # BP1753I) and 40μL 10% sodium dodecyl sulfate (SDS) and was vortexed for 10 minutes in a multi-tube vortexer. The tubes were then transferred to a 65C heat block for ten minutes, after which the mixture was transferred to a Heavy Phase-lock tube (VWR #10847-802) and spun down for 5 minutes at 17,000g. Then the aqueous layer was transferred into tubes containing 1mL 100% ethanol and 40μL 3M NaOAc and placed at -20C for 6 hours. Then tubes were spun at 17,000g for 30 minutes at 4°C, the ethanol was aspirated and 500μL 70% ethanol was added. The tubes were then centrifuged at 17,000g for 10 minutes at room temperature and the supernatant was aspirated. The RNA pellet was then dried in a speed vacuum concentrator for 5 minutes and resuspended in RNA-free molecular grade water. The extracted RNA was then treated with DNase (Ambion Life Technologies #AM1907) for an hour at 37°C and used for downstream processing.

5.7: RNA-sequencing

RNA was processed using the Ovation Complete Prokaryotic RNA-Seq Library System (NuGEN, #0363-32, 0326-32, 0327-32) according to the manufacturer's instructions to a final pooled library concentration of 3nM. Libraries were sequenced on an Illumina HiSeq 2500 (SR50) at The Genomics Resource at the Fred Hutchinson Cancer Research Center. Image analysis and base calling were performed using Illumina's Real Time Analysis v1.18.66.3 software, followed by 'demultiplexing' of indexed reads and generation of FASTQ files using Illumina's bcl2fastq Conversion Software v1.8.4. Reads determined by the RTA software to pass Illumina's default quality filters were concatenated for further analysis. The FASTQ files were aligned and analyzed using Rockhopper software [176]. These data have been deposited to the GEO and are accessible using accession number GSE150188.

5.8: qRT-PCR

Bacteria were grown in the same manner as for RNA-seq except 500μM of each aldehyde tested was added to the culture at mid-log (0.4-0.8 OD_{600}). The RNA was extracted by the acidified phenol method as listed above and DNase treated and reverse-transcribed using the iScript Reverse Transcription Supermix (Bio-Rad, #1708840). SYBR Green (Thermo Fisher Scientific # K0223) was then used to amplify genes of interest and CT values and relative expression were normalized using CFX Maestro Software (Bio-Rad #12004110).

5.9: Intracellular RNA extraction

RNA extraction from macrophages was performed as previously described [177]. J774 macrophages were seeded at a density of $2.0x10^7$ cells/dish in three 150 mm dishes in 30mL media and incubated overnight. The next day, overnight *L. monocytogenes* culture grown at 30ºC was washed twice with PBS and added to the cells at a MOI of 50. After one hour, the cells were washed twice with PBS and media containing gentamicin was added. Eight hours post-infection, cells were washed once with PBS and lysed by addition of cold nuclease-free water. Lysate was

collected by scraping and centrifugation at 800g for 3 min at 4ºC. Supernatants were passed through 0.45 µm filters in a vacuum apparatus, and filters were collected in conical tubes. Filters were vortexed with 650µL sterile AE buffer for one minute and centrifuged briefly. Bacteria-containing AE buffer was collected and used for immediate RNA extraction as described above.

5.10: Survival assays bacterial panel

Bacteria were inoculated overnight in TSBC (TSB + cysteine 0.1% required for *Francisella novicida* growth) and grown at 37°C. The next day the bacteria were subcultured 1:1000 into fresh TSBC and allowed to reach mid-log (0.4-0.8 OD_{600}). At mid-log the ODs of the bacteria were normalized to OD1, washed twice in sterile PBS and resuspended in sterile PBS. Then the bacteria were diluted 1:100 into sterile PBS in Eppendorf tubes and various concentrations of 4-HNE were added. The bacteria were then placed at 37°C for an hour, then plated on TSAC (TSA + cysteine 0.1%) plates. Colonies were enumerated after overnight growth at 37°C.

5.11: *L. monocytogenes* competition experiments

Colonies of *L. monocytogenes* were picked off BHI plates and inoculated into 2mL TSB which was then grown shaking at 37°C to mid-log (0.4-0.8 OD_{600}). At mid-log the bacteria were normalized to OD_{600} 1, washed twice in sterile PBS and resuspended in sterile PBS. Then the bacteria were diluted 1:100 into sterile PBS and appropriate strains were mixed together in a 1:1 ratio, after which 640µM of 4-HNE or vehicle (ethanol) was added. The bacteria were then placed at 37°C for one hour. 2x concentrated TSB media was added to the bacterial-PBS solution and the cells recovered for an hour at 37°C. The bacteria were then plated on BHI-streptomycin and BHI-chloramphenicol (5 plates for competitive strain differentiation. CFUs were enumerated after 24-48 hours of growth at 37°C. In competition between WT and WT, *Δrha1*, *Δrha2* and *ΔΔrha1/2*, the WT competition strain was the marked strain DPL-3903[178]. In competition between WT and

ΔΔrha1/2::rha1 and *ΔΔrha1/2::rha2*, WT *L. monocytogenes* were unmarked while the complemented strains carried resistance to chloramphenicol.

5.12: *L. monocytogenes* protein aggregation assay

The *L. monocytogenes* aggregation protocol was adapted from Tomoyasu et al with minor modifications [179] . *L. monocytogenes* were grown to mid-log (0.4-0.8 OD_{600}). Bacteria were normalized to 0.5 OD_{600} and resuspended in 3mL of sterile PBS. 640μM 4-HNE was added and the bacteria were placed at 37C for an hour. The bacteria were then removed, cooled on ice for 5 minutes and spun down at 5000g for 10 minutes at 4C. Pellets were then resuspended in 40μL buffer A1 [10mM potassium phosphate buffer, pH 6.5, 1mM EDTA, 20% w/vol sucrose, 50 units per sample mutanolysin (Sigma, #M9901)] and incubated on ice for 30 minutes. 360μL Buffer B1 [10mM potassium phosphate buffer, pH 6.5, 1mM EDTA] was added and the sample was sonicated with a microtip sonicator at 40% power, 6 seconds total, 1 second on, 1 second off. Intact cells were spun out at 2000g for 10 minutes at 4C and supernatant was transferred to a fresh tube. 50μL of sample supernatant was taken to measure total protein concentration by BCA. The insoluble fraction was isolated by centrifuging the supernatant a 15,000g for 20 minutes at 4C. The pellets were then frozen and stored at -80C. The pellets were resuspended in 400μL buffer B1 by brief sonication (40% power, 2 seconds total, 1 second on, 1 second off) and centrifuged at 15,000g for 20 minutes at 4C. The washed pellets were then resuspended in 320μL buffer B1 by brief sonication, after which, 80μL of 10% v/v IGEPAL was added to remove membrane proteins. The samples were mixed and then centrifuged at 15,000g for 30 minutes at 4C. This washing procedure was performed twice in total. Finally, the pellets were washed by 400μL buffer B1 and resuspended in 50μL PBS by brief sonication. The insoluble protein concentration was measured by microBCA (Thermo, #23235) and the percent of total protein was calculated and plotted.

5.13: Purified protein expression and enzyme kinetics

rha1 and *rha2* ORFs were cloned into pET20B vectors and transformed into BL21 *E. coli* and grown overnight in LB-ampicillin. The overnights were subcultured 1:100 in 2L baffled flasks until mid-log (0.4-0.8 OD_{600}) after which 0.5mM IPTG was added. The *pET20b::rha2 E. coli* were induced for 4 hours at 37°C shaking. 0.01% w/v riboflavin was added to *E. coli pET20B::rha1* and the flask was moved to grow at 17°C for 18 hours shaking. Upon completion, the bacteria were spun down, resuspended in buffer A (30mM K_2HPO_4, 300mM NaCl, pH 8) and sonicated on ice with a large sonicator tip at 80% power 1 sec on 1 sec off for 30 seconds total. They were then spun down at 15,000 g for 45 minutes at 4°C and the supernatant was passed over a nickel resin column (Thermo Fisher Scientific, # PI88222) and eluted using buffer B (30mM K_2HPO_4, 300mM NaCl, 500mM Imidazole, pH 8). The final protein was then transferred into PBS using a desalting column (Bio-Rad #7322010). For purification of Rha1 10μM FMN (Sigma #F2253) was added at every step of purification. Enzyme turnover assays were performed at 37°C in 96 well clear bottom plates (Genesee Scientific, #25-104) in a Synergy HTX plate reader in 200μL PBS 20% w/v PEG-8000 using 200μM NADPH, 0.2μM enzyme and a range of 4-HNE concentrations from 0 to 0.8mM. NADPH consumption was measured at the 340nm wavelength. Rha1 turnover was performed in the presence of 10μM FMN.

5.14: Chemical reduction of 4-HNE

100μL of 64mM 4-HNE was reduced by adding a molar excess (1mg) of sodium borohydride ($NaBH_4$), which was left to sit at room temperature for an hour. The reaction was quenched for one hour at room temperature with 100μL 1.5% v/v glacial acetic acid in water. The final product of the reaction was 1,4-dihydroxynonene (1,4-DHN) as confirmed by TLC (described below).

5.15: Thin layer chromatography (TLC)

Enzyme turnover assays performed as described above, except the reactions had final concentrations of 4μM enzyme, 1.6mM 4-HNE and 1.6mM NADPH. The reactions proceeded for 1 to 14 hours at room temperature. Once the reaction was complete, 6μL of reaction volume was spotted on the bottom of the TLC plate (Millipore Sigma, #105554) and run using a 2:1 mix of diethyl ether:hexanes (Sigma, #296082; Thermo Fisher, #H303). The TLC plate was visualized by dipping the plate in a 10% w/v phosphomolybdic acid (Sigma, #221856) absolute ethanol solution and then vigorously heating the TLC plate on a ceramic hot plate until the appearance of black bands on a light yellow background (15 seconds to 1 minute).

5.16: *B. subtilis* growth curves

B. subtilis expressing genes of interest on the pHT01 plasmid [180] were struck on LB-chloramphenicol plates on day 1 and grown overnight at 30°C. On day 2, colonies were re-struck on LB chloramphenicol IPTG 1mM LB plates overnight at 30°C. On day 3, biomass was scraped and processed as described in the "bacterial culturing" section above. The bacteria were then normalized to an OD_{600} of 1 and inoculated 1:100 into a 96-well plate containing TSB chloramphenicol and 0.5mM IPTG. 4-HNE was then added to the bacteria at various concentrations and the bacteria were allowed to grow at 37°C in Synergy HTX plate reader for 12 hours with shaking.

5.17: *B. subtilis* and *L. monocytogenes* rich media 4-HNE dot blots

B. subtilis were grown and processed in the same manner as for the growth curves above. *L. monocytogenes* were processed as described for competition experiments above. Upon OD_{600} 1 normalization *B. subtilis* were resuspended in TSB-chloramphenicol with 0.5mM IPTG and 250μL of this mix was transferred to a sterile Eppendorf tube into which 640μM 4-HNE was added. *L. monocytogenes* were resuspended in TSB with no antibiotic and no IPTG. The tubes were then incubated at 37°C for 3 hours. At 3 hours, the bacteria were spun down at 17,000g for 1 minute.

The supernatant was then aspirated and the pellet flash frozen in liquid nitrogen. At this point, the bacteria were stored at -80C until further processing. Once removed from the -80C, the bacteria were thawed at room temperature and resuspended in 250µL PBS. The bacteria were then sonicated using a microtip sonicator at 20% power, 1sec on 1sec off for 10 seconds and placed on ice. The bacteria were then spun at 4°C at 5,000g for 10 minutes. The subsequent lysate was transferred to fresh Eppendorf tubes containing Halt Proteinase and Phosphatase Inhibitor (Thermo Fisher Scientific, #78442) and stored at -80C until use. For the dot blots, the protein concentration was normalized using BCA (Fisher Scientific, #PI23227) and 3µg in 3µL was spotted onto nitrocellulose membrane (Bio-Rad, #1620115). The nitrocellulose was then dried, blocked for 45 minutes in 5% dry milk, washed three times with TBS-T and primary 4-HNE antibody was added at 1:200 dilution (Abcam, #ab46545). The antibody was left on overnight at 4°C rocking. The primary antibody was then washed off with TBS-T three times and secondary antibody (Licor, #926-32211) was added at 1:8000 for 45 minutes at RT. The secondary was then washed off with TBST twice, TBS once, and then the blot was imaged on a Licor Odyssey Fc. Relative densitometric analysis was performed using Licor Image Studio software.

5.18: *L. monocytogenes* macrophage infection

0.5×10^6 primary murine macrophages from WT C57BL/6 mice were plated in BMM media (DMEM with 10% heat inactivated fetal bovine serum, 1mM L-glutamine, 2mM sodium pyruvate and 10% L929-conditioned medium) in a tissue culture treated 24-well dish (Greiner Bio, #662165) with the addition of 100ng recombinant murine IFN-γ (Peprotech, #315-05) for 18 hours. Inoculants of *L. monocytogenes* were statically grown at 30°C overnight, washed twice with sterile PBS and resuspended in PBS before an MOI of 0.1 was added to each macrophage well. The cells were left to sit for an hour after which all wells were washed twice with PBS and gentamicin was added to all but one well, which was lysed in 500µL water and plated for CFU on LB plates.

The remainder of the wells were washed twice with PBS and then lysed and plated for CFU at hours 2, 6 and 9 post-infection.

5.19: *B. subtilis* macrophage survival assay

B. subtilis were grown on LB-chloramphenicol 1mM IPTG plates and processed into LB chloramphenicol as described above. Once the bacteria were normalized to OD_{600} 1 in LB chloramphenicol, an MOI of 100 was added to 0.5 x 10^6 primary murine macrophages from WT C57BL/6 or C57BL/6 deficient for phox (*gp91$^{phox-/-}$*) mice (The Jackson Laboratory, stock # 002365) that have been activated using 100ng/well recombinant murine IFN-γ (Peprotech, #315-05) for 18 hours. The cells were spinfected at 200g for 5 minutes. At 1.5 hours, cells were washed 2x with sterile PBS and gentamicin was added to the cells. pBMMs were lysed in 500µL cold water at hours 2, 6, 7, and 8 and plated for CFU. Colonies were enumerated after overnight growth at 30°C on LB plates.

5.20: Tn-seq library preparation and sequencing

Followed the TdT method of sample preparation as described in Gallagher et al [181] . Briefly, DNA samples were extracted using the Gram-positive DNA Purification Kit (Lucigen, #MGP04100), then sonicated to 300bp average length using a Covaris sonicator. The DNA was then end-repaired using the NEB Next End Repair Mix (NEB, #E6050), C-tailed using a Terminal transferase (Promega, #M1875) and bar-coded by PCR on a BioRad Real-Time PCR machine. The library was sequenced using an Illumina NextSeq Sequencer.

References

1. Bakshani, C. R. *et al.* Evolutionary conservation of the antimicrobial function of mucus: a first defence against infection. *NPJ Biofilms Microbiomes* **4**, 14 (2018).
2. Green, G. M., Jakab, G. J., Low, R. B. & Davis, G. S. Defense mechanisms of the respiratory membrane. *Am. Rev. Respir. Dis.* **115**, 479–514 (1977).
3. Schulz, J. T., 3rd, Tompkins, R. G. & Burke, J. F. Artificial skin. *Annu. Rev. Med.* **51**, 231–244 (2000).
4. Medzhitov, R. & Janeway, C., Jr. Innate immunity. *N. Engl. J. Med.* **343**, 338–344 (2000).
5. Mogensen, T. H. Pathogen recognition and inflammatory signaling in innate immune defenses. *Clin. Microbiol. Rev.* **22**, 240–73, Table of Contents (2009).
6. Vaure, C. & Liu, Y. A comparative review of toll-like receptor 4 expression and functionality in different animal species. *Front. Immunol.* **5**, 316 (2014).
7. Oliveira-Nascimento, L., Massari, P. & Wetzler, L. M. The Role of TLR2 in Infection and Immunity. *Front. Immunol.* **3**, 79 (2012).
8. Hajam, I. A., Dar, P. A., Shahnawaz, I., Jaume, J. C. & Lee, J. H. Bacterial flagellin-a potent immunomodulatory agent. *Exp. Mol. Med.* **49**, e373 (2017).
9. Lamphier, M. S., Sirois, C. M., Verma, A., Golenbock, D. T. & Latz, E. TLR9 and the recognition of self and non-self nucleic acids. *Ann. N. Y. Acad. Sci.* **1082**, 31–43 (2006).
10. Lund, J. M. *et al.* Recognition of single-stranded RNA viruses by Toll-like receptor 7. *Proc. Natl. Acad. Sci. U. S. A.* **101**, 5598–5603 (2004).
11. Balka, K. R. & De Nardo, D. Understanding early TLR signaling through the Myddosome. *J. Leukoc. Biol.* **105**, 339–351 (2019).
12. Kawasaki, T. & Kawai, T. Toll-like receptor signaling pathways. *Front. Immunol.* **5**, 461 (2014).
13. Bryan, N. *et al.* Reactive oxygen species (ROS)--a family of fate deciding molecules pivotal in constructive inflammation and wound healing. *Eur. Cell. Mater.* **24**, 249–265 (2012).
14. Ray, P. D., Huang, B.-W. & Tsuji, Y. Reactive oxygen species (ROS) homeostasis and redox regulation in cellular signaling. *Cellular Signalling* vol. 24 981–990 (2012).
15. Sies, H. & Jones, D. P. Reactive oxygen species (ROS) as pleiotropic physiological signalling agents. *Nat. Rev. Mol. Cell Biol.* **21**, 363–383 (2020).
16. van der Heijden, J., Bosman, E. S., Reynolds, L. A. & Finlay, B. B. Direct measurement of oxidative and nitrosative stress dynamics in Salmonella inside macrophages. *Proc. Natl. Acad. Sci. U. S. A.* **112**, 560–565 (2015).
17. Rhee, S. G. Redox signaling: hydrogen peroxide as intracellular messenger. *Experimental & Molecular Medicine* vol. 31 53–59 (1999).
18. Karin, M. NF- B as a Critical Link Between Inflammation and Cancer. *Cold Spring Harbor Perspectives in Biology* vol. 1 a000141–a000141 (2009).
19. Peralta, D. *et al.* A proton relay enhances H2O2 sensitivity of GAPDH to facilitate metabolic adaptation. *Nat. Chem. Biol.* **11**, 156–163 (2015).
20. Ruppersberg, J. P. *et al.* Regulation of fast inactivation of cloned mammalian IK(A) channels by cysteine oxidation. *Nature* **352**, 711–714 (1991).
21. Somyajit, K. *et al.* Redox-sensitive alteration of replisome architecture safeguards genome integrity. *Science* **358**, 797–802 (2017).
22. Iyer, G. Y. N., Islam, M. F. & Quastel, J. H. Biochemical Aspects of Phagocytosis. *Nature* vol. 192 535–541 (1961).
23. Nathan, C. F. & Root, R. K. Hydrogen peroxide release from mouse peritoneal macrophages: dependence on sequential activation and triggering. *J. Exp. Med.* **146**, 1648–1662 (1977).
24. Fang, F. C. Antimicrobial reactive oxygen and nitrogen species: concepts and controversies. *Nat. Rev. Microbiol.* **2**, 820–832 (2004).
25. Nathan, C. & Shiloh, M. U. Reactive oxygen and nitrogen intermediates in the relationship between mammalian hosts and microbial pathogens. *Proc. Natl. Acad. Sci. U. S. A.* **97**, 8841–8848 (2000).
26. El-Benna, J., Dang, P. M.-C., Gougerot-Pocidalo, M.-A. & Elbim, C. Phagocyte NADPH oxidase: a multicomponent enzyme essential for host defenses. *Arch. Immunol. Ther. Exp.* **53**, 199–206 (2005).
27. West, A. P. *et al.* TLR signalling augments macrophage bactericidal activity through mitochondrial

ROS. *Nature* **472**, 476–480 (2011).
28. Abuaita, B. H., Schultz, T. L. & O'Riordan, M. X. Mitochondria-Derived Vesicles Deliver Antimicrobial Reactive Oxygen Species to Control Phagosome-Localized Staphylococcus aureus. *Cell Host Microbe* **24**, 625-636.e5 (2018).
29. Kajiwara, C. *et al.* Metformin Mediates Protection against Legionella Pneumonia through Activation of AMPK and Mitochondrial Reactive Oxygen Species. *J. Immunol.* **200**, 623–631 (2018).
30. Khan, A. A., Alsahli, M. A. & Rahmani, A. H. Myeloperoxidase as an Active Disease Biomarker: Recent Biochemical and Pathological Perspectives. *Med Sci (Basel)* **6**, (2018).
31. Virág, L., Jaén, R. I., Regdon, Z., Boscá, L. & Prieto, P. Self-defense of macrophages against oxidative injury: Fighting for their own survival. *Redox Biol* **26**, 101261 (2019).
32. Prolo, C., Alvarez, M. N. & Radi, R. Peroxynitrite, a potent macrophage-derived oxidizing cytotoxin to combat invading pathogens. *Biofactors* **40**, 215–225 (2014).
33. Lowenstein, C. J. iNOS (NOS2) at a glance. *Journal of Cell Science* vol. 117 2865–2867 (2004).
34. Hong, Y., Zeng, J., Wang, X., Drlica, K. & Zhao, X. Post-stress bacterial cell death mediated by reactive oxygen species. *Proc. Natl. Acad. Sci. U. S. A.* **116**, 10064–10071 (2019).
35. Imlay, J. A. Iron-sulphur clusters and the problem with oxygen. *Mol. Microbiol.* **59**, 1073–1082 (2006).
36. Tamarit, J., Cabiscol, E. & Ros, J. Identification of the major oxidatively damaged proteins in Escherichia coli cells exposed to oxidative stress. *J. Biol. Chem.* **273**, 3027–3032 (1998).
37. Shohet, S. B., Pitt, J., Baehner, R. L. & Poplack, D. G. Lipid peroxidation in the killing of phagocytized pneumococci. *Infect. Immun.* **10**, 1321–1328 (1974).
38. Roos, D. Chronic granulomatous disease. *Br. Med. Bull.* **118**, 50–63 (2016).
39. Bustamante, J. *et al.* Germline CYBB mutations that selectively affect macrophages in kindreds with X-linked predisposition to tuberculous mycobacterial disease. *Nat. Immunol.* **12**, 213–221 (2011).
40. Vergis, N. *et al.* Defective monocyte oxidative burst predicts infection in alcoholic hepatitis and is associated with reduced expression of NADPH oxidase. *Gut* **66**, 519–529 (2017).
41. Calder, P. C. ω3 Polyunsaturated Fatty Acids, Inflammation and Immunity. *Fatty Acids and Lipids - New Findings* 109–116 (2000) doi:10.1159/000059774.
42. Hanna, V. S. & Hafez, E. A. A. Synopsis of arachidonic acid metabolism: A review. *J. Advert. Res.* **11**, 23–32 (2018).
43. Dennis, E. A. & Norris, P. C. Eicosanoid storm in infection and inflammation. *Nat. Rev. Immunol.* **15**, 511–523 (2015).
44. Long, E. K. & Picklo, M. J., Sr. Trans-4-hydroxy-2-hexenal, a product of n-3 fatty acid peroxidation: make some room HNE. *Free Radic. Biol. Med.* **49**, 1–8 (2010).
45. Ayala, A., Muñoz, M. F. & Argüelles, S. Lipid peroxidation: production, metabolism, and signaling mechanisms of malondialdehyde and 4-hydroxy-2-nonenal. *Oxid. Med. Cell. Longev.* **2014**, 360438 (2014).
46. Schwarzer, E., Arese, P. & Skorokhod, O. 4-Hydroxynonenal in the Physiology and Pathology of Malaria. *Encyclopedia of Malaria* 1–18 (2013) doi:10.1007/978-1-4614-8757-9_96-1.
47. Hauck, A. K. & Bernlohr, D. A. Oxidative stress and lipotoxicity. *J. Lipid Res.* **57**, 1976–1986 (2016).
48. Majima, H. J., Nakanishi-Ueda, T. & Ozawa, T. 4-Hydroxy-2-Nonenal (4-HNE) Staining by Anti-HNE Antibody. in *Oxidants and Antioxidants* 31–34 (Humana Press, 2002).
49. Voulgaridou, G.-P., Anestopoulos, I., Franco, R., Panayiotidis, M. I. & Pappa, A. DNA damage induced by endogenous aldehydes: Current state of knowledge. *Mutation Research/Fundamental and Molecular Mechanisms of Mutagenesis* vol. 711 13–27 (2011).
50. Castro, J.P., Jung T., Grune, T., Siems,W. 4-Hydroxynonenal (HNE) modified proteins in metabolic diseases. *Free Radical Biology and Medicine* **111**, 309–315 (2017).
51. Ullrich, O., Grune, T., Henke, W., Esterbauer, H. & Siems, W. G. Identification of metabolic pathways of the lipid peroxidation product 4-hydroxynonenal by mitochondria isolated from rat kidney cortex. *FEBS Letters* vol. 352 84–86 (1994).
52. Grimsrud, P. A., Xie, H., Griffin, T. J. & Bernlohr, D. A. Oxidative Stress and Covalent Modification of Protein with Bioactive Aldehydes. *Journal of Biological Chemistry* vol. 283 21837–21841 (2008).
53. Yang, Y., Sharma, R., Sharma, A., Awasthi, S. & Awasthi, Y. C. Lipid peroxidation and cell cycle signaling: 4-hydroxynonenal, a key molecule in stress mediated signaling. *Acta Biochimica Polonica* vol. 50 319–336 (2003).
54. Leonarduzzi, G., Robbesyn, F. & Poli, G. Signaling kinases modulated by 4-hydroxynonenal. *Free*

Radical Biology and Medicine vol. 37 1694–1702 (2004).
55. Patel, V. B., Spencer, C. H., Young, T. A., Lively, M. O. & Cunningham, C. C. Effects of 4-hydroxynonenal on mitochondrial 3-hydroxy-3-methylglutaryl (HMG-CoA) synthase. *Free Radical Biology and Medicine* vol. 43 1499–1507 (2007).
56. Bosch-Morell, F., Flohe, L., Marin, N., Romero, F.J. 4-hydroxynonenal inhibits glutathione peroxidase: protection by glutathione. *Free Radical Biology and Medicine* **26**, 1383–1387 (1999).
57. Ninfali, P., Ditroilo, M., Capellacci, S. & Biagiotti, E. Rabbit brain glucose-6-phosphate dehydrogenase: biochemical properties and inactivation by free radicals and 4-hydroxy-2-nonenal. *Neuroreport* vol. 12 4149–4153 (2001).
58. Mark, R. J., Pang, Z., Geddes, J. W., Uchida, K. & Mattson, M. P. Amyloid β-Peptide Impairs Glucose Transport in Hippocampal and Cortical Neurons: Involvement of Membrane Lipid Peroxidation. *The Journal of Neuroscience* vol. 17 1046–1054 (1997).
59. Siems, W., Capuozzo, E., Lucano, A., Salerno, C. & Crifò, C. High sensitivity of plasma membrane ion transport ATPases from human neutrophils towards 4-hydroxy-2,3-trans-nonenal. *Life Sciences* vol. 73 2583–2590 (2003).
60. Awasthi, Y. C. *et al.* Role of 4-hydroxynonenal in stress-mediated apoptosis signaling. *Molecular Aspects of Medicine* vol. 24 219–230 (2003).
61. Chaudhary, P. *et al.* Mechanisms of 4-Hydroxy-2-nonenal Induced Pro- and Anti-Apoptotic Signaling. *Biochemistry* vol. 49 6263–6275 (2010).
62. Shoeb, M., Ansari, N., Srivastava, S. & Ramana, K. 4-Hydroxynonenal in the Pathogenesis and Progression of Human Diseases. *Current Medicinal Chemistry* vol. 21 230–237 (2013).
63. Vindis, C. *et al.* Lipid oxidation products and oxidized low-density lipoproteins impair platelet-derived growth factor receptor activity in smooth muscle cells: implication in atherosclerosis. *Redox Rep.* **12**, 96–100 (2007).
64. Siegel, S. J., Bieschke, J., Powers, E. T. & Kelly, J. W. The oxidative stress metabolite 4-hydroxynonenal promotes Alzheimer protofibril formation. *Biochemistry* **46**, 1503–1510 (2007).
65. Benedetti, E. *et al.* Involvement of peroxisome proliferator-activated receptor β/δ (PPAR β/δ) in BDNF signaling during aging and in Alzheimer disease: possible role of 4-hydroxynonenal (4-HNE). *Cell Cycle* **13**, 1335–1344 (2014).
66. Selley, M. L. (E)-4-Hydroxy-2-Nonenal May be Involved in the Pathogenesis of Parkinson's Disease. *Free Radical Biology and Medicine* vol. 25 169–174 (1998).
67. Newcombe, J., Li, H. & Cuzner, M. L. Low density lipoprotein uptake by macrophages in multiple sclerosis plaques: implications for pathogenesis. *Neuropathol. Appl. Neurobiol.* **20**, 152–162 (1994).
68. Pillon, N. J. *et al.* The lipid peroxidation by-product 4-hydroxy-2-nonenal (4-HNE) induces insulin resistance in skeletal muscle through both carbonyl and oxidative stress. *Endocrinology* **153**, 2099–2111 (2012).
69. Zhong, H. & Yin, H. Role of lipid peroxidation derived 4-hydroxynonenal (4-HNE) in cancer: focusing on mitochondria. *Redox Biol* **4**, 193–199 (2015).
70. Hu, W. *et al.* The major lipid peroxidation product, trans-4-hydroxy-2-nonenal, preferentially forms DNA adducts at codon 249 of human p53 gene, a unique mutational hotspot in hepatocellular carcinoma. *Carcinogenesis* **23**, 1781–1789 (2002).
71. Wang, Y. *et al.* Intraperitoneal injection of 4-hydroxynonenal (4-HNE), a lipid peroxidation product, exacerbates colonic inflammation through activation of Toll-like receptor 4 signaling. *Free Radic. Biol. Med.* **131**, 237–242 (2019).
72. Srivastava, S. K. *et al.* Attenuation of 4-hydroxynonenal-induced cataractogenesis in rat lens by butylated hydroxytoluene. *Current Eye Research* vol. 15 749–754 (1996).
73. Dick, R. A., Kwak, M. K., Sutter, T. R. & Kensler, T. W. Antioxidative function and substrate specificity of NAD(P)H-dependent alkenal/one oxidoreductase. A new role for leukotriene B4 12-hydroxydehydrogenase/15-oxoprostaglandin 13-reductase. *J. Biol. Chem.* **276**, 40803–40810 (2001).
74. Mano, J. *et al.* The NADPH:quinone oxidoreductase P1-zeta-crystallin in Arabidopsis catalyzes the alpha,beta-hydrogenation of 2-alkenals: detoxication of the lipid peroxide-derived reactive aldehydes. *Plant Cell Physiol.* **43**, 1445–1455 (2002).
75. Hartley, D. P., Ruth, J. A. & Petersen, D. R. The hepatocellular metabolism of 4-hydroxynonenal by alcohol dehydrogenase, aldehyde dehydrogenase, and glutathione S-transferase. *Arch. Biochem. Biophys.* **316**, 197–205 (1995).

76. Amunom, I. *et al.* Cytochromes P450 catalyze oxidation of α,β-unsaturated aldehydes. *Archives of Biochemistry and Biophysics* vol. 464 187–196 (2007).
77. Guéraud, F. 4-Hydroxynonenal metabolites and adducts in pre-carcinogenic conditions and cancer. *Free Radic. Biol. Med.* **111**, 196–208 (2017).
78. Ramana, K. V. *et al.* Mitogenic responses of vascular smooth muscle cells to lipid peroxidation-derived aldehyde 4-hydroxy-trans-2-nonenal (HNE): role of aldose reductase-catalyzed reduction of the HNE-glutathione conjugates in regulating cell growth. *J. Biol. Chem.* **281**, 17652–17660 (2006).
79. Frohnert, B. I. & Bernlohr, D. A. Glutathionylated products of lipid peroxidation: A novel mechanism of adipocyte to macrophage signaling. *Adipocyte* **3**, 224–229 (2014).
80. Mol, M. *et al.* Enzymatic and non-enzymatic detoxification of 4-hydroxynonenal: Methodological aspects and biological consequences. *Free Radic. Biol. Med.* **111**, 328–344 (2017).
81. Grune, T. & Davies, K. J. A. The proteasomal system and HNE-modified proteins. *Mol. Aspects Med.* **24**, 195–204 (2003).
82. Jung, T. & Grune, T. The proteasome and its role in the degradation of oxidized proteins. *IUBMB Life* **60**, 743–752 (2008).
83. Kumar Deshmukh, F., Yaffe, D., Olshina, M. A., Ben-Nissan, G. & Sharon, M. The Contribution of the 20S Proteasome to Proteostasis. *Biomolecules* **9**, (2019).
84. Ferrington, D. A. & Kapphahn, R. J. Catalytic site-specific inhibition of the 20S proteasome by 4-hydroxynonenal. *FEBS Lett.* **578**, 217–223 (2004).
85. Friguet, B. & Szweda, L. I. Inhibition of the multicatalytic proteinase (proteasome) by 4-hydroxy-2-nonenal cross-linked protein. *FEBS Lett.* **405**, 21–25 (1997).
86. Mizushima, N. Autophagy: process and function. *Genes Dev.* **21**, 2861–2873 (2007).
87. Hill, B. G., Haberzettl, P., Ahmed, Y., Srivastava, S. & Bhatnagar, A. Unsaturated lipid peroxidation-derived aldehydes activate autophagy in vascular smooth-muscle cells. *Biochem. J* **410**, 525–534 (2008).
88. Bonet-Ponce, L. *et al.* Rotenone Induces the Formation of 4-Hydroxynonenal Aggresomes. Role of ROS-Mediated Tubulin Hyperacetylation and Autophagic Flux Disruption. *Mol. Neurobiol.* **53**, 6194–6208 (2016).
89. Chondrogianni, N. *et al.* Protein damage, repair and proteolysis. *Mol. Aspects Med.* **35**, 1–71 (2014).
90. Minko, I. G. *et al.* Chemistry and biology of DNA containing 1,N(2)-deoxyguanosine adducts of the alpha,beta-unsaturated aldehydes acrolein, crotonaldehyde, and 4-hydroxynonenal. *Chem. Res. Toxicol.* **22**, 759–778 (2009).
91. Feng, Z., Hu, W., Amin, S. & Tang, M.-S. Mutational spectrum and genotoxicity of the major lipid peroxidation product, trans-4-hydroxy-2-nonenal, induced DNA adducts in nucleotide excision repair-proficient and -deficient human cells. *Biochemistry* **42**, 7848–7854 (2003).
92. Douki, T. & Ames, B. N. An HPLC-EC assay for 1,N2-propano adducts of 2'-deoxyguanosine with 4-hydroxynonenal and other alpha,beta-unsaturated aldehydes. *Chem. Res. Toxicol.* **7**, 511–518 (1994).
93. McGarry, T. *et al.* Resolution of TLR2-induced inflammation through manipulation of metabolic pathways in Rheumatoid Arthritis. *Sci. Rep.* **7**, 43165 (2017).
94. Pepi, M. *et al.* Toxicity of diatom polyunsaturated aldehydes to marine bacterial isolates reveals their mode of action. *Chemosphere* **177**, 258–265 (2017).
95. Wang, X., Yang, Y. & Huycke, M. M. Commensal bacteria drive endogenous transformation and tumour stem cell marker expression through a bystander effect. *Gut* **64**, 459–468 (2015).
96. Donath, B. *et al.* Chlamydia pneumoniae activates IKK/IκB-mediated signaling, which is inhibited by 4-HNE and following primary exposure. *Atherosclerosis* vol. 165 79–88 (2002).
97. Kurita-Ochiai, T. *et al.* Porphyromonas gingivalis promotes low-density lipoprotein oxidation and atherosclerosis. *Journal of Oral Biosciences* vol. 59 44–49 (2017).
98. Freitag, N. E., Port, G. C. & Miner, M. D. Listeria monocytogenes — from saprophyte to intracellular pathogen. *Nature Reviews Microbiology* vol. 7 623–628 (2009).
99. Kvenberg, J. E. Outbreaks of listeriosis/Listeria-contaminated foods. *Microbiol. Sci.* **5**, 355–358 (1988).
100. Heras, A. de las, de las Heras, A., Cain, R. J., Bielecka, M. K. & Vázquez-Boland, J. A. Regulation of Listeria virulence: PrfA master and commander. *Current Opinion in Microbiology* vol. 14 118–127 (2011).
101. Vázquez-Boland, J. A. *et al.* Listeria Pathogenesis and Molecular Virulence Determinants. *Clinical*

Microbiology Reviews vol. 14 584–640 (2001).
102. Tilney, L. G. & Portnoy, D. A. Actin filaments and the growth, movement, and spread of the intracellular bacterial parasite, Listeria monocytogenes. *Journal of Cell Biology* vol. 109 1597–1608 (1989).
103. Magalhaes, R., Mena, C., Ferreira, V., Silva, J., Almeida, G., Gibbs, P., and Teixeira, P. Bacteria: Listeria monocytogenes. *Encyclopedia of Food Safety* 450–461 (2014).
104. Disease Control, C. Biosafety in Microbiological and Biomedical Laboratories. (2009).
105. Woodward, J. J., Iavarone, A. T. & Portnoy, D. A. c-di-AMP secreted by intracellular Listeria monocytogenes activates a host type I interferon response. *Science* **328**, 1703–1705 (2010).
106. Dey, B. *et al.* A bacterial cyclic dinucleotide activates the cytosolic surveillance pathway and mediates innate resistance to tuberculosis. *Nat. Med.* **21**, 401–406 (2015).
107. Goldberg, M. B. Actin-based motility of intracellular microbial pathogens. *Microbiol. Mol. Biol. Rev.* **65**, 595–626, table of contents (2001).
108. O'Riordan, M., Moors, M. A. & Portnoy, D. A. Listeria intracellular growth and virulence require host-derived lipoic acid. *Science* **302**, 462–464 (2003).
109. Zorzoli, A., Grayczyk, J. P. & Alonzo, F., 3rd. Staphylococcus aureus Tissue Infection During Sepsis Is Supported by Differential Use of Bacterial or Host-Derived Lipoic Acid. *PLoS Pathog.* **12**, e1005933 (2016).
110. Nathan, C. & Cunningham-Bussel, A. Beyond oxidative stress: an immunologist's guide to reactive oxygen species. *Nature Reviews Immunology* vol. 13 349–361 (2013).
111. Patel, R. P. *et al.* Biological aspects of reactive nitrogen species. *Biochim. Biophys. Acta* **1411**, 385–400 (1999).
112. Jacobson, M. D. Reactive oxygen species and programmed cell death. *Trends in Biochemical Sciences* vol. 21 83–86 (1996).
113. Staerck, C. *et al.* Microbial antioxidant defense enzymes. *Microb. Pathog.* **110**, 56–65 (2017).
114. Uchida, K. *et al.* Michael addition-type 4-hydroxy-2-nonenal adducts in modified low-density lipoproteins: markers for atherosclerosis. *Biochemistry* **33**, 12487–12494 (1994).
115. Sayre, L. M. *et al.* 4-Hydroxynonenal-derived advanced lipid peroxidation end products are increased in Alzheimer's disease. *J. Neurochem.* **68**, 2092–2097 (1997).
116. Rahman, I. *et al.* 4-Hydroxy-2-nonenal, a specific lipid peroxidation product, is elevated in lungs of patients with chronic obstructive pulmonary disease. *Am. J. Respir. Crit. Care Med.* **166**, 490–495 (2002).
117. Paradis, V. *et al.* In situ detection of lipid peroxidation by-products in chronic liver diseases. *Hepatology* **26**, 135–142 (1997).
118. Zheng, R. *et al.* Differential metabolism of 4-hydroxynonenal in liver, lung and brain of mice and rats. *Toxicol. Appl. Pharmacol.* **279**, 43–52 (2014).
119. Dalleau, S., Baradat, M., Guéraud, F. & Huc, L. Cell death and diseases related to oxidative stress: 4-hydroxynonenal (HNE) in the balance. *Cell Death Differ.* **20**, 1615–1630 (2013).
120. Zimniak, P. Relationship of electrophilic stress to aging. *Free Radic. Biol. Med.* **51**, 1087–1105 (2011).
121. Esterbauer, H., Schaur, R. J. & Zollner, H. Chemistry and biochemistry of 4-hydroxynonenal, malonaldehyde and related aldehydes. *Free Radic. Biol. Med.* **11**, 81–128 (1991).
122. Uchida, K. 4-Hydroxy-2-nonenal: a product and mediator of oxidative stress. *Prog. Lipid Res.* **42**, 318–343 (2003).
123. Mohapatra, N. P. *et al.* Francisella acid phosphatases inactivate the NADPH oxidase in human phagocytes. *J. Immunol.* **184**, 5141–5150 (2010).
124. Fayram, D. C. Characterization of the neutrophil respiratory burst during infection with Francisella novicida. (2013).
125. Zhang, H. & Forman, H. J. Signaling by 4-hydroxy-2-nonenal: Exposure protocols, target selectivity and degradation. *Arch. Biochem. Biophys.* **617**, 145–154 (2017).
126. Parsell, D. A. & Lindquist, S. The function of heat-shock proteins in stress tolerance: degradation and reactivation of damaged proteins. *Annu. Rev. Genet.* **27**, 437–496 (1993).
127. Yura, T., Nagai, H. & Mori, H. Regulation of the heat-shock response in bacteria. *Annu. Rev. Microbiol.* **47**, 321–350 (1993).
128. Roncarati, D. & Scarlato, V. Regulation of heat-shock genes in bacteria: from signal sensing to gene expression output. *FEMS Microbiol. Rev.* **41**, 549–574 (2017).

129. Hou, F. *et al.* Structure and reaction mechanism of a novel enone reductase. *FEBS J.* **282**, 1526–1537 (2015).
130. Awada, M. *et al.* Dietary oxidized n-3 PUFA induce oxidative stress and inflammation: role of intestinal absorption of 4-HHE and reactivity in intestinal cells. *J. Lipid Res.* **53**, 2069–2080 (2012).
131. Schaur, R. J., Siems, W., Bresgen, N. & Eckl, P. M. 4-Hydroxy-nonenal-A Bioactive Lipid Peroxidation Product. *Biomolecules* **5**, 2247–2337 (2015).
132. Burczynski, M. E., Sridhar, G. R., Palackal, N. T. & Penning, T. M. The reactive oxygen species--and Michael acceptor-inducible human aldo-keto reductase AKR1C1 reduces the alpha,beta-unsaturated aldehyde 4-hydroxy-2-nonenal to 1,4-dihydroxy-2-nonene. *J. Biol. Chem.* **276**, 2890–2897 (2001).
133. Stuehr, D. J. & Marletta, M. A. Mammalian nitrate biosynthesis: mouse macrophages produce nitrite and nitrate in response to Escherichia coli lipopolysaccharide. *Proc. Natl. Acad. Sci. U. S. A.* **82**, 7738–7742 (1985).
134. Iyengar, R., Stuehr, D. J. & Marletta, M. A. Macrophage synthesis of nitrite, nitrate, and N-nitrosamines: precursors and role of the respiratory burst. *Proc. Natl. Acad. Sci. U. S. A.* **84**, 6369–6373 (1987).
135. Nathan, C. F. & Hibbs, J. B., Jr. Role of nitric oxide synthesis in macrophage antimicrobial activity. *Curr. Opin. Immunol.* **3**, 65–70 (1991).
136. Nagafuji, T., Sugiyama, M., Matsui, T., Muto, A. & Naito, S. Nitric oxide synthase in cerebral ischemia. Possible contribution of nitric oxide synthase activation in brain microvessels to cerebral ischemic injury. *Mol. Chem. Neuropathol.* **26**, 107–157 (1995).
137. Galley, H. F. & Webster, N. R. Nitric oxide in a nutshell: genetics, physiology and pathology. *Curr. Anaesth. Crit. Care* **9**, 209–213 (1998).
138. Prost, I. *et al.* Evaluation of the antimicrobial activities of plant oxylipins supports their involvement in defense against pathogens. *Plant Physiol.* **139**, 1902–1913 (2005).
139. Vaughn, S. F. & Gardner, H. W. Lipoxygenase-derived aldehydes inhibit fungi pathogenic on soybean. *J. Chem. Ecol.* **19**, 2337–2345 (1993).
140. Hébrard, M., Viala, J. P. M., Méresse, S., Barras, F. & Aussel, L. Redundant hydrogen peroxide scavengers contribute to Salmonella virulence and oxidative stress resistance. *J. Bacteriol.* **191**, 4605–4614 (2009).
141. Cybulski, R. J., Jr *et al.* Four superoxide dismutases contribute to Bacillus anthracis virulence and provide spores with redundant protection from oxidative stress. *Infect. Immun.* **77**, 274–285 (2009).
142. El-Halfawy, O. M. *et al.* Antibiotic Capture by Bacterial Lipocalins Uncovers an Extracellular Mechanism of Intrinsic Antibiotic Resistance. *MBio* **8**, (2017).
143. LoPachin, R. M. & Gavin, T. Molecular mechanisms of aldehyde toxicity: a chemical perspective. *Chem. Res. Toxicol.* **27**, 1081–1091 (2014).
144. Leichert, L. I. O., Scharf, C. & Hecker, M. Global characterization of disulfide stress in Bacillus subtilis. *J. Bacteriol.* **185**, 1967–1975 (2003).
145. Schmitz, J., Rossoni, A. W. & Maurino, V. G. Dissecting the Physiological Function of Plant Glyoxalase I and Glyoxalase I-Like Proteins. *Front. Plant Sci.* **9**, 1618 (2018).
146. van Opijnen, T., Bodi, K. L. & Camilli, A. Tn-seq: high-throughput parallel sequencing for fitness and genetic interaction studies in microorganisms. *Nat. Methods* **6**, 767–772 (2009).
147. DeJesus, M. A. *et al.* Comprehensive Essentiality Analysis of the Mycobacterium tuberculosis Genome via Saturating Transposon Mutagenesis. *MBio* **8**, (2017).
148. Ramsey, K. M. *et al.* Tn-Seq reveals hidden complexity in the utilization of host-derived glutathione in Francisella tularensis. *PLoS Pathog.* **16**, e1008566 (2020).
149. Troy, E. B. *et al.* Global Tn-seq analysis of carbohydrate utilization and vertebrate infectivity of Borrelia burgdorferi. *Mol. Microbiol.* **101**, 1003–1023 (2016).
150. Solaimanpour, S., Sarmiento, F. & Mrázek, J. Tn-seq explorer: a tool for analysis of high-throughput sequencing data of transposon mutant libraries. *PLoS One* **10**, e0126070 (2015).
151. Orsi, R. H., Bergholz, T. M., Wiedmann, M. & Boor, K. J. The Listeria monocytogenes strain 10403S BioCyc database. *Database* **2015**, (2015).
152. Kobayashi, K. *et al.* Essential Bacillus subtilis genes. *Proc. Natl. Acad. Sci. U. S. A.* **100**, 4678–4683 (2003).
153. Goodall, E. C. A. *et al.* The Essential Genome of Escherichia coli K-12. *MBio* **9**, (2018).
154. Poulsen, B. E. *et al.* Defining the core essential genome of Pseudomonas aeruginosa. *Proc. Natl. Acad. Sci. U. S. A.* **116**, 10072–10080 (2019).

155. Commichau, F. M., Heidemann, J. L., Ficner, R. & Stülke, J. Making and Breaking of an Essential Poison: the Cyclases and Phosphodiesterases That Produce and Degrade the Essential Second Messenger Cyclic di-AMP in Bacteria. *J. Bacteriol.* **201**, (2019).
156. Wagner, W. P., Helmig, D. & Fall, R. Isoprene biosynthesis in Bacillus subtilis via the methylerythritol phosphate pathway. *J. Nat. Prod.* **63**, 37–40 (2000).
157. Deuerling, E., Schulze-Specking, A., Tomoyasu, T., Mogk, A. & Bukau, B. Trigger factor and DnaK cooperate in folding of newly synthesized proteins. *Nature* **400**, 693–696 (1999).
158. Lupoli, T. J., Fay, A., Adura, C., Glickman, M. S. & Nathan, C. F. Reconstitution of a Mycobacterium tuberculosis proteostasis network highlights essential cofactor interactions with chaperone DnaK. *Proc. Natl. Acad. Sci. U. S. A.* **113**, E7947–E7956 (2016).
159. Fay, A. & Glickman, M. S. An essential nonredundant role for mycobacterial DnaK in native protein folding. *PLoS Genet.* **10**, e1004516 (2014).
160. Schramm, F. D., Heinrich, K., Thüring, M., Bernhardt, J. & Jonas, K. An essential regulatory function of the DnaK chaperone dictates the decision between proliferation and maintenance in Caulobacter crescentus. *PLoS Genet.* **13**, e1007148 (2017).
161. Muchaamba, F., Eshwar, A. K., von Ah, U., Stevens, M. J. A. & Tasara, T. Evolution of Listeria monocytogenes During a Persistent Human Prosthetic Hip Joint Infection. *Front. Microbiol.* **11**, (2020).
162. Flores-Kim, J. & Darwin, A. J. Phage shock protein C (PspC) of Yersinia enterocolitica is a polytopic membrane protein with implications for regulation of the Psp stress response. *J. Bacteriol.* **194**, 6548–6559 (2012).
163. Kelley, L. A., Mezulis, S., Yates, C. M., Wass, M. N. & Sternberg, M. J. E. The Phyre2 web portal for protein modeling, prediction and analysis. *Nat. Protoc.* **10**, 845–858 (2015).
164. Pettersen, E. F. *et al.* UCSF Chimera--a visualization system for exploratory research and analysis. *J. Comput. Chem.* **25**, (2004).
165. Yu, N. Y. *et al.* PSORTb 3.0: improved protein subcellular localization prediction with refined localization subcategories and predictive capabilities for all prokaryotes. *Bioinformatics* **26**, 1608 (2010).
166. Jeffery, C. Intracellular proteins moonlighting as bacterial adhesion factors. *AIMS Microbiology* **4**, 362 (2018).
167. Cotter, P. D., Guinane, C. M. & Hill, C. The LisRK signal transduction system determines the sensitivity of Listeria monocytogenes to nisin and cephalosporins. *Antimicrob. Agents Chemother.* **46**, 2784–2790 (2002).
168. Nielsen, P. K. *et al.* Genome-wide transcriptional profiling of the cell envelope stress response and the role of LisRK and CesRK in Listeria monocytogenes. *Microbiology* **158**, 963–974 (2012).
169. Nguyen, T. T. H. *et al.* Genome-wide responses to carbonyl electrophiles in Bacillus subtilis: control of the thiol-dependent formaldehyde dehydrogenase AdhA and cysteine proteinase YraA by the MerR-family regulator YraB (AdhR). *Mol. Microbiol.* **71**, 876–894 (2009).
170. Jo, J.-E. *et al.* Cloning, expression, and characterization of an aldehyde dehydrogenase from Escherichia coli K-12 that utilizes 3-Hydroxypropionaldehyde as a substrate. *Appl. Microbiol. Biotechnol.* **81**, 51–60 (2008).
171. Jang, E. J. *et al.* Activation of proinflammatory signaling by 4-hydroxynonenal-Src adducts in aged kidneys. *Oncotarget* **7**, 50864–50874 (2016).
172. Yang, H.-J. *et al.* 4-HNE induces proinflammatory cytokines of human retinal pigment epithelial cells by promoting extracellular efflux of HSP70. *Exp. Eye Res.* **188**, 107792 (2019).
173. Zhang, X.-M., Guo, L., Huang, X., Li, Q.-M. & Chi, M.-H. 4-Hydroxynonenal Regulates TNF-α Gene Transcription Indirectly via ETS1 and microRNA-29b in Human Adipocytes Induced From Adipose Tissue-Derived Stromal Cells. *Anat. Rec.* **299**, 1145–1152 (2016).
174. Breitzig, M., Bhimineni, C., Lockey, R. & Kolliputi, N. 4-Hydroxy-2-nonenal: a critical target in oxidative stress? *Am. J. Physiol. Cell Physiol.* **311**, C537–C543 (2016).
175. McFarland, A. P. *et al.* Sensing of Bacterial Cyclic Dinucleotides by the Oxidoreductase RECON Promotes NF-κB Activation and Shapes a Proinflammatory Antibacterial State. *Immunity* **46**, 433–445 (2017).
176. McClure, R. *et al.* Computational analysis of bacterial RNA-Seq data. *Nucleic Acids Res.* **41**, e140 (2013).
177. Sigal, N., Pasechnek, A. & Herskovits, A. A. RNA Purification from Intracellularly Grown Listeria

monocytogenes in Macrophage Cells. *J. Vis. Exp.* (2016) doi:10.3791/54044.
178. Humann, J., Bjordahl, R., Andreasen, K. & Lenz, L. L. Expression of the p60 autolysin enhances NK cell activation and is required for listeria monocytogenes expansion in IFN-gamma-responsive mice. *J. Immunol.* **178**, 2407–2414 (2007).
179. Tomoyasu, T., Mogk, A., Langen, H., Goloubinoff, P. & Bukau, B. Genetic dissection of the roles of chaperones and proteases in protein folding and degradation in the Escherichia coli cytosol. *Mol. Microbiol.* **40**, 397–413 (2001).
180. Nguyen, H. D., Phan, T. T. P. & Schumann, W. Expression vectors for the rapid purification of recombinant proteins in Bacillus subtilis. *Curr. Microbiol.* **55**, 89–93 (2007).
181. Gallagher, L. A. Methods for Tn-seq analysis in Acinetobacter baumannii. *Methods Mol. Biol.* **1946**, 115–134 (2019).

Table 1: RNA-seq dataset of L. monocytogenes treated with 4-HNE versus mock

Data presented here are sorted by q-value (statistical significance) < 0.05						
Synonym	Product	Expression mock	Expression HNE	qValue wt vs HNE	hne fold over mock	lmo numbers
LMRG_00296	oxidoreductase	3	716	0	238.6666667	lmo0613
LMRG_00295	hypothetical protein	3	542	0	180.6666667	lmo0612
predicted RNA	antisense: LMRG_00484	15	2673	0	178.2	#N/A
LMRG_00999	mercuric ion binding protein	2	332	0	166	lmo1852
LMRG_01869	hypothetical protein	41	6735	0	164.2682927	lmo2829
LMRG_02304	peptidoglycan bound protein	1	137	0	137	lmo0880
predicted RNA	-	19	2296	0	120.8421053	#N/A
LMRG_00177	hypothetical protein	63	6244	0	99.11111111	lmo0496
LMRG_02097	ATP-dependent Clp protease ATP-binding subunit ClpE	47	4494	0	95.61702128	lmo0997
LMRG_01000	Cu2+-exporting ATPase	33	2999	0	90.87878788	lmo1853
LMRG_01001	hypothetical protein	18	1628	0	90.44444444	lmo1854
LMRG_02351	hypothetical protein	3	260	0	86.66666667	lmo0102
LMRG_00484	YceI like family protein	75	5695	0	75.93333333	lmo0796
LMRG_01602	hypothetical protein	30	1977	0	65.9	lmo2230
predicted RNA	antisense: LMRG_02097	8	527	0	65.875	#N/A
LMRG_02352	hypothetical protein	2	123	0	61.5	lmo0103
LMRG_00333	hypothetical protein	5	306	0	61.2	lmo0646
predicted RNA	antisense: LMRG_01626	3	183	0	61	#N/A
LMRG_01633	OsmC/Ohr family protein	12	668	0	55.66666667	lmo2199
LMRG_02052	hypothetical protein	2	83	0	41.5	lmo0953
LMRG_01632	MarR family transcriptional regulator	69	2700	0	39.13043478	lmo2200
predicted RNA	antisense: LMRG_00177	6	226	0	37.66666667	#N/A
LMRG_00482	hypothetical protein	19	714	0	37.57894737	lmo0794
predicted RNA	-	14	476	0	34	#N/A
LMRG_02677	CtsR family transcriptional regulator	6	188	0	31.33333333	lmo0229
predicted RNA	-	8	244	0	30.5	#N/A
LMRG_00129	hypothetical protein	8	239	0	29.875	lmo0437
LMRG_01948	general stress protein 26	33	973	0	29.48484848	lmo2748
LMRG_00446	hypothetical protein	13	378	0	29.07692308	lmo0758
LMRG_02675	ATP:guanido phosphotransferase	12	344	0	28.66666667	lmo0231
LMRG_01674	hypothetical protein	59	1650	0	27.96610169	lmo2158
LMRG_02676	hypothetical protein	12	319	0	26.58333333	lmo0230
LMRG_00581	Clp protease	51	1311	0	25.70588235	lmo1138
LMRG_00448	hypothetical protein	6	154	0	25.66666667	lmo0760
LMRG_00137	hypothetical protein	15	374	0	24.93333333	lmo0445
LMRG_02646	internalin C2	6	140	1.17E-285	23.33333333	lmo0263
LMRG_00447	glyoxylase	4	92	1.91E-252	23	lmo0759
predicted RNA	-	7	159	7.63E-193	22.71428571	#N/A
LMRG_00583	hypothetical protein	16	344	1.04E-243	21.5	lmo1140
LMRG_01626	ATP-dependent chaperone ClpB	80	1707	2.00E-230	21.3375	lmo2206

Table 1: RNA-seq dataset of L. monocytogenes treated with 4-HNE versus mock

LMRG_01029	30S ribosomal protein S14	40	852	4.55E-255	21.3	lmo1882
LMRG_01627	phosphoglycerate mutase	154	3240	4.37E-233	21.03896104	lmo2205
LMRG_00334	hypothetical protein	37	771	4.93E-241	20.83783784	lmo0647
LMRG_02768	hypothetical protein	4	83	9.40E-207	20.75	lmo1694
LMRG_01754	phosphate transport system regulatory protein PhoU	5	102	6.31E-187	20.4	lmo2494
LMRG_00489	hypothetical protein	14	276	4.94E-214	19.71428571	lmo0800
LMRG_02611	succinyl-diaminopimelate desuccinylase	6	117	2.33E-182	19.5	lmo0265
LMRG_01764	membrane protein	72	1388	3.23E-219	19.27777778	lmo2484
LMRG_02736	hypothetical protein	9	171	3.09E-199	19	lmo2391
predicted RNA	-	43	815	1.23E-167	18.95348837	#N/A
predicted RNA	antisense: LMRG_00335	22	414	7.52E-178	18.81818182	#N/A
LMRG_01219	chaperonin GroS	81	1484	4.17E-188	18.32098765	lmo2069
LMRG_02000	dihydroxyacetone kinase	4	72	1.49E-144	18	lmo2697
predicted RNA	antisense: LMRG_01296	13	233	1.77E-235	17.92307692	#N/A
LMRG_00285	hypothetical protein	6	107	2.64E-116	17.83333333	lmo0602
LMRG_00449	hypothetical protein	4	71	3.23E-110	17.75	lmo0761
LMRG_02693	CDF family cation efflux system protein	22	389	1.54E-161	17.68181818	lmo2575
LMRG_02002	dihydroxyacetone kinase DhaK subunit	23	405	5.57E-165	17.60869565	lmo2695
predicted RNA	-	14	241	9.22E-157	17.21428571	#N/A
LMRG_02674	ATP-dependent Clp protease ATP-binding subunit ClpC	37	626	9.91E-140	16.91891892	lmo0232
LMRG_02808	hypothetical protein	7	118	2.54E-130	16.85714286	lmo2132
LMRG_02146	Mg2+ transporter-C family protein	16	269	5.53E-139	16.8125	lmo2602
LMRG_02218	universal stress protein	12	201	1.25E-136	16.75	lmo2673
LMRG_00666	hypothetical protein	14	234	4.12E-137	16.71428571	lmo1220
LMRG_00293	internalin	6	100	2.29E-133	16.66666667	lmo0610
LMRG_00411	pyruvate oxidase	42	697	3.15E-148	16.5952381	lmo0722
LMRG_02697	nicotinamidase	24	398	8.74E-139	16.58333333	lmo2571
LMRG_02701	hypothetical protein	22	359	3.17E-133	16.31818182	lmo2567
LMRG_01972	DNA binding 3-demethylubiquinone-9 3-methyltransferase domain-containing protein	51	784	3.22E-127	15.37254902	lmo2724
predicted RNA	antisense: LMRG_02046	14	213	3.84E-177	15.21428571	#N/A
LMRG_01675	hypothetical protein	9	134	8.77E-110	14.88888889	lmo2157
LMRG_00221	tagatose 1,6-diphosphate aldolase	183	2721	1.34E-99	14.86885246	lmo0539
LMRG_01814	glutamate decarboxylase	33	484	1.49E-147	14.66666667	lmo2434
LMRG_02001	dihydroxyacetone kinase L subunit	16	233	1.17E-98	14.5625	lmo2696
predicted RNA	antisense: LMRG_02042	16	232	1.45E-174	14.5	#N/A
predicted RNA	antisense: LMRG_00221	15	214	9.08E-169	14.26666667	#N/A
LMRG_02003	OsmC/Ohr family protein	35	499	1.57E-103	14.25714286	lmo0903
predicted RNA	antisense: LMRG_00364	14	198	4.14E-134	14.14285714	#N/A
LMRG_01780	Clp protease	241	3361	2.53E-101	13.94605809	lmo2468
predicted RNA	antisense: LMRG_02779	31	431	8.30E-100	13.90322581	#N/A
LMRG_02382	hypothetical protein	5	67	1.75E-124	13.4	lmo0133
predicted RNA	-	35	469	6.70E-92	13.4	#N/A

Table 1: RNA-seq dataset of L. monocytogenes treated with 4-HNE versus mock

predicted RNA	antisense: LMRG_00073	15	199	1.12E-122	13.26666667	#N/A
predicted RNA	antisense: LMRG_00704	24	317	5.17E-154	13.20833333	#N/A
LMRG_00131	hypothetical protein	6	79	3.36E-70	13.16666667	lmo0439
LMRG_01236	peptidoglycan binding protein	16	207	4.29E-84	12.9375	lmo2085
LMRG_02633	50S ribosomal protein L25 Ctc-form	13	167	3.18E-71	12.84615385	lmo0211
predicted RNA	antisense: LMRG_01869	23	295	1.89E-146	12.82608696	#N/A
predicted RNA	-	37	465	4.87E-132	12.56756757	#N/A
LMRG_02472	arginine deiminase	42	527	1.70E-94	12.54761905	lmo0043
LMRG_00273	hypothetical protein	5	62	1.74E-56	12.4	lmo0591
LMRG_01761	hypothetical protein	20	241	1.17E-69	12.05	lmo2487
LMRG_02147	amidase	10	120	3.25E-63	12	lmo2603
LMRG_01619	hypothetical protein	41	486	2.61E-69	11.85365854	lmo2213
LMRG_02290	hypothetical protein	46	514	4.62E-52	11.17391304	#N/A
LMRG_02036	hypothetical protein	7	77	1.99E-69	11	lmo0937
LMRG_02295	hypothetical protein	11	121	8.24E-51	11	lmo0871
LMRG_01753	phosphate ABC transporter ATP-binding protein	13	142	2.10E-50	10.92307692	lmo2495
predicted RNA	-	36	390	1.30E-88	10.83333333	#N/A
predicted RNA	-	23	247	1.02E-92	10.73913043	#N/A
LMRG_01763	PspC domain-containing protein	46	485	9.81E-47	10.54347826	lmo2485
predicted RNA	antisense: LMRG_00365	79	826	2.26E-45	10.4556962	#N/A
LMRG_02013	succinate-semialdehyde dehydrogenase	31	322	1.48E-65	10.38709677	lmo0913
LMRG_00341	hypothetical protein	81	831	1.21E-48	10.25925926	lmo0654
LMRG_02696	riboflavin biosynthesis protein RibD domain-containing protein	35	355	2.82E-47	10.14285714	lmo2572
LMRG_02695	NADPH2:quinone reductase	14	142	9.70E-42	10.14285714	lmo2573
LMRG_02247	hypothetical protein	113	1146	3.80E-61	10.14159292	lmo0822
LMRG_00272	hypothetical protein	16	158	4.99E-44	9.875	lmo0590
LMRG_02732	hypothetical protein	7	69	3.37E-37	9.857142857	lmo2387
LMRG_02398	zinc transport system substrate-binding protein	9	86	1.56E-31	9.555555556	lmo0153
predicted RNA	-	30	285	1.62E-51	9.5	#N/A
LMRG_02094	hypothetical protein	8	76	1.20E-33	9.5	lmo0994
predicted RNA	antisense: LMRG_00288	29	266	1.50E-55	9.172413793	#N/A
LMRG_02622	listeriolysin regulatory protein	55	490	1.14E-42	8.909090909	lmo0200
predicted RNA	-	128	1134	3.82E-31	8.859375	#N/A
LMRG_02011	hypothetical protein	24	211	4.50E-33	8.791666667	lmo0911
predicted RNA	-	36	315	5.00E-29	8.75	#N/A
LMRG_02042	hypothetical protein	574	4865	2.49E-28	8.475609756	lmo0944
predicted RNA	-	24	201	3.30E-25	8.375	#N/A
LMRG_01757	hydrolase	58	475	2.44E-33	8.189655172	lmo2491
LMRG_01153	aryl-alcohol dehydrogenase	11	90	2.59E-25	8.181818182	lmo2005
LMRG_01816	hypothetical protein	26	212	1.29E-25	8.153846154	lmo2432
LMRG_01353	hypothetical protein	15	120	9.60E-25	8	lmo1613
predicted RNA	-	26	207	6.40E-37	7.961538462	#N/A

Table 1: RNA-seq dataset of L. monocytogenes treated with 4-HNE versus mock

predicted RNA	antisense: LMRG_01149	29	229	1.18E-33	7.896551724	#N/A
LMRG_02734	hypothetical protein	58	456	1.24E-26	7.862068966	lmo2389
predicted RNA	-	36	277	1.50E-21	7.694444444	#N/A
LMRG_00897	transcriptional regulator ZurR	91	699	3.06E-30	7.681318681	lmo1445
LMRG_02476	hypothetical protein	17	130	3.36E-23	7.647058824	lmo0047
predicted RNA	-	82	622	1.82E-21	7.585365854	#N/A
LMRG_02738	hypothetical protein	14	106	9.18E-22	7.571428571	lmo2393
LMRG_01680	thioredoxin	99	742	6.82E-26	7.494949495	lmo2152
predicted RNA	-	104	778	4.76E-23	7.480769231	#N/A
LMRG_01444	hypothetical protein	111	823	2.31E-27	7.414414414	lmo1526
LMRG_01755	HTH-type transcriptional repressor czrA	25	185	2.83E-19	7.4	lmo2493
LMRG_02579	hypothetical protein	284	2051	5.97E-09	7.221830986	lmo0292
predicted RNA	antisense: LMRG_00364	33	235	8.76E-27	7.121212121	#N/A
LMRG_00357	hypothetical protein	10	71	8.56E-18	7.1	lmo0669
LMRG_02415	hypothetical protein	174	1233	2.19E-17	7.086206897	lmo0170
predicted RNA	antisense: LMRG_02779	31	216	4.02E-31	6.967741935	#N/A
LMRG_01296	zinc transport system substrate-binding protein	339	2339	7.35E-14	6.899705015	lmo1671
LMRG_00928	heat-inducible transcription repressor HrcA	139	954	1.44E-19	6.863309353	lmo1475
LMRG_00292	hypothetical protein	38	259	2.51E-19	6.815789474	lmo0609
LMRG_01737	sigma-54 modulation protein	92	619	9.23E-23	6.72826087	lmo2511
LMRG_02884	secreted protein	18	121	4.42E-17	6.722222222	lmo0479
LMRG_00926	chaperone DnaK	276	1849	6.39E-07	6.699275362	lmo1473
LMRG_01028	hypothetical protein	81	537	1.75E-17	6.62962963	lmo1881
LMRG_02679	hypothetical protein	10	66	3.04E-17	6.6	lmo2588
predicted RNA	-	31	202	2.61E-26	6.516129032	#N/A
LMRG_02215	hypothetical protein	14	91	4.97E-16	6.5	lmo2670
LMRG_02239	hypothetical protein	269	1736	1.84E-15	6.453531599	lmo2692
LMRG_02731	hypothetical protein	13	83	5.22E-14	6.384615385	lmo2386
LMRG_01140	alpha-acetolactate decarboxylase	347	2173	1.58E-12	6.262247839	lmo1992
LMRG_00521	hypothetical protein	17	106	2.08E-13	6.235294118	lmo1059
predicted RNA	-	133	829	5.00E-14	6.233082707	#N/A
LMRG_00743	glycerol-3-phosphate dehydrogenase	32	198	5.21E-18	6.1875	lmo1293
LMRG_01431	glycerol uptake facilitator protein	12	73	6.40E-12	6.083333333	lmo1539
predicted RNA	-	56	340	7.37E-17	6.071428571	#N/A
LMRG_01762	hypothetical protein	31	188	2.63E-16	6.064516129	lmo2486
LMRG_01218	chaperonin GroL	281	1684	5.23E-06	5.992882562	lmo2068
LMRG_02694	hypothetical protein	241	1407	4.30E-14	5.838174274	lmo2574
LMRG_01756	hypothetical protein	338	1964	2.88E-13	5.810650888	lmo2492
predicted RNA	-	168	971	2.98E-13	5.779761905	#N/A
LMRG_02700	hypothetical protein	14	80	2.05E-11	5.714285714	lmo2568
LMRG_01573	hypothetical protein	14	79	1.95E-09	5.642857143	lmo2258
LMRG_02331	hypothetical protein	24	133	3.16E-10	5.541666667	lmo0083

Table 1: RNA-seq dataset of L. monocytogenes treated with 4-HNE versus mock

LMRG_00472	mannose-specific PTS system IIA component	21	116	1.38E-10	5.523809524	lmo0784
LMRG_01815	tributyrin esterase	120	658	1.48E-10	5.483333333	lmo2433
LMRG_00679	thioredoxin	104	569	2.18E-12	5.471153846	lmo1233
LMRG_02248	aldo/keto reductase	111	604	2.23E-10	5.441441441	lmo0823
LMRG_02813	hypothetical protein	13	70	3.75E-09	5.384615385	lmo1789
predicted RNA	antisense: LMRG_00288	144	768	7.93E-11	5.333333333	#N/A
LMRG_02609	hypothetical protein	25	131	1.77E-10	5.24	lmo0267
LMRG_02055	N-acetylglucosamine-6-phosphate deacetylase	168	880	5.95E-09	5.238095238	lmo0956
LMRG_01656	hypothetical protein	17	89	1.72E-09	5.235294118	lmo2176
LMRG_01794	hypothetical protein	13	68	9.42E-10	5.230769231	lmo2454
LMRG_02812	MarR family transcriptional regulator	39	202	6.79E-10	5.179487179	lmo1788
LMRG_01384	thiol peroxidase	43	222	4.11E-10	5.162790698	lmo1583
LMRG_00345	endonuclease III	13	66	1.24E-08	5.076923077	lmo0658
LMRG_00879	osmoprotectant transport system permease	43	218	2.60E-10	5.069767442	lmo1427
LMRG_02056	glucosamine-6-phosphate isomerase	59	299	8.90E-12	5.06779661	lmo0957
predicted RNA	antisense: LMRG_02397	80	403	8.77E-09	5.0375	#N/A
LMRG_05029	Met tRNA	81	403	5.84E-09	4.975308642	#N/A
LMRG_00878	osmoprotectant transport system substrate-binding protein	79	391	4.62E-09	4.949367089	lmo1426
LMRG_01641	arsenate reductase	24	118	1.05E-07	4.916666667	lmo2191
LMRG_02054	hypothetical protein	50	243	8.38E-11	4.86	lmo0955
LMRG_01491	HTH-type transcriptional regulator ytlI	27	131	1.45E-08	4.851851852	lmo2352
LMRG_01795	hypothetical protein	161	779	2.32E-08	4.838509317	lmo2453
predicted RNA	antisense: LMRG_02397	53	256	1.65E-08	4.830188679	#N/A
LMRG_01822	arsenate reductase	72	346	9.16E-09	4.805555556	lmo2426
predicted RNA	antisense: LMRG_01678	93	446	3.44E-08	4.795698925	#N/A
LMRG_00469	mannose-specific PTS system IID component	13	62	1.15E-08	4.769230769	lmo0781
LMRG_02397	peptide/nickel transport system substrate-binding protein	1002	4775	0.005247719	4.765469062	lmo0152
LMRG_00488	hypothetical protein	107	509	3.27E-08	4.757009346	lmo0799
LMRG_00826	peptidase T-like protein	62	294	2.14E-08	4.741935484	lmo1375
LMRG_00877	osmoprotectant transport system permease	43	203	7.10E-09	4.720930233	lmo1425
predicted RNA	antisense: LMRG_01840 LMRG_01839	272	1280	5.55E-09	4.705882353	#N/A
LMRG_01066	hypothetical protein	73	340	3.46E-10	4.657534247	lmo1919
LMRG_01679	ribonucleotide reductase-associated flavodoxin	204	949	1.84E-07	4.651960784	lmo2153
LMRG_00470	mannose-specific PTS system IIC component	43	200	7.17E-09	4.651162791	lmo0782
LMRG_00294	FMN-dependent NADH-azoreductase 1	24	111	2.83E-07	4.625	lmo0611
LMRG_01469	hypothetical protein	95	436	2.53E-08	4.589473684	lmo1501
LMRG_00132	hypothetical protein	50	227	1.15E-07	4.54	lmo0440
LMRG_00925	chaperone DnaJ	105	471	3.15E-07	4.485714286	lmo1472
LMRG_02764	hypothetical protein	228	1021	2.47E-06	4.478070175	lmo1690
LMRG_01207	protoheme IX farnesyltransferase	15	67	1.93E-06	4.466666667	lmo2057
LMRG_01068	hypothetical protein	24	107	3.84E-07	4.458333333	lmo1921
predicted RNA	-	47	209	2.45E-11	4.446808511	#N/A

Table 1: RNA-seq dataset of L. monocytogenes treated with 4-HNE versus mock

LMRG_00885	glutathione reductase	18	80	1.03E-06	4.444444444	lmo1433
LMRG_02076	hypothetical protein	18	80	3.98E-06	4.444444444	lmo0976
LMRG_00290	ABC transporter	70	311	4.35E-07	4.442857143	lmo0607
predicted RNA	antisense: LMRG_01556	60	266	2.64E-06	4.433333333	#N/A
LMRG_01154	acetolactate synthase catabolic	85	376	2.83E-07	4.423529412	lmo2006
LMRG_00927	co-chaperone GrpE	74	326	9.01E-09	4.405405405	lmo1474
LMRG_02350	hypothetical protein	164	704	9.58E-09	4.292682927	lmo0101
LMRG_02320	sigma-B negative regulator	24	103	2.85E-06	4.291666667	lmo0896
LMRG_00836	hypothetical protein	207	885	8.45E-06	4.275362319	lmo1384
LMRG_00880	osmoprotectant transport system ATP-binding protein	62	264	2.14E-06	4.258064516	lmo1428
predicted RNA	antisense: LMRG_02384	72	306	6.76E-06	4.25	#N/A
predicted RNA	-	42	177	2.49E-09	4.214285714	#N/A
LMRG_02053	hypothetical protein	32	133	8.57E-06	4.15625	lmo0954
LMRG_02666	ribonuclease III family protein	25	103	1.17E-05	4.12	lmo0240
predicted RNA	antisense: LMRG_02397	54	221	7.03E-06	4.092592593	#N/A
LMRG_00891	superoxide dismutase	110	450	2.97E-06	4.090909091	lmo1439
LMRG_00289	transcription regulator MarR family protein	183	748	8.08E-06	4.087431694	lmo0606
LMRG_02216	hypothetical protein	16	65	2.31E-05	4.0625	lmo2671
LMRG_01690	hypothetical protein	34	138	2.03E-06	4.058823529	lmo2557
LMRG_01850	phosphatidylglycerophosphatase A	76	307	9.10E-07	4.039473684	lmo2398
LMRG_02758	hypothetical protein	26	105	9.71E-06	4.038461538	lmo1684
LMRG_02845	GntR family transcriptional regulator	34	137	6.75E-06	4.029411765	lmo0902
LMRG_00291	ABC transporter	152	610	1.44E-04	4.013157895	lmo0608
LMRG_02414	sugar uptake protein	28	112	1.18E-05	4	lmo0169
predicted RNA	antisense: LMRG_05509	42	167	3.33E-06	3.976190476	#N/A
LMRG_01770	thioredoxin-disulfide reductase	90	356	2.26E-05	3.955555556	lmo2478
LMRG_02869	mannose-specific PTS system IIB component	17	67	8.85E-05	3.941176471	lmo0783
predicted RNA	antisense: LMRG_05515	42	165	5.69E-06	3.928571429	#N/A
LMRG_00261	hypothetical protein	56	220	1.95E-05	3.928571429	lmo0579
LMRG_01851	thioredoxin-like protein	23	89	1.88E-05	3.869565217	lmo2397
LMRG_01678	ribonucleoside-diphosphate reductase	617	2371	0.039824699	3.842787682	lmo2154
LMRG_02667	cysteinyl-tRNA synthetase	54	207	3.60E-05	3.833333333	lmo0239
LMRG_02665	TrmH family RNA methyltransferase group 3	63	241	1.51E-06	3.825396825	lmo0241
LMRG_00884	hypothetical protein	337	1276	2.19E-04	3.786350148	lmo1432
LMRG_02082	deblocking aminopeptidase	22	83	5.76E-05	3.772727273	lmo0982
LMRG_00266	hypothetical protein	135	508	5.74E-05	3.762962963	lmo0584
LMRG_00707	hypothetical protein	54	203	2.40E-06	3.759259259	lmo1258
predicted RNA	antisense: LMRG_02771	49	184	7.32E-08	3.755102041	#N/A
LMRG_00032	hypothetical protein	27	101	1.99E-04	3.740740741	lmo0341
LMRG_05008	Arg tRNA	50	187	1.45E-04	3.74	#N/A
LMRG_00898	zinc transport system permease	61	228	1.63E-05	3.737704918	lmo1446
LMRG_02663	RNA polymerase sporulation-specific sigma factor	181	673	1.27E-04	3.718232044	lmo0243

Table 1: RNA-seq dataset of L. monocytogenes treated with 4-HNE versus mock

LMRG_01937	hypothetical protein	21	78	9.21E-05	3.714285714	lmo2759
LMRG_00278	hypothetical protein	78	289	7.49E-06	3.705128205	lmo0596
LMRG_02786	carbonic anhydrase	33	122	8.27E-05	3.696969697	lmo0811
LMRG_01114	hypothetical protein	153	558	3.50E-04	3.647058824	lmo1967
LMRG_01297	hypothetical protein	117	425	5.59E-05	3.632478632	lmo1670
predicted RNA	antisense: LMRG_00515 LMRG_00514	119	430	1.75E-04	3.613445378	#N/A
LMRG_01870	hypothetical protein	53	190	2.12E-04	3.58490566	lmo2828
LMRG_00337	membrane protein	31	111	2.04E-04	3.580645161	lmo0650
LMRG_02349	hypothetical protein	169	605	6.05E-05	3.579881657	lmo0100
LMRG_00753	cell division suppressor protein yneA	19	68	5.66E-04	3.578947368	lmo1303
LMRG_00745	host factor-I protein	243	867	5.76E-05	3.567901235	lmo1295
LMRG_02959	multidrug resistance protein	37	131	1.00E-05	3.540540541	lmo1712
predicted RNA	antisense: LMRG_01609	75	262	5.43E-04	3.493333333	#N/A
LMRG_00835	isopentenyl-diphosphate delta-isomerase type 2	292	1019	0.002406516	3.489726027	lmo1383
LMRG_02063	hypothetical protein	70	244	1.20E-04	3.485714286	lmo0964
LMRG_02317	anti-sigma-B factor antagonist	77	267	1.85E-04	3.467532468	lmo0893
LMRG_00354	antibiotic transport system ATP-binding protein	82	282	4.34E-04	3.43902439	lmo0667
LMRG_00899	zinc uptake system ATP-binding protein zurA	55	189	3.94E-05	3.436363636	lmo1447
LMRG_01823	glycine cleavage system H protein	37	127	4.03E-04	3.432432432	lmo2425
LMRG_02050	hypothetical protein	38	130	2.17E-04	3.421052632	lmo0951
LMRG_01811	hypothetical protein	56	191	4.20E-04	3.410714286	lmo2437
LMRG_00258	hypothetical protein	18	61	3.96E-04	3.388888889	lmo0576
LMRG_02643	type III pantothenate kinase	149	504	5.73E-04	3.382550336	lmo0221
LMRG_02644	chaperonin HslO	41	138	1.68E-04	3.365853659	lmo0222
LMRG_01556	gp27	114	383	4.07E-04	3.359649123	#N/A
LMRG_02714	general stress protein 13	143	480	6.94E-05	3.356643357	lmo2369
LMRG_01615	hypothetical protein	87	292	3.01E-04	3.356321839	lmo2217
LMRG_02735	hypothetical protein	159	527	7.10E-04	3.314465409	lmo2390
LMRG_02445	cytochrome aa3 quinol oxidase subunit IV	31	102	0.00194844	3.290322581	lmo0016
LMRG_00520	hypothetical protein	58	190	0.001066446	3.275862069	lmo1058
LMRG_01365	hypothetical protein	81	265	2.92E-04	3.271604938	lmo1602
predicted RNA	antisense: LMRG_02224	73	238	0.001730138	3.260273973	#N/A
LMRG_01796	carboxylesterase	47	153	4.39E-04	3.255319149	lmo2452
predicted RNA	antisense: LMRG_05511	75	244	0.001100033	3.253333333	#N/A
LMRG_01357	thioredoxin-like protein ytpP	29	93	0.003804507	3.206896552	lmo1609
LMRG_02718	cellobiose-specific PTS system IIB component	31	99	0.002545682	3.193548387	lmo2373
LMRG_00235	hypothetical protein	410	1307	0.006174283	3.187804878	lmo0553
LMRG_02293	hypothetical protein	22	70	0.001841892	3.181818182	lmo0869
predicted RNA	antisense: LMRG_02834	111	353	0.001722101	3.18018018	#N/A
LMRG_02245	hypothetical protein	29	92	0.001924661	3.172413793	lmo0820
LMRG_05032	Arg tRNA	58	184	0.002078209	3.172413793	#N/A
predicted RNA	antisense: LMRG_01571	112	355	0.001936706	3.169642857	#N/A

Table 1: RNA-seq dataset of L. monocytogenes treated with 4-HNE versus mock

LMRG_00103	pyruvate,water dikinase	25	79	0.001765837	3.16	lmo0410
LMRG_02041	starvation-inducible DNA-binding protein	846	2651	0.029780284	3.13356974	lmo0943
LMRG_01113	hypothetical protein	94	293	0.001053115	3.117021277	lmo1966
LMRG_02007	hypothetical protein	83	258	0.001066446	3.108433735	lmo0907
LMRG_02057	GntR family transcriptional regulator	48	149	0.001066276	3.104166667	lmo0958
LMRG_02610	hypothetical protein	31	96	0.002731204	3.096774194	lmo0266
LMRG_01575	protease I	32	99	0.002100988	3.09375	lmo2256
LMRG_02263	MarR family transcriptional regulator	32	99	0.002865296	3.09375	lmo0840
LMRG_01833	FeS assembly ATPase SufC	278	857	0.006208014	3.082733813	lmo2415
LMRG_02437	diamine N-acetyltransferase	33	101	0.002572121	3.060606061	lmo0009
LMRG_02792	hypothetical protein	76	231	0.001558446	3.039473684	#N/A
predicted RNA	-	73	220	0.00451781	3.01369863	#N/A
LMRG_02375	hypothetical protein	33	99	0.004438201	3	lmo0126
LMRG_00417	hypothetical protein	45	133	0.004725323	2.955555556	lmo0729
LMRG_01568	hypothetical protein	42	124	0.002673939	2.952380952	lmo2263
predicted RNA	-	88	256	0.005176832	2.909090909	#N/A
LMRG_02343	hypothetical protein	21	61	0.008216044	2.904761905	lmo0094
predicted RNA	-	82	236	0.003455037	2.87804878	#N/A
LMRG_02077	hypothetical protein	37	106	0.00581421	2.864864865	lmo0977
LMRG_02938	serine O-acetyltransferase	22	63	0.013315824	2.863636364	lmo0238
predicted RNA	antisense: LMRG_00233	117	333	0.008711523	2.846153846	#N/A
LMRG_01576	hypothetical protein	37	105	0.017136024	2.837837838	lmo2255
LMRG_01402	DNA polymerase I	55	156	0.005065534	2.836363636	lmo1565
LMRG_02117	PTS system glucose-specific transporter subunit IIA	82	230	0.0032698	2.804878049	lmo1017
LMRG_00080	hypothetical protein	209	584	0.010165448	2.794258373	lmo0387
LMRG_02274	hypothetical protein	99	275	0.010550408	2.777777778	lmo0851
LMRG_01777	NADPH dehydrogenase	31	86	0.006728628	2.774193548	lmo2471
predicted RNA	antisense: LMRG_05504	63	174	0.018568862	2.761904762	#N/A
LMRG_02089	hypothetical protein	57	157	0.013197896	2.754385965	lmo0989
LMRG_00336	hypothetical protein	23	63	0.025737754	2.739130435	lmo0649
predicted RNA	antisense: LMRG_05508	87	237	0.012951781	2.724137931	#N/A
LMRG_00236	hypothetical protein	89	242	0.018535735	2.719101124	lmo0554
LMRG_02259	hypothetical protein	109	295	0.003559122	2.706422018	lmo0836
LMRG_00512	polypeptide deformylase	243	649	0.008885988	2.670781893	lmo1051
LMRG_00081	hypothetical protein	48	128	0.018674629	2.666666667	lmo0388
LMRG_00173	transcription regulator LysR	29	77	0.018961544	2.655172414	lmo0492
LMRG_01007	peptide-methionine (S)-S-oxide reductase	482	1278	0.041761156	2.651452282	lmo1860
predicted RNA	antisense: LMRG_05517	97	257	0.014391515	2.649484536	#N/A
predicted RNA	antisense: LMRG_00479	94	248	0.023529652	2.638297872	#N/A
LMRG_02673	DNA repair protein RadA	41	108	0.010760569	2.634146341	lmo0233
LMRG_01624	hypothetical protein	63	165	0.005014105	2.619047619	lmo2208
LMRG_00519	L-lactate dehydrogenase	79	206	0.021438437	2.607594937	lmo1057

Table 1: RNA-seq dataset of L. monocytogenes treated with 4-HNE versus mock

LMRG_00458	transcriptional regulator	25	65	0.018961544	2.6	lmo0770
LMRG_01623	hypothetical protein	25	65	0.021265447	2.6	lmo2209
LMRG_01403	formamidopyrimidine-DNA glycosylase	34	88	0.021453834	2.588235294	lmo1564
predicted RNA	antisense: LMRG_05505	123	317	0.025246604	2.577235772	#N/A
LMRG_00701	hypothetical protein	178	457	0.02523123	2.56741573	#N/A
LMRG_02615	HlyD family secretion protein	39	100	0.021634833	2.564102564	lmo0193
predicted RNA	antisense: LMRG_05514	96	245	0.03036087	2.552083333	#N/A
LMRG_01055	hypothetical protein	42	107	0.043428349	2.547619048	lmo1908
predicted RNA	antisense: LMRG_00554	67	170	8.34E-04	2.537313433	#N/A
LMRG_02244	hypothetical protein	89	225	0.030493736	2.528089888	lmo0819
LMRG_01069	hypothetical protein	42	106	0.01320132	2.523809524	lmo1922
LMRG_00205	hypothetical protein	48	121	0.033431119	2.520833333	lmo0524
LMRG_00090	hypothetical protein	52	131	0.032359701	2.519230769	lmo0397
LMRG_00442	hypothetical protein	54	136	0.019786837	2.518518519	lmo0754
LMRG_02037	protein-tyrosine phosphatase	157	392	0.033431119	2.496815287	lmo0938
predicted RNA	-	238	591	0.026337976	2.483193277	#N/A
LMRG_02386	peptide/nickel transport system permease	146	362	0.020624817	2.479452055	lmo0137
LMRG_02635	peptidyl-tRNA hydrolase	54	131	0.039822953	2.425925926	lmo0213
LMRG_00280	transcription regulator CRP/FNR family protein	26	63	0.044916888	2.423076923	lmo0597
LMRG_01847	hydrolase	43	104	0.032798066	2.418604651	lmo2401
LMRG_01856	transcriptional regulator	46	111	0.016880131	2.413043478	lmo2842
LMRG_01036	hypothetical protein	107	255	0.033198142	2.38317757	lmo1889
LMRG_01051	hypothetical protein	47	112	0.020005519	2.382978723	lmo1904
LMRG_02049	hypothetical protein	134	319	0.044879257	2.380597015	lmo0950
LMRG_02946	hypothetical protein	252	595	0.021633399	2.361111111	#N/A
LMRG_02108	hypothetical protein	252	586	0.041761156	2.325396825	lmo1008
LMRG_00452	lipoate-protein ligase A	37	86	0.038929387	2.324324324	lmo0764
LMRG_01834	FeS assembly protein SufD	118	273	0.042967549	2.313559322	lmo2414
LMRG_01047	aspartate 1-decarboxylase	341	784	0.044283805	2.299120235	lmo1900
LMRG_01054	dihydrodipicolinate reductase	64	147	0.02980491	2.296875	lmo1907
LMRG_02444	cytochrome aa3 quinol oxidase subunit III	64	145	0.038929387	2.265625	lmo0015
predicted RNA	-	353	799	0.04803035	2.263456091	#N/A
LMRG_01210	hypothetical protein	76	169	0.035520736	2.223684211	lmo2060
LMRG_02727	multicomponent Na+:H+ antiporter subunit E	124	63	0.032125345	0.508064516	lmo2382
LMRG_02008	hypothetical protein	65	33	0.020005519	0.507692308	lmo0908
LMRG_01700	homoserine dehydrogenase	201	101	0.047175323	0.502487562	lmo2547
LMRG_02800	sodium transport system permease	48	24	0.035658352	0.5	lmo2140
LMRG_02585	aminotransferase	52	26	0.038929387	0.5	lmo0286
LMRG_02250	hydroxymethylglutaryl-CoA reductase	48	24	0.03981199	0.5	lmo0825
LMRG_00681	aspartate kinase	182	91	0.040562131	0.5	lmo1235
LMRG_02620	UDP-N-acetylglucosamine diphosphorylase/glucosamine-1-phosphate N-acetyltransferase	130	65	0.04364084	0.5	lmo0198

Table 1: RNA-seq dataset of L. monocytogenes treated with 4-HNE versus mock

LMRG_01394	acetyl-CoA carboxylase carboxyl transferase subunit beta	48	24	0.044283805	0.5	lmo1573
LMRG_02124	hypothetical protein	44	22	0.047789583	0.5	lmo1024
LMRG_02312	hypothetical protein	283	141	0.04803035	0.498233216	lmo0888
LMRG_00784	secreted protein	257	128	0.04215241	0.498054475	lmo1334
LMRG_00413	hypothetical protein	350	173	0.039495623	0.494285714	lmo0724
LMRG_01002	D-alanyl-D-alanine carboxypeptidase	81	40	0.023124458	0.49382716	lmo1855
predicted RNA	-	1606	790	0.033748261	0.491905355	#N/A
LMRG_02641	tRNA(Ile)-lysidine synthetase	147	72	0.03871668	0.489795918	lmo0219
LMRG_01347	D-amino acid aminotransferase	333	163	0.03990536	0.489489489	lmo1619
LMRG_00908	hypothetical protein	190	93	0.002408231	0.489473684	lmo1456
LMRG_00995	manganese transport system membrane protein mntC	178	87	0.029152211	0.488764045	lmo1848
LMRG_00537	teichoic acids export ATP-binding protein tagH	84	41	0.020653577	0.488095238	lmo1075
LMRG_02621	ribose-phosphate pyrophosphokinase 1	355	173	0.038289935	0.487323944	lmo0199
LMRG_01143	deoxyribose-phosphate aldolase	142	69	0.037493838	0.485915493	lmo1995
LMRG_00883	hypothetical protein	266	129	0.041730146	0.484962406	lmo1431
LMRG_02502	phosphoribosylformylglycinamidine synthase II	31	15	0.021382699	0.483870968	lmo1769
LMRG_02167	30S ribosomal protein S17	461	223	0.034746604	0.48373102	lmo2623
LMRG_01773	phosphoglucomutase/phosphomannomutase	54	26	0.03885516	0.481481481	lmo2475
LMRG_01892	hypothetical protein	52	25	0.016954793	0.480769231	lmo2804
LMRG_00993	multidrug resistance protein norM	50	24	0.015638073	0.48	lmo1846
LMRG_00685	rdgB/HAM1 family non-canonical purine NTP pyrophosphatase	221	106	0.026237749	0.479638009	lmo1239
predicted RNA	-	1672	800	0.013365301	0.4784689	#N/A
LMRG_01697	hypothetical protein	46	22	0.034356578	0.47826087	lmo2550
LMRG_02180	1,4-dihydroxy-2-naphthoate octaprenyltransferase	67	32	0.018674629	0.47761194	lmo2635
LMRG_02684	response regulator	74	35	0.023677106	0.472972973	lmo2583
LMRG_02879	hypothetical protein	55	26	0.009199536	0.472727273	lmo0528
LMRG_01168	isoleucyl-tRNA synthetase	70	33	5.73E-04	0.471428571	lmo2019
LMRG_00536	teichoic acid transport system permease	51	24	0.029891732	0.470588235	lmo1074
LMRG_00965	ribulose-phosphate 3-epimerase	149	70	0.026728806	0.469798658	lmo1818
LMRG_02252	pyruvate:ferredoxin oxidoreductase	66	31	0.026347347	0.46969697	lmo0829
LMRG_01406	replication initiation and membrane attachment protein	330	155	0.035630534	0.46969697	lmo1561
LMRG_01374	NifS/icsS protein	49	23	0.013354675	0.469387755	lmo1593
predicted RNA	-	868	406	0.020408525	0.467741935	#N/A
LMRG_00211	N-acetylglucosaminyltransferase	30	14	0.044813253	0.466666667	lmo0529
LMRG_00281	biotin biosynthesis protein BioY	133	62	0.010993339	0.466165414	#N/A
LMRG_01793	phosphopyruvate hydratase	1243	579	0.02779667	0.465808528	lmo2455
LMRG_00301	hypothetical protein	41	19	0.021453834	0.463414634	lmo0618
LMRG_01330	ABC transporter ATP-binding protein	237	109	0.021382699	0.459915612	lmo1636
LMRG_01284	hypothetical protein	192	88	0.023052624	0.458333333	lmo2130
LMRG_01373	septation ring formation regulator EzrA	313	143	0.030958788	0.45686901	lmo1594
LMRG_00905	hypothetical protein	125	57	0.007034615	0.456	lmo1453
LMRG_01063	beta-lactamase	145	66	0.015455111	0.455172414	lmo1916

Table 1: RNA-seq dataset of L. monocytogenes treated with 4-HNE versus mock

LMRG_01685	hypothetical protein	33	15	0.047803696	0.454545455	lmo2147
LMRG_00758	hypothetical protein	97	44	0.008216044	0.453608247	lmo1308
LMRG_00703	alpha-phosphotrehalase	181	82	0.02165941	0.453038674	lmo1254
LMRG_02699	peptide/nickel transport system substrate-binding protein	371	168	0.032359701	0.452830189	lmo2569
LMRG_02168	50S ribosomal protein L29	349	158	0.009456532	0.452722063	lmo2624
LMRG_02150	DNA-directed RNA polymerase subunit alpha	685	310	0.045972061	0.452554745	lmo2606
LMRG_00952	ribonuclease III	250	113	0.011835797	0.452	lmo1805
LMRG_01062	malate dehydrogenase	113	51	0.014960466	0.451327434	lmo1915
LMRG_02185	heptaprenyl diphosphate synthase component I	246	111	0.018334167	0.451219512	lmo2640
LMRG_00534	pyruvate carboxylase	404	182	0.038260918	0.45049505	lmo1072
LMRG_00961	hypothetical protein	60	27	0.014081458	0.45	lmo1814
LMRG_02820	hypothetical protein	145	65	0.0383802	0.448275862	lmo1796
predicted RNA	antisense: LMRG_02657	654	293	0.03871668	0.448012232	#N/A
LMRG_01034	N6-adenine-specific DNA methylase	76	34	0.005810536	0.447368421	lmo1887
LMRG_02656	large subunit ribosomal protein L10	1275	569	0.032743346	0.44627451	lmo0250
LMRG_01253	glutamine amidotransferase subunit pdxT	299	133	0.009044345	0.444816054	lmo2102
LMRG_00941	nicotinate nucleotide adenylyltransferase	135	60	0.006294116	0.444444444	lmo1488
LMRG_00765	di-trans,poly-cis-decaprenylcistransferase	187	83	0.013134209	0.443850267	lmo1315
LMRG_02051	hypothetical protein	210	93	0.006922704	0.442857143	lmo0952
LMRG_02360	hypothetical protein	113	50	0.004666342	0.442477876	lmo0111
LMRG_02181	thiamine biosynthesis lipoprotein	118	52	0.016805534	0.440677966	lmo2636
LMRG_02599	hypothetical protein	66	29	0.007640077	0.439393939	lmo0276
LMRG_02177	30S ribosomal protein S10	746	327	0.013197896	0.438337802	lmo2633
LMRG_02712	glucose-6-phosphate isomerase	963	422	0.037643237	0.438213915	lmo2367
LMRG_02088	peptide chain release factor 3	176	77	0.013046027	0.4375	lmo0988
LMRG_01408	threonyl-tRNA synthetase	112	49	0.015305858	0.4375	lmo1559
LMRG_02432	hypothetical protein	117	51	0.031589071	0.435897436	lmo0004
LMRG_00802	hypothetical protein	590	254	0.006832118	0.430508475	lmo1352
LMRG_00550	hypothetical protein	135	58	0.007061656	0.42962963	lmo1088
LMRG_00147	hypothetical protein	35	15	0.004337716	0.428571429	lmo0455
LMRG_02348	hypothetical protein	138	59	0.004955323	0.427536232	lmo0099
LMRG_00771	hypothetical protein	134	57	0.004312974	0.425373134	lmo1321
LMRG_02278	D-alanine--D-alanine ligase	146	62	0.005807016	0.424657534	lmo0855
LMRG_01638	peptide/nickel transport system permease	721	305	0.04919203	0.423023578	lmo2194
LMRG_02501	phosphoribosylformylglycinamidine synthase I	31	13	0.049232295	0.419354839	lmo1770
LMRG_05006	Gly tRNA	5433	2278	0.010459305	0.419289527	#N/A
LMRG_01772	aldose 1-epimerase	456	191	0.010762338	0.418859649	lmo2476
LMRG_00744	tRNA delta(2)-isopentenylpyrophosphate transferase	203	85	0.004477661	0.418719212	lmo1294
LMRG_00944	ribosome biogenesis GTPase YqeH	696	291	0.049164568	0.418103448	lmo1491
LMRG_01303	methionine adenosyltransferase	137	57	0.004283812	0.416058394	lmo1664
LMRG_01473	uridine kinase	41	17	0.04301591	0.414634146	lmo1497
LMRG_01360	DNA segregation ATPase FtsK/SpoIIIE	152	63	0.010095766	0.414473684	lmo1606

Table 1: RNA-seq dataset of L. monocytogenes treated with 4-HNE versus mock

LMRG_00704	trehalose-specific PTS system IIBC component	162	67	0.0063181	0.413580247	lmo1255
LMRG_01038	recombination protein U	179	74	0.005263869	0.413407821	lmo1891
LMRG_00275	formate/nitrite transporter	119	49	0.001306163	0.411764706	lmo0593
LMRG_02176	50S ribosomal protein L3	506	207	0.006832118	0.409090909	lmo2632
LMRG_00870	nucleotide pyrophosphatase	93	38	0.008061528	0.408602151	lmo1418
LMRG_00966	ribosome small subunit-dependent GTPase A	142	58	0.008512739	0.408450704	lmo1819
LMRG_00901	endonuclease 4	130	53	0.006954465	0.407692308	lmo1449
LMRG_01124	ribonuclease Z	32	13	0.030716609	0.40625	lmo1977
predicted RNA	antisense: LMRG_01720	160	65	0.04102053	0.40625	#N/A
LMRG_00674	ribonuclease HIII	32	13	0.043051938	0.40625	lmo1228
LMRG_02280	alpha/beta fold family hydrolase	106	43	0.001883725	0.405660377	lmo0857
LMRG_05034	Gly tRNA	4718	1889	0.005916195	0.400381518	#N/A
LMRG_01084	ribosome-associated GTPase EngA	200	80	0.004192147	0.4	lmo1937
LMRG_00954	3-oxoacyl-ACP reductase	45	18	0.014038157	0.4	lmo1807
LMRG_01714	F-type H+-transporting ATPase subunit C	484	193	0.001306163	0.398760331	lmo2534
LMRG_00529	GTP-binding protein TypA/BipA	224	89	0.006238853	0.397321429	lmo1067
LMRG_01169	cell division initiation protein	68	27	0.014408909	0.397058824	lmo2020
LMRG_01582	PiT family inorganic phosphate transporter	754	298	0.017102841	0.395225464	lmo2249
LMRG_00773	hypothetical protein	947	373	0.003406903	0.393875396	lmo1323
LMRG_02271	polar amino acid transport system ATP-binding protein	112	44	0.001070677	0.392857143	lmo0848
LMRG_00832	hypothetical protein	396	155	0.001640079	0.391414141	lmo1380
LMRG_00318	2-haloalkanoic acid dehalogenase	296	114	0.002014978	0.385135135	lmo0635
LMRG_02770	hypothetical protein	65	25	0.007034615	0.384615385	lmo1696
LMRG_01926	antibiotic transport system ATP-binding protein	39	15	0.012232232	0.384615385	lmo2769
LMRG_01340	hypothetical protein	136	52	0.001194099	0.382352941	lmo1626
LMRG_05045	Lys tRNA	1810	690	0.00345001	0.38121547	#N/A
LMRG_01099	diaminopimelate decarboxylase	108	41	0.002777291	0.37962963	lmo1952
LMRG_01079	trans-hexaprenyltranstransferase	467	177	0.002933682	0.379014989	lmo1932
LMRG_01090	hypothetical protein	45	17	0.005014008	0.377777778	lmo1943
LMRG_02586	D-methionine transport system substrate-binding protein	398	150	0.002200451	0.376884422	lmo0285
LMRG_02315	serine/threonine-protein kinase rsbT	146	55	7.89E-04	0.376712329	lmo0891
LMRG_02119	hypothetical protein	77	29	6.28E-04	0.376623377	lmo1019
LMRG_00657	integral membrane protein	40	15	0.036269745	0.375	lmo1211
LMRG_02175	50S ribosomal protein L4/L1	884	331	0.002853719	0.374434389	lmo2631
LMRG_01243	glycine betaine transporter	59	22	3.96E-04	0.372881356	lmo2092
LMRG_00419	hypothetical protein	43	16	0.039856044	0.372093023	lmo0731
LMRG_01363	peroxiredoxin	250	93	0.002708912	0.372	lmo1604
LMRG_01792	2,3-bisphosphoglycerate-independent phosphoglycerate mutase	1390	517	0.002493673	0.371942446	lmo2456
LMRG_00812	exodeoxyribonuclease VII small subunit	119	44	0.012379762	0.369747899	lmo1362
LMRG_00612	threonine-phosphate decarboxylase	38	14	0.00563131	0.368421053	lmo1169
LMRG_05036	Lys tRNA	3699	1354	0.001375696	0.366044877	#N/A
LMRG_01414	delta-aminolevulinic acid dehydratase	41	15	0.004441472	0.365853659	lmo1554

Table 1: RNA-seq dataset of L. monocytogenes treated with 4-HNE versus mock

predicted RNA	antisense: LMRG_01081	707	257	0.006238853	0.363507779	#N/A
LMRG_00392	hypothetical protein	295	107	0.0016435	0.362711864	lmo0703
LMRG_02759	glutamate-1-semialdehyde 2,1-aminomutase 2	91	33	5.05E-04	0.362637363	lmo1685
LMRG_01412	porphobilinogen deaminase	50	18	0.002877714	0.36	lmo1556
predicted RNA	-	225	81	0.011560716	0.36	#N/A
LMRG_02744	multiple sugar transport system permease	53	19	0.002233874	0.358490566	lmo0179
LMRG_02784	fructokinase	90	32	1.69E-04	0.355555556	lmo0813
LMRG_01443	bifunctional preprotein translocase subunit SecD/SecF	249	88	0.001306163	0.353413655	lmo1527
predicted RNA	-	2015	710	3.40E-04	0.35235732	#N/A
predicted RNA	-	375	132	4.83E-05	0.352	#N/A
LMRG_01141	pyrimidine-nucleoside phosphorylase	37	13	0.002721735	0.351351351	lmo1993
LMRG_01033	carboxypeptidase Taq	180	63	8.59E-04	0.35	lmo1886
LMRG_01717	ATP synthase F1 alpha subunit	277	96	9.11E-04	0.346570397	lmo2531
LMRG_00171	shikimate 5-dehydrogenase	52	18	0.002151164	0.346153846	lmo0490
LMRG_01691	fructose-16-bisphosphate aldolase class II	2798	968	0.001156859	0.345961401	lmo2556
LMRG_01630	3-oxoacyl-ACP synthase	67	23	2.92E-04	0.343283582	lmo2202
LMRG_01696	transcription termination factor Rho	35	12	0.001999326	0.342857143	lmo2551
LMRG_01097	segregation and condensation protein B	794	272	7.23E-04	0.34256927	lmo1950
LMRG_01425	septum site-determining protein minC	38	13	0.006680086	0.342105263	lmo1545
LMRG_00852	acetyltransferase	328	112	3.96E-04	0.341463415	lmo1400
LMRG_01385	site-specific DNA-methyltransferase	484	163	5.43E-04	0.33677686	lmo1582
LMRG_02473	30S ribosomal protein S6	520	175	4.20E-04	0.336538462	lmo0044
predicted RNA	-	4219	1411	0.003535268	0.334439441	#N/A
predicted RNA	-	560	187	0.001804117	0.333928571	#N/A
LMRG_02187	serine/threonine protein phosphatase	105	35	3.64E-04	0.333333333	lmo2642
LMRG_01230	hypothetical protein	42	14	9.19E-04	0.333333333	lmo2079
LMRG_01382	protease IV	36	12	0.002942662	0.333333333	lmo1585
LMRG_01195	2-dehydropantoate 2-reductase	30	10	0.004772802	0.333333333	lmo2046
LMRG_01790	phosphoglycerate kinase	686	228	5.42E-04	0.332361516	lmo2458
LMRG_01098	ScpA/B protein	103	34	2.76E-05	0.330097087	lmo1951
LMRG_01059	hypothetical protein	73	24	3.33E-05	0.328767123	lmo1912
predicted RNA	-	229	75	0.039007579	0.327510917	#N/A
LMRG_00736	DNA topoisomerase IV B subunit	513	168	0.005301755	0.32748538	lmo1286
LMRG_01058	hypothetical protein	43	14	8.40E-04	0.325581395	lmo1911
LMRG_01997	aldo/keto reductase family oxidoreductase	83	27	4.52E-05	0.325301205	lmo2700
LMRG_02122	response regulator LiaR	163	53	1.52E-05	0.325153374	lmo1022
LMRG_00084	hypothetical protein	114	37	0.00194844	0.324561404	lmo0391
LMRG_00762	hypothetical protein	37	12	0.027913956	0.324324324	lmo1312
LMRG_00085	hypothetical protein	130	42	5.72E-06	0.323076923	lmo0392
LMRG_01441	hypothetical protein	78	25	0.003860523	0.320512821	lmo1529
LMRG_02900	beta-glucoside operon transcriptional antiterminator	94	30	8.10E-06	0.319148936	lmo2773
LMRG_01713	ATP synthase F0 A subunit	421	134	1.23E-04	0.318289786	lmo2535

Table 1: RNA-seq dataset of L. monocytogenes treated with 4-HNE versus mock

LMRG_02658	50S ribosomal protein L11	2141	680	5.50E-04	0.317608594	lmo0248
LMRG_00287	hypothetical protein	41	13	0.019268586	0.317073171	lmo0604
LMRG_00871	hypothetical protein	121	38	5.23E-06	0.314049587	lmo1419
LMRG_00475	amino acid transporter AAT family protein	287	90	9.08E-05	0.31358885	lmo0787
predicted RNA	-	354	111	0.003199764	0.313559322	#N/A
LMRG_02425	membrane protein OxaA	428	134	6.66E-05	0.313084112	lmo2854
LMRG_00759	hypothetical protein	48	15	0.004644073	0.3125	lmo1309
LMRG_02516	glutamyl-tRNA(Gln) amidotransferase subunit A	308	96	1.24E-04	0.311688312	lmo1755
LMRG_00163	cfr family radical SAM enzyme	289	90	7.62E-05	0.311418685	lmo0482
LMRG_00749	glutamine synthetase type I	621	191	1.08E-04	0.307568438	lmo1299
LMRG_02485	adenylosuccinate synthetase	154	47	2.18E-05	0.305194805	lmo0055
LMRG_00942	hypothetical protein	59	18	0.009270389	0.305084746	lmo1489
LMRG_00216	hypothetical protein	69	21	5.69E-06	0.304347826	lmo0534
LMRG_00774	hypothetical protein	793	241	8.03E-06	0.303909206	lmo1324
LMRG_02868	AAT family amino acid transporter	33	10	4.88E-04	0.303030303	lmo0798
LMRG_00377	hypothetical protein	33	10	0.001095668	0.303030303	lmo0689
LMRG_01981	ABC transporter CydDC cysteine exporter CydC	308	93	5.50E-05	0.301948052	lmo2715
LMRG_02279	UDP-N-acetylmuramoylalanyl-D-glutamyl-2	170	51	7.76E-06	0.3	lmo0856
LMRG_01891	hypothetical protein	47	14	0.004544726	0.29787234	lmo2805
LMRG_01637	peptide/nickel transport system permease	1132	336	7.25E-04	0.296819788	lmo2195
LMRG_02751	hypothetical protein	118	35	7.56E-06	0.296610169	lmo0186
LMRG_00955	malonyl CoA-acyl carrier protein transacylase	98	29	2.02E-06	0.295918367	lmo1808
LMRG_00223	iron complex transport system substrate-binding protein	122	36	1.29E-06	0.295081967	lmo0541
LMRG_00288	hypothetical protein	75	22	3.80E-06	0.293333333	lmo0605
LMRG_01979	cytochrome d ubiquinol oxidase subunit II	580	170	2.49E-05	0.293103448	lmo2717
LMRG_02153	50S ribosomal protein L36	3824	1111	1.42E-05	0.290533473	lmo2609
LMRG_01252	pyridoxine biosynthesis protein	341	99	1.11E-05	0.290322581	lmo2101
LMRG_01182	cell division protein FtsA	428	124	1.93E-05	0.289719626	lmo2033
LMRG_02671	2-C-methyl-D-erythritol 4-phosphate cytidylyltransferase	2304	665	2.72E-04	0.288628472	lmo0235
predicted RNA	antisense: LMRG_01430 LMRG_01429	427	123	0.001841892	0.288056206	#N/A
LMRG_02114	glycine betaine/proline transport system ATP-binding protein	293	84	9.67E-06	0.28668942	lmo1014
LMRG_00263	SAM-dependent methyltransferase	155	44	1.07E-05	0.283870968	lmo0581
LMRG_05004	Lys tRNA	2329	660	7.03E-06	0.283383426	#N/A
LMRG_01489	hypothetical protein	120	34	1.09E-05	0.283333333	lmo2354
LMRG_01771	UDP-glucose 4-epimerase	110	31	3.42E-07	0.281818182	lmo2477
LMRG_02510	neurotransmitter:Na+ symporter	64	18	3.12E-07	0.28125	lmo1761
LMRG_01242	argininosuccinate lyase	25	7	3.35E-04	0.28	lmo2091
LMRG_01331	DNA binding 3-demethylubiquinone-9 3-methyltransferase domain-containing protein	193	54	3.19E-07	0.279792746	lmo1635
LMRG_02081	hypothetical protein	175	48	6.10E-07	0.274285714	lmo0981
LMRG_01866	glycerate kinase	77	21	1.60E-07	0.272727273	lmo2832
predicted RNA	-	837	228	2.67E-05	0.272401434	#N/A
LMRG_01718	ATP synthase F1 gamma subunit	788	213	2.31E-06	0.270304569	lmo2530

Table 1: RNA-seq dataset of L. monocytogenes treated with 4-HNE versus mock

LMRG_01018	phosphomannomutase	37	10	1.37E-05	0.27027027	lmo1871
LMRG_02183	NADH dehydrogenase	592	160	5.06E-05	0.27027027	lmo2638
LMRG_01013	phosphotransferase	26	7	0.00230137	0.269230769	lmo1866
LMRG_02798	hypothetical protein	272	73	2.06E-06	0.268382353	lmo2142
predicted RNA	-	358	96	0.011052388	0.268156425	#N/A
LMRG_02864	hypothetical protein	64	17	0.001034586	0.265625	#N/A
LMRG_00810	hypothetical protein	57	15	2.40E-05	0.263157895	lmo1360
LMRG_02626	actin-assembly inducing protein ActA	153	40	1.42E-07	0.261437908	lmo0204
LMRG_01364	aminopeptidase	153	40	2.03E-07	0.261437908	lmo1603
LMRG_01003	purine nucleoside phosphorylase	81	21	2.60E-06	0.259259259	lmo1856
LMRG_00381	flagellar motor switch protein FliN/FliY	722	185	2.34E-07	0.256232687	lmo0693
LMRG_02710	CTP synthase	594	152	6.70E-07	0.255892256	lmo2559
LMRG_01341	hypothetical protein	43	11	7.57E-07	0.255813953	lmo1625
LMRG_05050	His tRNA	232	59	6.68E-04	0.254310345	#N/A
predicted RNA	-	284	72	0.005807016	0.253521127	#N/A
predicted RNA	-	222	56	0.005060871	0.252252252	#N/A
LMRG_01488	hypothetical protein	282	71	1.21E-07	0.25177305	lmo2355
LMRG_00553	hypothetical protein	64	16	7.57E-07	0.25	lmo1091
LMRG_00393	hypothetical protein	128	32	2.24E-06	0.25	lmo0704
LMRG_02496	AIR carboxylase	40	10	3.98E-04	0.25	lmo1775
LMRG_02070	D-alanine transfer protein	1034	255	2.17E-05	0.246615087	lmo0971
LMRG_02872	hypothetical protein	1602	393	8.01E-08	0.245318352	lmo0694
predicted RNA	-	213	52	0.001184674	0.244131455	#N/A
LMRG_02827	translation initiation factor IF-3	4106	997	2.11E-06	0.242815392	lmo1785
predicted RNA	-	5311	1286	3.68E-08	0.242138957	#N/A
LMRG_00384	hypothetical protein	2429	588	3.52E-07	0.242074928	lmo0695
LMRG_00843	simple sugar transport system permease	87	21	4.89E-09	0.24137931	lmo1391
LMRG_01659	hypothetical protein	29	7	1.10E-05	0.24137931	lmo2173
LMRG_00772	transcription termination factor NusA	287	69	2.34E-09	0.240418118	lmo1322
predicted RNA	-	887	213	1.16E-07	0.240135287	#N/A
LMRG_01712	ATP synthase I	150	36	2.41E-07	0.24	lmo2536
LMRG_00394	flagellar hook-associated protein FlgK	573	137	3.41E-08	0.239092496	lmo0705
predicted RNA	antisense: LMRG_01792	176	42	8.59E-04	0.238636364	#N/A
LMRG_02307	membrane protein	202	48	1.26E-09	0.237623762	lmo0883
LMRG_00819	phosphate butyryltransferase	131	31	7.29E-11	0.236641221	lmo1369
LMRG_00811	exodeoxyribonuclease VII large subunit	89	21	4.10E-10	0.235955056	lmo1361
LMRG_01867	beta-phosphoglucomutase	51	12	1.08E-05	0.235294118	lmo2831
predicted RNA	-	290	68	0.001100033	0.234482759	#N/A
LMRG_02321	SulP family sulfate permease	64	15	1.99E-10	0.234375	lmo0897
LMRG_02978	hypothetical protein	64	15	0.001125382	0.234375	#N/A
LMRG_01636	peptide/nickel transport system substrate-binding protein	2391	560	1.75E-07	0.234211627	lmo2196
LMRG_00987	pyrimidine operon attenuation protein/uracil phosphoribosyltransferase	47	11	6.92E-05	0.234042553	lmo1840

Table 1: RNA-seq dataset of L. monocytogenes treated with 4-HNE versus mock

LMRG_01978	cytochrome bd-I oxidase subunit I	159	37	1.15E-08	0.232704403	lmo2718
LMRG_00803	hypothetical protein	86	20	5.80E-09	0.23255814	lmo1353
LMRG_02136	CRISPR-associated protein cas2	56	13	3.17E-04	0.232142857	#N/A
predicted RNA	-	358	83	0.001804117	0.231843575	#N/A
LMRG_01583	hypothetical protein	986	228	8.19E-09	0.231237323	lmo2248
LMRG_01213	hypothetical protein	39	9	7.00E-04	0.230769231	lmo2063
LMRG_01676	hypothetical protein	39	9	7.11E-04	0.230769231	lmo2156
LMRG_02071	D-alanine--poly(phosphoribitol) ligase subunit 2	1124	259	7.20E-10	0.230427046	lmo0972
LMRG_02426	ribonuclease P	211	48	4.46E-09	0.227488152	lmo2855
LMRG_01741	cell division ATP-binding protein FtsE	721	163	6.66E-10	0.226074896	lmo2507
LMRG_00981	dihydroorotate dehydrogenase electron transfer subunit	49	11	3.31E-06	0.224489796	lmo1834
LMRG_01743	D-glutamyl-L-m-Dpm peptidase P45	1944	436	9.47E-08	0.224279835	lmo2505
LMRG_00956	fatty acid/phospholipid synthesis protein PlsX	90	20	1.29E-10	0.222222222	lmo1809
predicted RNA	-	389	86	3.72E-05	0.221079692	#N/A
predicted RNA	-	242	53	2.11E-04	0.219008264	#N/A
predicted RNA	-	256	56	2.67E-04	0.21875	#N/A
LMRG_01788	transcriptional regulator	719	156	3.22E-10	0.216968011	lmo2460
LMRG_00957	fatty acid biosynthesis transcriptional regulator	598	129	4.58E-12	0.215719064	lmo1810
LMRG_01577	AGZA family MFS transporter xanthine/uracil permease	182	39	2.34E-10	0.214285714	lmo2254
LMRG_01453	nitrogen regulatory protein P-II	33	7	5.43E-04	0.212121212	lmo1517
LMRG_00391	hypothetical protein	496	105	3.72E-11	0.211693548	lmo0702
LMRG_02060	protease	177	37	7.11E-12	0.209039548	lmo0961
LMRG_02270	glutamine ABC transporter	144	30	2.32E-13	0.208333333	lmo0847
predicted RNA	-	221	46	7.94E-06	0.208144796	#N/A
LMRG_00087	extracellular P60 protein	135	28	2.80E-11	0.207407407	lmo0394
LMRG_00151	hypothetical protein	92	19	6.63E-08	0.206521739	#N/A
LMRG_01742	cell division transport system permease	762	157	2.04E-11	0.206036745	lmo2506
LMRG_00535	iron complex transport system substrate-binding protein	68	14	2.93E-09	0.205882353	lmo1073
predicted RNA	-	787	162	4.55E-09	0.205844981	#N/A
predicted RNA	-	254	52	7.39E-06	0.204724409	#N/A
LMRG_00386	flagellar hook protein FlgE	362	74	8.09E-12	0.20441989	lmo0697
LMRG_02607	oligopeptide transport system permease oppC	54	11	2.17E-12	0.203703704	lmo0269
LMRG_00370	flagellar basal-body rod protein FlgG	54	11	2.43E-07	0.203703704	lmo0682
LMRG_01980	ABC transporter CydDC cysteine exporter CydD	430	87	1.19E-11	0.202325581	lmo2716
LMRG_01073	chorismate mutase	195	39	4.57E-11	0.2	lmo1926
LMRG_01428	50S ribosomal protein L21	6089	1215	3.38E-08	0.199540154	lmo1542
LMRG_00395	flagellar hook-associated protein 3	517	101	2.40E-13	0.195357834	lmo0706
LMRG_02773	hypothetical protein	385	75	4.01E-15	0.194805195	lmo1699
LMRG_02134	hypothetical protein	423	82	1.41E-16	0.193853428	lmo2594
predicted RNA	-	301	58	9.22E-06	0.19269103	#N/A
LMRG_02073	D-alanine--poly(phosphoribitol) ligase subunit 1	270	52	2.81E-14	0.192592593	lmo0974
predicted RNA	antisense: LMRG_01691	203	39	1.42E-05	0.192118227	#N/A

Table 1: RNA-seq dataset of L. monocytogenes treated with 4-HNE versus mock

LMRG_01472	O-methyltransferase	73	14	1.24E-09	0.191780822	lmo1498
predicted RNA	-	335	64	1.11E-05	0.191044776	#N/A
LMRG_02624	listeriolysin O	168	32	1.15E-13	0.19047619	lmo0202
LMRG_00398	hypothetical protein	2607	494	7.01E-14	0.189489835	lmo0709
predicted RNA	antisense: LMRG_02182	431	81	9.73E-15	0.187935035	#N/A
LMRG_02783	enoyl-(acyl carrier protein) reductase	256	48	5.67E-15	0.1875	lmo0814
LMRG_01791	triosephosphate isomerase	659	123	9.75E-15	0.186646434	lmo2457
LMRG_00761	hypothetical protein	70	13	2.10E-12	0.185714286	lmo1311
LMRG_00389	flagellar motor switch protein FliN/FliY	890	165	2.56E-14	0.185393258	lmo0700
LMRG_01744	hypothetical protein	65	12	5.56E-12	0.184615385	lmo2504
predicted RNA	-	378	68	2.00E-06	0.17989418	#N/A
LMRG_00388	flagellar motor switch protein FliM	1078	191	2.38E-16	0.177179963	lmo0699
LMRG_00953	acyl carrier protein	362	64	1.58E-14	0.17679558	lmo1806
predicted RNA	-	665	117	1.11E-10	0.17593985	#N/A
LMRG_00104	hypothetical protein	74	13	2.12E-11	0.175675676	lmo0412
LMRG_00215	ACT domain-containing protein	74	13	2.26E-07	0.175675676	lmo0533
LMRG_00390	hypothetical protein	274	48	5.67E-19	0.175182482	lmo0701
LMRG_00662	bax protein	190	33	7.49E-21	0.173684211	lmo1216
LMRG_01508	hypothetical protein	1747	301	1.15E-14	0.172295363	lmo2335
LMRG_00404	flagellar assembly protein H	2207	379	3.22E-17	0.171726325	lmo0715
LMRG_02138	CRISPR-associated protein	47	8	1.46E-21	0.170212766	#N/A
predicted RNA	-	259	44	7.88E-07	0.16988417	#N/A
predicted RNA	-	282	47	2.32E-07	0.166666667	#N/A
LMRG_00365	flagellar biosynthetic protein FliQ	571	95	4.06E-24	0.166374781	lmo0677
LMRG_00407	hypothetical protein	319	53	5.84E-24	0.166144201	lmo0718
LMRG_02746	multiple sugar transport system substrate-binding protein	103	17	3.42E-21	0.165048544	lmo0181
LMRG_00385	flagellar hook capping protein	1003	165	2.51E-22	0.164506481	lmo0696
LMRG_01715	ATP synthase F0 subunit B	1436	236	6.64E-20	0.164345404	lmo2533
LMRG_02238	autolysin	1956	321	1.78E-16	0.164110429	lmo2691
predicted RNA	-	476	78	1.71E-10	0.163865546	#N/A
LMRG_00476	hypothetical protein	55	9	3.69E-21	0.163636364	lmo0788
LMRG_02379	hypothetical protein	110	18	9.32E-20	0.163636364	lmo0130
predicted RNA	-	385	63	6.88E-08	0.163636364	#N/A
LMRG_01487	hypothetical protein	44	7	2.13E-06	0.159090909	#N/A
predicted RNA	-	1512	236	6.50E-18	0.156084656	#N/A
LMRG_02059	hypothetical protein	154	24	2.94E-25	0.155844156	lmo0960
predicted RNA	-	2547	383	7.86E-27	0.150372988	#N/A
LMRG_00840	ABC transporter	293	44	1.28E-24	0.150170648	lmo1388
predicted RNA	-	181	27	1.95E-09	0.149171271	#N/A
predicted RNA	-	222	33	1.25E-09	0.148648649	#N/A
LMRG_02072	membrane protein	622	92	6.60E-26	0.147909968	lmo0973
predicted RNA	-	325	48	1.43E-10	0.147692308	#N/A

Table 1: RNA-seq dataset of L. monocytogenes treated with 4-HNE versus mock

LMRG_02623	1-phosphatidylinositol phosphodiesterase	299	44	3.76E-31	0.147157191	lmo0201
LMRG_02306	hypothetical protein	367	54	2.22E-31	0.147138965	lmo0882
LMRG_00859	pyruvate formate-lyase activating enzyme	48	7	1.99E-11	0.145833333	lmo1407
LMRG_02137	CRISPR-associated protein cas1	69	10	4.98E-17	0.144927536	#N/A
LMRG_00045	long-chain fatty acid CoA ligase (AMP-binding)	152	22	2.06E-33	0.144736842	lmo0354
LMRG_00402	flagellar M-ring protein FliF	1309	189	4.43E-19	0.144385027	lmo0713
LMRG_01507	1-phosphofructokinase	791	111	3.77E-29	0.140328698	lmo2336
LMRG_01506	hypothetical protein	679	95	9.72E-33	0.139911635	lmo2337
LMRG_05005	Leu tRNA	1696	237	1.78E-30	0.139740566	#N/A
predicted RNA	-	266	37	8.02E-10	0.139097744	#N/A
LMRG_01779	APA family basic amino acid/polyamine antiporter	72	10	3.67E-23	0.138888889	lmo2469
LMRG_00760	hypothetical protein	36	5	1.02E-13	0.138888889	lmo1310
LMRG_01376	N-acetyl-gamma-glutamyl-phosphate reductase	58	8	2.16E-18	0.137931034	lmo1591
LMRG_00980	dihydroorotate oxidase	51	7	5.29E-14	0.137254902	lmo1833
LMRG_00400	flagellar basal-body rod protein FlgC	633	85	8.02E-41	0.134281201	lmo0711
LMRG_05035	Leu tRNA	1337	178	1.08E-27	0.133133882	#N/A
predicted RNA	-	370	49	3.61E-11	0.132432432	#N/A
LMRG_00778	tRNA pseudouridine synthase B	152	20	1.08E-32	0.131578947	lmo1328
LMRG_00399	flagellar basal-body rod protein FlgB	604	79	1.27E-41	0.130794702	lmo0710
predicted RNA	antisense: LMRG_01743	177	23	1.17E-10	0.129943503	#N/A
predicted RNA	-	524	68	5.21E-20	0.129770992	#N/A
LMRG_02012	nitrite transporter NirC	509	66	3.81E-33	0.129666012	lmo0912
predicted RNA	-	324	42	2.16E-18	0.12962963	#N/A
LMRG_01584	hypothetical protein	124	16	2.06E-16	0.129032258	#N/A
LMRG_00397	flagellar biosynthesis protein fliS	1993	257	5.01E-35	0.12895133	lmo0708
LMRG_00406	hypothetical protein	1247	160	1.60E-36	0.128307939	lmo0717
predicted RNA	-	219	28	1.83E-13	0.127853881	#N/A
LMRG_01241	argininosuccinate synthase	90	11	5.43E-32	0.122222222	lmo2090
LMRG_00405	flagellar protein export ATPase FliI	550	66	1.79E-41	0.12	lmo0716
LMRG_00985	aspartate carbamoyltransferase	34	4	3.73E-18	0.117647059	lmo1838
predicted RNA	-	1199	134	3.87E-22	0.1117598	#N/A
LMRG_00841	simple sugar transport system ATP-binding protein	127	14	1.26E-55	0.11023622	lmo1389
LMRG_00978	orotate phosphoribosyltransferase	37	4	3.01E-15	0.108108108	lmo1831
predicted RNA	-	192	20	8.11E-19	0.104166667	#N/A
predicted RNA	-	279	29	5.63E-31	0.103942652	#N/A
LMRG_00842	simple sugar transport system permease	165	17	5.55E-56	0.103030303	lmo1390
LMRG_01579	aspartate aminotransferase	235	24	1.18E-75	0.10212766	lmo2252
LMRG_00403	flagellar motor switch protein FliG	592	60	8.87E-68	0.101351351	lmo0714
LMRG_01976	acetyl-CoA synthetase	773	78	8.55E-63	0.100905563	lmo2720
LMRG_00858	formate acetyltransferase	355	35	9.14E-72	0.098591549	lmo1406
LMRG_00984	dihydroorotase	64	6	1.11E-35	0.09375	lmo1837
LMRG_00376	hypothetical protein	270	25	2.17E-74	0.092592593	lmo0688

Table 1: RNA-seq dataset of L. monocytogenes treated with 4-HNE versus mock

LMRG_00366	flagellar biosynthesis protein FliR	119	11	1.32E-41	0.092436975	lmo0678
LMRG_00387	hypothetical protein	338	31	2.43E-45	0.091715976	lmo0698
predicted RNA	-	1163	105	1.17E-62	0.090283749	#N/A
LMRG_00706	hypothetical protein	1530	137	4.97E-90	0.089542484	lmo1257
LMRG_00396	flagellar hook-associated protein 2	1259	111	3.48E-82	0.08816521	lmo0707
LMRG_00401	flagellar hook-basal body complex protein FliE	337	29	6.46E-57	0.086053412	lmo0712
LMRG_00368	flagellar biosynthesis protein FlhA	95	8	1.26E-74	0.084210526	lmo0680
LMRG_02347	mannose-specific PTS system IID component	216	18	2.87E-83	0.083333333	lmo0098
LMRG_00364	flagellar biosynthetic protein FliP	410	34	6.85E-123	0.082926829	lmo0676
LMRG_05037	Thr tRNA	401	33	1.30E-37	0.082294264	#N/A
predicted RNA	-	379	30	2.01E-36	0.079155673	#N/A
LMRG_00982	carbamoyl-phosphate synthase large subunit	89	7	2.07E-117	0.078651685	lmo1835
LMRG_02908	hypothetical protein	140	11	1.14E-38	0.078571429	#N/A
LMRG_00367	flagellar biosynthetic protein FlhB	272	21	5.76E-133	0.077205882	lmo0679
LMRG_01064	formate acetyltransferase	689	53	4.57E-119	0.076923077	lmo1917
predicted RNA	-	281	21	3.94E-48	0.074733096	#N/A
LMRG_01580	polar amino acid transport system ATP-binding protein	436	32	5.02E-157	0.073394495	lmo2251
LMRG_01838	hypothetical protein	151	11	1.30E-66	0.072847682	lmo2410
LMRG_00979	orotidine 5'-phosphate decarboxylase	127	9	3.19E-70	0.070866142	lmo1832
LMRG_01269	hypothetical protein	466	33	3.13E-154	0.070815451	lmo2115
predicted RNA	-	505	35	3.98E-56	0.069306931	#N/A
LMRG_00983	carbamoyl-phosphate synthase small subunit	130	9	8.52E-85	0.069230769	lmo1836
predicted RNA	-	188	13	2.11E-45	0.069148936	#N/A
predicted RNA	-	772	52	5.12E-116	0.067357513	#N/A
LMRG_02874	flagellar motor switch protein FliN	611	40	2.69E-133	0.065466448	lmo0675
LMRG_00374	chemotaxis protein MotB	872	54	7.09E-193	0.061926606	lmo0686
predicted RNA	-	326	20	3.99E-66	0.061349693	#N/A
LMRG_00748	HTH-type transcriptional regulator glnR	87	5	1.99E-60	0.057471264	lmo1298
LMRG_01268	hypothetical protein	301	17	1.10E-188	0.056478405	lmo2114
predicted RNA	-	341	19	2.61E-95	0.055718475	#N/A
LMRG_00369	flagellar biosynthesis regulator FlhF	222	12	2.50E-219	0.054054054	lmo0681
predicted RNA	-	674	36	5.75E-87	0.053412463	#N/A
LMRG_00375	hypothetical protein	512	26	5.22E-242	0.05078125	lmo0687
predicted RNA	antisense: LMRG_01332	355	17	1.73E-116	0.047887324	#N/A
predicted RNA	-	315	15	1.95E-118	0.047619048	#N/A
LMRG_02345	mannose-specific PTS system IIAB component manL	939	42	0	0.044728435	lmo0096
predicted RNA	-	249	11	1.37E-135	0.044176707	#N/A
LMRG_00046	fumarate reductase flavoprotein subunit	570	25	0	0.043859649	lmo0355
LMRG_05003	Thr tRNA	412	18	1.15E-143	0.04368932	#N/A
predicted RNA	-	208	9	1.68E-121	0.043269231	#N/A
LMRG_00373	chemotaxis protein MotA	849	36	0	0.042402827	lmo0685
predicted RNA	-	386	15	7.22E-180	0.038860104	#N/A

Table 1: RNA-seq dataset of L. monocytogenes treated with 4-HNE versus mock

predicted RNA	antisense: LMRG_01332	284	11	5.53E-170	0.038732394	#N/A
LMRG_02346	mannose-specific PTS system IIC component	549	20	0	0.036429872	lmo0097
LMRG_00371	chemotaxis protein methyltransferase	191	6	0	0.031413613	lmo0683
LMRG_00986	uracil permease	535	16	0	0.029906542	lmo1839
predicted RNA	-	373	11	0	0.029490617	#N/A
predicted RNA	-	606	13	0	0.021452145	#N/A
LMRG_01332	bifunctional acetaldehyde-CoA/alcohol dehydrogenase	4772	98	0	0.020536463	lmo1634
predicted RNA	-	3702	61	0	0.01647758	#N/A
LMRG_00372	hypothetical protein	1276	21	0	0.01645768	lmo0684
LMRG_01479	glutamate decarboxylase	809	12	0	0.014833127	lmo2363
predicted RNA	-	237	3	0	0.012658228	#N/A
predicted RNA	-	660	8	0	0.012121212	#N/A
LMRG_01480	glutamate/gamma-aminobutyrate antiporter	1094	12	0	0.010968921	lmo2362

Table 2. Tn-seq dataset of essential *L. monocytogenes* genes matched with essential *B. subtilis* genes.

lmrg #	annotation	cutoff value	cutoff value	average	lmo #	gene name (Bs)	essential in Bs? Yes is x
LMRG_00550	hypothetical protein	0	1	0.5	lmo1088	tagB	x
LMRG_02430	DNA polymerase III beta subunit	0	1	0.5	lmo0002	dnaN	x
LMRG_02434	DNA gyrase, B subunit	0	0	0	lmo0006	gyrB	x
LMRG_02435	DNA gyrase subunit A	0	1	0.5	lmo0007	gyrA	x
LMRG_02474	single-strand DNA-binding protein	0	2	1	lmo0045	ssbA	x
LMRG_02483	replicative DNA helicase	0	2	1	lmo0054	dnaC	x
LMRG_02407	DNA polymerase III subunit delta	1	1	1	lmo0162	holB	x
LMRG_02620	UDP-N-acetylglucosamine diphosphorylase/glucosamine-1-phosphate N-acetyltransferase	1	1	1	lmo0198	glmU/gcaD	x
LMRG_02621	ribose-phosphate pyrophosphokinase 1	0	0	0	lmo0199	prs	x
LMRG_02635	peptidyl-tRNA hydrolase	1	1	1	lmo0213	pth/spoVC	x
LMRG_02839	dihydroneopterin aldolase	1	1	1	lmo0225	folB	x
LMRG_02836	lysyl-tRNA synthetase	0	0	0	lmo0228	lysS	x
LMRG_02667	cysteinyl-tRNA synthetase	1	1	1	lmo0239	cysS	x
LMRG_02656	large subunit ribosomal protein L10	0	1	0.5	lmo0250	rplJ	x
LMRG_02650	DNA-directed RNA polymerase beta' subunit	1	1	1	lmo0259	rpoC	x
LMRG_02584	response regulator VicR	0	1	0.5	lmo0287	walR	x
LMRG_00415	glutamine-fructose-6-phosphate transaminase	1	1	1	lmo0727	glmS	x
LMRG_02278	D-alanine-D-alanine ligase	0	0	0	lmo0855	ddl	x
LMRG_02279	UDP-N-acetylmuramoylalanyl-D-glutamyl-2	1	1	1	lmo0856	murF	x
LMRG_02067	inorganic polyphosphate/ATP-NAD kinase 1	0	0	0	lmo0968	nadF	x
LMRG_02106	aminotransferase	1	1	1	lmo1006	patA	x
LMRG_02111	2,3,4,5-tetrahydropyridine-2,6-dicarboxylate N-acetyltransferase	0	0	0	lmo1011	dapH	x
LMRG_02112	N-acetyl-L,L-diaminopimelate deacetylase	1	1	1	lmo1012	dapL	x
LMRG_00533	cell division protein FtsW	0	1	0.5	lmo1071	ftsW	x
LMRG_00536	teichoic acid transport system permease	0	1	0.5	lmo1074	tagG	x
LMRG_00537	teichoic acids export ATP-binding protein tagH	0	1	0.5	lmo1075	tagH	x
LMRG_00539	hypothetical protein	0	2	1	lmo1077	tagB	x
LMRG_00547	CDP-ribitol:poly(ribitol phosphate) ribitol phosphotransferase	0	0	0	lmo1085	tagB	x
LMRG_00548	2-C-methyl-D-erythritol 4-phosphate cytidylyltransferase	0	0	0	lmo1086	ispD	x
LMRG_00551	glycerol-3-phosphate cytidylyltransferase	0	0	0	lmo1089	tagD	x
LMRG_00554	nicotinate phosphoribosyltransferase	0	1	0.5	lmo1092	pncB	x
LMRG_00555	NAD+ synthetase	0	0	0	lmo1093	nadE	x
LMRG_00683	glutamate racemase	0	0	0	lmo1237	racE	x
LMRG_00722	ribosome biogenesis GTP-binding protein YlqF	0	1	0.5	lmo1272	rbgA	x
LMRG_00734	hypothetical protein	0	1	0.5	lmo1284	plsY	x
LMRG_00736	DNA topoisomerase IV B subunit	0	1	0.5	lmo1286	parE	x
LMRG_00737	DNA topoisomerase IV A subunit	0	0	0	lmo1287	parC	x
LMRG_00763	UMP kinase	0	0	0	lmo1313	pyrH	x
LMRG_00764	ribosome recycling factor	0	0	0	lmo1314	frr	x
LMRG_00765	di-trans,poly-cis-decaprenylcistransferase	0	0	0	lmo1315	uppS	x

Table 2. Tn-seq dataset of essential *L. monocytogenes* genes matched with essential *B. subtilis* genes.

LMRG_00766	phosphatidate cytidylyltransferase	0	0	0	lmo1316	cdsA	x
LMRG_00772	transcription termination factor NusA	1	1	1	lmo1322	nusA	x
LMRG_00807	acetyl-CoA carboxylase	0	2	1	lmo1357	accC	x
LMRG_00848	CDP-diacylglycerol-glycerol-3-phosphate 3-phosphatidyltransferase	0	1	0.5	lmo1396	pgsA	x
LMRG_00872	UDP-N-acetylenolpyruvoylglucosamine reductase	0	2	1	lmo1420	murB	x
LMRG_00887	dihydrodipicolinate synthase	0	0	0	lmo1435	dapA	x
LMRG_00888	aspartate kinase	0	1	0.5	lmo1436	dapG	x
LMRG_00889	aspartate-semialdehyde dehydrogenase	0	1	0.5	lmo1437	asd	x
LMRG_00900	manganese-dependent inorganic pyrophosphatase	0	1	0.5	lmo1448	ppaC	x
LMRG_00906	RNA polymerase sigma factor rpoD	0	0	0	lmo1454	sigA	x
LMRG_00910	glycyl-tRNA synthetase beta subunit	0	0	0	lmo1458	glyS	x
LMRG_00911	glycyl-tRNA synthetase alpha subunit	0	0	0	lmo1459	glyQ	X
LMRG_00917	metalloprotease	0	1	0.5	lmo1465	yqfG	x
LMRG_00934	DNA polymerase III delta subunit	0	1	0.5	lmo1481	holA	x
LMRG_00941	nicotinate nucleotide adenylyltransferase	0	2	1	lmo1488	nadD	x
LMRG_00945	HAD superfamily phosphatase	0	0	0	lmo1492	yqeG	x
LMRG_01458	tRNA methyl transferase	0	1	0.5	lmo1512	trmU	x
LMRG_01457	cysteine desulfurase	0	0	0	lmo1513	yrvO	x
LMRG_01451	aspartyl-tRNA synthetase	0	0	0	lmo1519	aspS	x
LMRG_01430	50S ribosomal protein L27	1	1	1	lmo1540	rpmA	x
LMRG_01429	hypothetical protein	0	0	0	lmo1541	prp	x
LMRG_01428	50S ribosomal protein L21	0	0	0	lmo1542	rplU	x
LMRG_01424	rod shape-determining protein MreD	1	1	1	lmo1546	mreD	x
LMRG_01423	rod shape-determining protein MreC	0	0	0	lmo1547	mreC	x
LMRG_01422	rod shape-determining protein mreB	0	2	1	lmo1548	mreB	x
LMRG_01417	folylpolyglutamate synthase	0	0	0	lmo1551	folC	x
LMRG_01416	valyl-tRNA synthetase	0	2	1	lmo1552	valS	x
LMRG_01409	ribosome biogenesis GTP-binding protein YsxC	0	0	0	lmo1558	ysxC	x
LMRG_01406	replication initiation and membrane attachment protein	1	1	1	lmo1561	dnaB	x
LMRG_01404	dephospho-CoA kinase	0	0	0	lmo1563	ytaG	x
LMRG_01395	acetyl-CoA carboxylase carboxyl transferase alpha subunit	1	1	1	lmo1572	accA	x
LMRG_01394	acetyl-CoA carboxylase carboxyl transferase beta subunit	1	1	1	lmo1573	accD	x
LMRG_02943	DNA polymerase III subunit alpha	0	1	0.5	lmo1574	dnaE	x
LMRG_01371	30S ribosomal protein S4	0	0	0	lmo1596	rpsD	x
LMRG_01369	tyrosyl-tRNA synthetase	0	2	1	lmo1598	tyrS	x
LMRG_01361	UDP-N-acetylmuramate-alanine ligase	0	1	0.5	lmo1605	murC	x
LMRG_01319	1-acyl-sn-glycerol-3-phosphate acyltransferase	0	0	0	lmo1647	plsC	x
LMRG_01310	translation elongation factor Ts	0	0	0	lmo1657	tsf	x
LMRG_01309	30S ribosomal protein S2	0	0	0	lmo1658	rpsB	x
LMRG_01307	leucyl-tRNA synthetase	0	2	1	lmo1660	leuS	x
LMRG_01303	methionine adenosyltransferase	0	0	0	lmo1664	metK	x

Table 2. Tn-seq dataset of essential *L. monocytogenes* genes matched with essential *B. subtilis* genes.

LMRG_02517	aspartyl/glutamyl-tRNA(Asn/Gln) amidotransferase subunit B	0	0	0	lmo1754	gatB	x
LMRG_02516	glutamyl-tRNA(Gln) amidotransferase subunit A	0	0	0	lmo1755	gatA	x
LMRG_02827	translation initiation factor IF-3	0	0	0	lmo1785	infC	x
LMRG_02816	tRNA (guanine-N1)-methyltransferase	0	2	1	lmo1792	trmD	x
LMRG_00948	signal recognition particle protein	0	1	0.5	lmo1801	ffh	x
LMRG_00950	signal recognition particle-docking protein FtsY	0	1	0.5	lmo1803	ftsY	x
LMRG_00954	3-oxoacyl-[acyl-carrier-protein] reductase	0	1	0.5	lmo1807	fabG	x
LMRG_00955	malonyl CoA-acyl carrier protein transacylase	0	0	0	lmo1808	fabD	x
LMRG_00971	primosomal protein N'	0	1	0.5	lmo1824	priA	x
LMRG_00974	guanylate kinase	0	0	0	lmo1827	gmk	x
LMRG_01021	thymidylate synthase	0	0	0	lmo1874	thyA	x
LMRG_01042	DNA replication protein	0	0	0	lmo1895	dnaD	x
LMRG_01051	hypothetical protein	0	1	0.5	lmo1904	birA	x
LMRG_01052	CCA-adding enzyme	0	0	0	lmo1905	cca	x
LMRG_01054	dihydrodipicolinate reductase	0	0	0	lmo1907	dapB	x
LMRG_01084	ribosome-associated GTPase EngA	0	1	0.5	lmo1937	engA	x
LMRG_01168	isoleucyl-tRNA synthetase	0	1	0.5	lmo2019	ileS	x
LMRG_01181	cell division protein FtsZ	0	1	0.5	lmo2032	ftsZ	x
LMRG_01183	cell division protein FtsQ	0	0	0	lmo2034	divIB	x
LMRG_01187	UDP-N-acetylmuramoyl-L-alanyl-D-glutamate-2	0	0	0	lmo2038	murE	x
LMRG_01189	cell division protein FtsL	0	0	0	lmo2040	ftsL	x
LMRG_01202	pantetheine-phosphate adenylyltransferase	0	1	0.5	lmo2052	coaD	x
LMRG_01218	chaperonin GroEL	0	2	1	lmo2068	groEL	x
LMRG_01226	O-sialoglycoprotein endopeptidase	0	2	1	lmo2075	gcp	x
LMRG_01228	hypothetical protein	1	1	1	lmo2077	tsaB	x
LMRG_01272	phosphoglucosamine mutase	0	2	1	lmo2118	glmM	x
LMRG_01680	thioredoxin	1	1	1	lmo2152	trxA	x
LMRG_01678	ribonucleoside-diphosphate reductase	1	1	1	lmo2154	nrdF	x
LMRG_01677	ribonucleoside-diphosphate reductase subunit alpha	0	2	1	lmo2155	nrdE	x
LMRG_01634	tryptophanyl-tRNA synthetase	1	1	1	lmo2198	trpS	x
LMRG_02723	multicomponent Na+:H+ antiporter subunit A	0	2	1	lmo2378	mrpA	x
LMRG_02724	multicomponent Na+:H+ antiporter subunit B	0	1	0.5	lmo2379	mrpB	x
LMRG_02726	multicomponent Na+:H+ antiporter subunit D	0	0	0	lmo2381	mrpD	x
LMRG_02728	multicomponent Na+:H+ antiporter subunit F	0	1	0.5	lmo2383	mrpF	x
LMRG_02735	hypothetical protein	0	1	0.5	lmo2390	yumC	x
LMRG_01837	FeS assembly protein SufB	0	2	1	lmo2411	sufB	x
LMRG_01836	NifU family SUF system FeS assembly protein	0	1	0.5	lmo2412	sufU	x
LMRG_01835	selenocysteine lyase	0	0	0	lmo2413	sufS	x
LMRG_01834	FeS assembly protein SufD	1	1	1	lmo2414	sufD	x
LMRG_01833	FeS assembly ATPase SufC	0	0	0	lmo2415	sufC	x
LMRG_01793	phosphopyruvate hydratase	1	1	1	lmo2455	eno	x

Table 2. Tn-seq dataset of essential *L. monocytogenes* genes matched with essential *B. subtilis* genes.

LMRG_01789	glyceraldehyde-3-phosphate dehydrogenase	0	0	0	lmo2459	gapA	x
LMRG_01770	thioredoxin-disulfide reductase	0	1	0.5	lmo2478	trxB	x
LMRG_01739	peptide chain release factor 2	0	0	0	lmo2509	prfB	x
LMRG_01727	N-acetylglucosaminyldiphosphoundecaprenol	0	0	0	lmo2521	tagA	x
LMRG_01722	UDP-N-acetylglucosamine 1-carboxyvinyltransferase	0	2	1	lmo2526	murA	x
LMRG_01710	UDP-N-acetylglucosamine 2-epimerase	0	1	0.5	lmo2537	mnaA	x
LMRG_01704	peptide chain release factor 1	0	1	0.5	lmo2543	prfA	x
LMRG_02710	CTP synthase	0	2	1	lmo2559	pyrG	x
LMRG_02708	arginyl-tRNA synthetase	0	1	0.5	lmo2561	argS	x
LMRG_02149	50S ribosomal protein L17	0	0	0	lmo2605	rplQ	x
LMRG_02150	DNA-directed RNA polymerase alpha subunit	0	1	0.5	lmo2606	rpoA	x
LMRG_02155	adenylate kinase	0	0	0	lmo2611	adk	x
LMRG_02156	preprotein translocase SecY subunit	0	0	0	lmo2612	secY	x
LMRG_02160	50S ribosomal protein L18	0	0	0	lmo2616	rplR	x
LMRG_02161	50S ribosomal protein L6	0	1	0.5	lmo2617	rplF	x
LMRG_02162	30S ribosomal protein S8	0	0	0	lmo2618	rpsH	x
LMRG_02163	30S ribosomal protein S14p/S29e	0	0	0	lmo2619	rpsN	x
LMRG_02164	large subunit ribosomal protein L5	0	0	0	lmo2620	rplE	x
LMRG_02165	50S ribosomal protein L24	0	0	0	lmo2621	rplX	x
LMRG_02166	50S ribosomal protein L14	0	0	0	lmo2622	rplN	x
LMRG_02167	30S ribosomal protein S17	0	0	0	lmo2623	rpsQ	x
LMRG_02169	50S ribosomal protein L16	0	0	0	lmo2625	rplP	x
LMRG_02170	30S ribosomal protein S3	0	1	0.5	lmo2626	rpsC	x
LMRG_02171	50S ribosomal protein L22	0	0	0	lmo2627	rplV	x
LMRG_02172	30S ribosomal protein S19	0	0	0	lmo2628	rpsS	x
LMRG_02173	50S ribosomal protein L2	0	1	0.5	lmo2629	rplB	x
LMRG_02175	50S ribosomal protein L4/L1	0	1	0.5	lmo2631	rplD	x
LMRG_02176	50S ribosomal protein L3	0	1	0.5	lmo2632	rplC	x
LMRG_02198	translation elongation factor Tu	0	1	0.5	lmo2653	tufA	x
LMRG_02199	translation elongation factor G	1	1	1	lmo2654	fusA	x
LMRG_02200	30S ribosomal protein S7	1	1	1	lmo2655	rpsG	x
LMRG_02240	thymidylate kinase	0	0	0	lmo2693	tmk	x
LMRG_01993	DNA polymerase III subunit gamma/tau	0	2	1	lmo2704	dnaX	x
LMRG_01949	seryl-tRNA synthetase	0	2	1	lmo2747	serS	x
LMRG_02439	mevalonate kinase	0	0	0	lmo0010		
LMRG_02440	diphosphomevalonate decarboxylase	0	2	1	lmo0011		
LMRG_02441	phosphomevalonate kinase	0	2	1	lmo0012		
LMRG_02386	peptide/nickel transport system permease	0	1	0.5	lmo0137		
LMRG_02938	serine O-acetyltransferase	0	0	0	lmo0238	cysE	
LMRG_02658	50S ribosomal protein L11	0	0	0	lmo0248	rplK/relC	
LMRG_02657	50S ribosomal protein L1	0	0	0	lmo0249	rplA	

Table 2. Tn-seq dataset of essential *L. monocytogenes* genes matched with essential *B. subtilis* genes.

LMRG_02786	carbonic anhydrase	0	0	0	lmo0811		
LMRG_02250	hydroxymethylglutaryl-CoA reductase	0	1	0.5	lmo0825		
LMRG_02026	phosphoglycerol transferase	1	1	1	lmo0927	itaS	
LMRG_02069	enoyl-[acyl-carrier protein] reductase I	1	1	1	lmo0970	fabI	
LMRG_02127	hypothetical protein	0	2	1	lmo1027	rnJA	
LMRG_02128	hypothetical protein	0	0	0	lmo1028	no close homolog	
LMRG_00512	polypeptide deformylase	0	1	0.5	lmo1051	defB	
LMRG_00549	alcohol dehydrogenase	0	0	0	lmo1087	no close homolog, this component of pentose pathway missing Bs	
LMRG_00553	hypothetical protein	0	1	0.5	lmo1091	epsH	
LMRG_00590	adenosylcobinamide kinase/adenosylcobinamide-phosphate guanylyltransferase	0	2	1	lmo1147	cobalamin synthesis pathway missing in Bs	
LMRG_00674	ribonuclease HIII	0	0	0	lmo1228	rnhC	
LMRG_00752	LexA repressor	0	0	0	lmo1302	lexA	
LMRG_00773	hypothetical protein	0	2	1	lmo1323	ylxR	
LMRG_00774	hypothetical protein	0	2	1	lmo1324	rplGA	
LMRG_00805	translation elongation factor P	0	1	0.5	lmo1355	efp	
LMRG_00828	6-phosphogluconate dehydrogenase	0	1	0.5	lmo1376	gndA	
LMRG_00835	isopentenyl-diphosphate delta-isomerase type 2	0	1	0.5	lmo1383	fni	
LMRG_00851	hypothetical protein	0	0	0	lmo1399	rny	
LMRG_00866	acetyl-CoA C-acetyltransferase	0	2	1	lmo1414	mmgA	
LMRG_00867	hydroxymethylglutaryl-CoA synthase	1	1	1	lmo1415	pksG	
LMRG_00890	hypothetical protein	0	1	0.5	lmo1438	pbpA	
LMRG_00925	chaperone DnaJ	0	0	0	lmo1472	dnaJ	
LMRG_00926	chaperone DnaK	1	1	1	lmo1473	dnaK	
LMRG_00927	co-chaperone GrpE	0	0	0	lmo1474	grpE	
LMRG_00944	ribosome biogenesis GTPase YqeH	0	1	0.5	lmo1491	yqeH	
LMRG_01474	transcription elongation factor greA	0	0	0	lmo1496	greA	
LMRG_01427	hypothetical protein	0	2	1	lmo1543		
LMRG_01408	threonyl-tRNA synthetase	0	1	0.5	lmo1559	thrS	
LMRG_02561	methionine aminopeptidase type I	0	0	0	lmo1709	mapA	
LMRG_02817	16S rRNA processing protein RimM	0	0	0	lmo1793	rimM	
LMRG_00970	methionyl-tRNA formyltransferase	0	2	1	lmo1823	fmt	
LMRG_01044	aspartate aminotransferase	0	1	0.5	lmo1897	aspB	
LMRG_01092	hypothetical protein	0	1	0.5	lmo1945	ribU	
LMRG_01274	hypothetical protein	0	2	1	lmo2120	cdaA	
LMRG_01679	ribonucleotide reductase-associated flavodoxin	0	1	0.5	lmo2153	ykuP	
LMRG_01630	3-oxoacyl-[acyl-carrier-protein] synthase 3	0	0	0	lmo2202	fabHA	
LMRG_01791	triosephosphate isomerase	0	1	0.5	lmo2457	tpiA	
LMRG_01790	phosphoglycerate kinase	0	1	0.5	lmo2458	pgk	
LMRG_01780	Clp protease	0	1	0.5	lmo2468	clpP	
LMRG_01776	hypothetical protein	0	1	0.5	lmo2472	whiA	
LMRG_01773	phosphoglucomutase/phosphomannomutase	0	2	1	lmo2475	pgcA	

Table 2. Tn-seq dataset of essential *L. monocytogenes* genes matched with essential *B. subtilis* genes.

LMRG_01761	hypothetical protein	0	0	0	lmo2487	yvlB	
LMRG_01743	D-glutamyl-L-m-Dpm peptidase P45	0	1	0.5	lmo2505	cwlO	
LMRG_01742	cell division transport system permease	1	1	1	lmo2506	ftsX	
LMRG_01741	cell division ATP-binding protein FtsE	0	0	0	lmo2507	ftsE	
LMRG_02707	hypothetical protein	0	0	0	lmo2562		
LMRG_02144	cobalt/nickel transport system ATP-binding protein	0	1	0.5	lmo2600	ybaE	
LMRG_02145	cobalt import ATP-binding protein cbiO 2	0	1	0.5	lmo2601	ybxA	
LMRG_02157	50S ribosomal protein L15	0	1	0.5	lmo2613	rplO	
LMRG_02168	50S ribosomal protein L29	0	0	0	lmo2624	rpmC	